HYBRID EPOXY FILMS CONTAINING WELL-EXFOLIATED MULTI-WALLED CARBON NANOTUBES AND NYLON-12 WITH ENHANCED TENSILE PROPERTIES, FRACTURE TOUGHNESS, AND ELECTRICAL CONDUCTIVITY

A Dissertation

by

SPENCER ALLISTOR HAWKINS

Submitted to the Office of Graduate and Professional Studies of
Texas A&M University
in partial fulfillment of the requirements for the degree of

DOCTOR OF PHILOSOPHY

Chair of Committee,	Hung-Jue Sue
Committee Members,	Perla Balbuena
	Mohammad Naraghi
	John Whitcomb
Head of Department,	Ibrahim Karaman

August 2017

Major Subject: Materials Science and Engineering

ABSTRACT

In order to gain a more fundamental understanding of multifunctional epoxy nanocomposites, model systems containing surface functionalized multi-walled carbon nanotubes (MWCNTs) and thermoplastic microparticles were fabricated and studied. Epoxies are inherently brittle and electrically insulative and therefore require the introduction of fillers with different functionalities to produce a truly multifunctional epoxy composite. The mechanical, electrical, and fracture properties of a conventional aerospace-grade epoxy resin were enhanced by the addition of ZnO-functionalized MWCNTs and nylon 12 (PA) microparticles.

Carbon nanotubes (CNTs) are an emerging class of carbon-based materials that have dominated polymer nanocomposite research in recent years due to their potential application in energy storage, electronic thin films, biotechnology, multifunctional materials, etc. The strong push for fundamental research is driven by their superior mechanical, electrical, and thermal properties. However, there are numerous problems related to processability and fabrication of nanocomposites. In order to solve these problems, which include insolubility in organic solvents and polymers and dispersability, surface functionalization is used to break up large aggregates of CNTs resulting in better dispersion and enhanced compatibility with various solvents and polymers. Traditional approaches such as chemical functionalization of the CNT surface are less commonly used due to their lacking efficiency and effectiveness at controlling the exfoliation of CNTs, which are critical to the development of tailored nanocomposites with superior mechanical and electrical behavior. Further advances in the field are required whereby a fundamental

understanding of the necessary steps involved is gained. MWCNTs were decorated with ZnO quantum dots (QDs) by refluxing zinc acetate dihydrate and potassium hydroxide in the presence of pristine (P-MWCNTs) or oxidized (O-MWCNTs). The physical decoration of ZnO QDs on MWCNTs yielded a system of well-exfoliated CNTs with little to no degradation of their material properties.

PA was introduced to enhance the ductility and fracture toughness of the epoxy resin by undergoing a severe level of plastic deformation when under tensile stress with and without a pre-existing crack. The glass transition and elastic modulus of epoxy tends to decrease when a large concentration of a relatively soft filler is introduced resulting in a somewhat softer material. This was not observed when ZnO/MWCNTs were introduced into the PA toughened epoxy systems, which contradicts findings currently found in the literature.

The morphology and dispersion of the various fillers was unambiguously confirmed via X-ray diffraction (XRD), transmission electron microscopy (TEM), UV-Vis-NIR spectroscopy, x-ray photoelectron spectroscopy (XPS), and optical microscopy (OM). The tensile, fracture, and thermos-mechanical properties of the model hybrid epoxy nanocomposites have been investigated. This dissertation has expanded the understanding of the effects of filler, and filler-filler interaction on the thermal, mechanical, and fracture behavior of epoxy nanocomposites.

DEDICATION

To my wife, Melissa, and son, Silas, you have given me the love and support that I needed to finish this. Day in and day out, I couldn't have done it without you. I'm pretty sure that I would've quit a long time ago, and if not, I don't think that I would've been in a good place when I had finished. To my parents, Scott and Arlene, and in-laws, Leon and Shirley, thanks for listening to my struggles throughout this process and always telling me that I'd make it. To my brothers and sisters, Sean, Taylor, Sullivan, Preston, and Hope, for always helping me remember that I'm not alone and for picking me up, even when you didn't know that I needed it. To my grandparents, John and Fausta, and Phillip and Connie, for giving me perspective on life: what is was, is, and can be if I want it bad enough. All of you were the cornerstone upon which I was supported throughout my graduate career. Without you, I wouldn't have finished. Plain and simple.

"As the Father has loved me, so I have loved you; abide in my love. If you keep my commandments, you will abide in my love, just as I have kept my Father's commandments and abide in his love. These things I have spoken to you, that my joy may be in you, and that your joy may be full. 'This is my commandment, that you love one another as I have loved you. Greater love has no man than this, that a man lay down his life for his friends.'" John 15:9-13.

"You shall love the Lord your God with all your heart, and with all your soul, and with all your mind. This the great and first commandment. And a second is like it, You shall love your neighbor as yourself." Matthew 22:37-39

ACKNOWLEDGEMENTS

First and foremost, I want to thank God for giving me the strength and patience to see this through to the end.

Melissa, thank you for standing by me through my ups and downs, there were times that I didn't think that I was good enough to get a Ph.D. or be a good husband to you or a good father to Silas. I definitely had doubts throughout the whole process, but you were always there in my mind and there at home to welcome me. I was always able to cheer myself up a bit by knowing that you'd be there when I was done for the day. Silas, thank you for giving me renewed hope for the next chapter in my life. Knowing that you loved me regardless of what I thought about myself gave me hope. Wanting to be a better father for you kept me going through all of this. Mom, Dad, Sean, Taylor, Sullivan, Preston, and Hope, I can't tell you how much it meant to me that you guys were only an hour away. Going home for the weekend, even if I worked, really helped me relieve the stress of grad school. You guys are part of the reason that I'm still sane and actually finished it with a smile. Mom and Dad (Shirley and Leon) the same can be said to you as well, I'm so glad that I could take a break at your home for the weekend. You also listened to me vent during those weekends and I really appreciate it. To my extended family, I couldn't do it without y'all either. I had some of the best times in Cleveland when I stayed over the past summers.

I want to also thank the members of my research group that have helped me in numerous and varied ways throughout my time in graduate school. Ehsan Moghbelli, thanks for making the lab a place that I wanted to come to every day. I especially enjoyed

our shenanigans throughout the years and our workouts. Haiqing Yao, thank you for putting up with me and my lack of chemistry knowledge. Without you, I never could have gotten this far, let alone finished my Ph.D. Hongfeng Wang, thanks for helping me with my first paper and teaching me about French culture and for your advice on raising my son. Kevin Laux, thanks for putting up with me as an office mate and allowing us to become friends, even if it was near the end of our time here at graduate school. Kevin White, thank you for taking me under your wing all those years ago and teaching me the trade. I've come to consider you one of my best friends, especially during my time here at Texas A&M. Fringe, right? Mohammad Hossain, thanks for always being open to my questions about solid mechanics and fracture and for inviting me into your home for an awesome night of festivities. Peng Liu, thank you for sticking with me until the end, I know that it wasn't easy for either of us. I really appreciated your honesty throughout my time here. They took our jobs! Tatsuya Hirata, thanks for being my friend while you were here, I really enjoyed having you over to my place to play some video games. I'm also thankful for your help with my project and for teaching me about Japan. Farhad Daneshvar, thank you for being my best friend at the end of all of this. I should also thank you for putting up with me as well, I know that I blew you off sometimes (gym, research, etc.). I will always think of you as a brother, remember that. Isabel Cantu, it goes without saying that you are and always will be my mama bear here at Texas A&M University. You always helped me when I needed something taken care of, you listened to me when I was struggling, and you welcomed me into your family by sharing so much of your life with me. James Chrisman, thanks for being my friend through all of this; it hasn't been

easy, but talking with you day in and day out about whatever grounded me and helped me remember that I was not alone in my suffering here. Dr. Michael Mullins, I can't tell you how much it meant to me over the years that your door was always open. You were the advisor that I never had. I always looked forward to talking with you about my research progress, papers that I'd read, how to get a job, family stuff, etc. I want you to know that I'm forever grateful for your generosity and warmth during this cold and dark period in my life. Bart Stevens, thank you for also listening to my struggles, but also for letting me bounce research ideas off of you. I'll never forget how much I looked forward to and enjoyed our discussions, over a pop, about Game of Thrones, Sherlock, The Walking Dead, etc. Cong Liu, thank you so much for helping me with the final stages of my Ph.D., especially working with the microtome and the dielectric spectrometer. I always enjoyed talking with you about your research and your life; I know that it hasn't been easy for you. Just remember that you always have a friend in me. To all of my friends mentioned above (and unmentioned) and those past, current, and future group members, nobody makes it through graduate school by themselves. We're all running a race and some of us stumble along the way. Let's make sure that we always reach out to those that can help us and also extend a helping hand to those who need it. I hope that I've left the group with an example of what we can be if we all work together and support each other through these trying times. I hope that if I come back to the group in 1, 5, or 10 years, that I'll be able to see the influence that I made during my time here. If we ever see each other in the future, just know that I'm forever grateful for anything that you ever helped me with and good luck with the rest of your life.

Dr. Sue, thank you for giving me the opportunity to work in your lab and your constant support throughout the years. I admit that I wasn't always very motivated about my work and was constantly thinking about doing other things and being in other places. I'd also like to thank my committee members, Dr. Perla Balbuena, Dr. Mohammad Naraghi, and Dr. John Whitcomb, for your guidance and support. I know that you were trying to help me along this journey.

"Even though I walk through the valley of the shadow of death, I fear no evil; for you are with me; your rod and your staff, they comfort me. You prepare a table before me in the presence of my enemies; you anoint my head with oil, my cup overflows. Surely goodness and mercy shall follow me all the days of my life; and I shall dwell in the house of the Lord forever." Psalm 23:4-6

"You have heard that it was said, 'You shall love your neighbor and hate your enemy.' But I say to you, love your enemies and pray for those who persecute you, so that you may be sons of your Father who is in heaven; for He makes his sun rise on the evil and on the good, and sends rain on the just and on the unjust. For if you love those who love you, what reward have you?" And if you salute only your brethren, what more are you doing than others? Do not even the Gentiles do the same? You, therefore, must be perfect, as your heavenly Father is perfect." Matthew 5:43-48

"Behold, I am with you always, to the end of the age." Matthew 28:20

CONTRIBUTORS AND FUNDING SOURCES

Contributors

This work was supervised by a dissertation committee consisting of Professor Hung-Jue Sue of the Department of Materials Science and Engineering and Professor Perla Balbuena of the Department of Chemical Engineering and Professors Mohammad Naraghi and John Whitcomb of the Department of Aerospace Engineering.

The functionalization method was developed by Haiqing Yao, the scanning electron microscopy images were obtained by Farhad Daneshvar, and the transmission electron microscopy images were obtained by Hongfeng Wang and Xi Zhang.

All other work conducted for the dissertation was completed by the student independently.

Funding Sources

Graduate study was supported by the NSF TAMUS LSAMP BTD Fellowship from the Louis Stokes Alliance for Minority Participation in Research and the National Science Foundation and the NASA Harriet G. Jenkins Graduate Fellowship from the National Aeronautics and Space Administration (Grant #: NNX13AT13H).

NOMENCLATURE

CNT:	Carbon nanotube
SWCNT:	Single-walled carbon nanotube
P-SWCNT:	Pristine single-walled carbon nanotube
O-SWCNT:	Oxidized single-walled carbon nanotube
F-SWCNT:	Functionalized single-walled carbon nanotube
MWCNT:	Multi-walled carbon nanotube
P-MWCNT:	Pristine multi-walled carbon nanotube
O-MWCNT:	Oxidized multi-walled carbon nanotube
F-MWCNT:	Functionalized multi-walled carbon nanotube
PA:	Polyamide-12, Nylon-12
α-ZrP:	α-zirconium phosphate
VaRTM:	Vacuum-assisted resin transfer molding
CFRC:	Carbon fiber-reinforced composite
EMI:	Electromagnetic interference shielding
Zn:	Zinc
ZnO;	Zinc oxide
QD:	Quantum dot
MeOH:	Methanol
KOH:	Potassium hydroxide
PDMS:	Polydimethylsiloxane
DI-H_2O:	Deionized water

PVDF:	Polyvinylidene fluoride
DGEBF:	Diglycidylether of bisphenol F
DETDA:	Diethyltoluene diamine
DSC:	Differential scanning calorimetry
DMA:	Dynamic mechanical analysis
TGA:	Thermogravimetric analysis
XRD:	X-ray diffraction
XPS:	X-ray photoelectron spectroscopy
UV-Vis-NIR:	Ultraviolet-Visual-Near Infrared Spectroscopy
FTIR:	Fourier transform infrared spectroscopy
TOM:	Transmission optical microscopy
LCM:	Laser scanning microscope
SEM:	Scanning electron microscope
TEM:	Transmission electron microscope
E':	Tensile storage modulus
E":	Tensile loss modulus
δ:	Phase shift
tan δ:	Damping factor
T_g:	Glass transition temperature
ρ:	Electrical resistivity
σ:	Electrical conductivity
ν:	Poisson's ratio

E:	Young’s modulus
$\Sigma\sigma_U$:	Ultimate tensile strength
ε_B:	Strain at break
K_{IC}:	Critical stress intensity factor
G_{IC}:	Critical strain energy release rate
vdW:	Van der Waals
FRP:	Fiber-reinforced polymer

TABLE OF CONTENTS

Page

LIST OF FIGURES

Page

LIST OF TABLES

Page

CHAPTER I

INTRODUCTION

1.1 Background

The history of materials science as it relates to the development of commercial and military aircraft over the years has exhibited a trend from using flexible, low-density materials, towards denser, and stiffer materials with the ability to sustain heavier payloads at higher speeds. The discovery of polymers, development of polymer science, and the more recent progress in fabricating advanced polymer composites with extraordinary strength-to-weight ratios led many to believe that a new era would begin whereby the use of polymeric composites in aircraft would see exponential growth. However, with the development of advanced joining techniques, lightweight metallic alloys, high-speed machining, and low-cost manufacturing of castings, that prediction has been met with a much slower rate [1]. Furthermore, the lack of a complete understanding of the fatigue life of polymeric materials, let alone their composites, coupled with the poor fracture toughness and compression after impact (CAI) strength of brittle thermoset materials commonly has also negatively impacted the growth of polymer material use in the aerospace industry.

Over the last three decades, there has been an enormous push towards the development of multifunctional polymer nanocomposites with CNTs and/or thermoplastic particles. These polymeric composite materials are expected to be less dense than metals, be stiffer and stronger than conventional polymers, and electrically and thermally conductive as well. However, the number of negative reports in the literature far outweigh

the positive ones, specifically when it comes to effectively dispersing the fillers, maintaining or improving T_g, or driving whatever property is desired without compromising another.

CNTs have been a focal point of polymer composite research for decades due to their excellent mechanical strength and stiffness, and superior electrical and thermal conductivities [2-39]. Numerous research efforts have investigated whether CNTs are able to be introduced into a polymer matrix of interest to impart their excellent inherent properties to the final composite part [6-8, 13, 18, 19, 25, 39-60]. Due to their large surface area-to-volume ratio and aspect ratio, CNTs exhibit unparalleled properties such as: 1) the highest modulus and tensile strength of any discovered material, 2) high potential for surface functionalization due to high surface energy, 3) exceptional thermal and chemical stability, and 4) superior electrical and thermal conductivities compared to other conductive fillers. As a result, CNTs are an attractive nanofiller for research into diverse applications such as polymer composites for structural or electrical/thermal environments, batteries, dielectrics, and anti-corrosive coatings, and many others [51, 54, 61-63].

In light of their previously mentioned properties, CNTs are not without their share of problems, especially when it comes to processing and integration into polymer matrices. They are difficult to manipulate and are not soluble in organic solvents, which decreases the amount of usable material and also tend to destroy their inherent properties. Furthermore, the techniques used to synthesize CNTs usually yield bunded tubes, entanglements, and aggregates, which are composed of hundreds, if not thousands of single nanotubes. The atomically smooth surface of CNTs makes it difficult to disperse

them in solvents and react with various functional groups [62]. The extremely large surface area-to-volume ratio and high aspect ratio, coupled with the high surface energy and strong vdW interactions, tend to result in single tubes bundling and entangling.

Surface functionalization is therefore used to overcome these challenges to successfully integrate CNTs into polymer matrices. The addition of various chemical groups, small molecules, or short chain oligomers to the tube surface breaks up the aggregates, which are further broken into bundles and individual tubes via ultrasonication [60]. Once the CNTs are individually exfoliated, they can be dispersed into a polymer matrix of interest. The surface functionalization of CNTs is commonly accomplished with two methods: 1) covalent attachment of various molecules via chemical reactions with or without previous surface oxidation, and 2) non-covalent or physical functionalization of molecules onto the tube surface.

Thermoplastic particles, particularly nylons, have been dispersed into thermoset polymer matrices to improve their inherently low fracture toughness [29, 64-74]. The primary mechanism involved in dissipating energy is crack bridging whereby, assuming the dispersed particle is of a comparable size as that of the natural crack tip radius of a given polymer matrix, it is able to bridge the crack after the crack front has passed beyond the location of the particle. Subsequently, the crack continues to propagate causing the crack wake to continue opening resulting in severe plastic deformation of the nylon particle. Unfortunately, the concentration of particles used is sufficiently high, such that, the modulus of the matrix is adversely effected This is only the case for soft-rigid systems,

wherein the toughening phase is relatively soft (low T_g) compared to the relatively hard matrix (high T_g).

1.2 Research objectives and significance

The proposed research aims to probe the effect of a newly developed, physical functionalization approach to exfoliating multi-walled carbon nanotubes (MWCNTs) on the bulk behavior of epoxy nanocomposites. The intrinsic properties of the MWCNTs are marginally effected by the proposed functionalization method and should result in enhanced bulk performance when used as the reinforcing phase. Pristine (P-MWCNTs) and oxidized (O-MWCNTs) MWCNTs will be used to observe any changes in the bonding strength between ZnO quantum dots (QDs) and the carbon nanotube (CNT) surface. This research aims to understand the interaction between functionalized MWCNTs and nylon-12 (PA) microspheres in an epoxy matrix. With this knowledge, ternary systems may be intelligently developed with the intent of improving the mechanical and electrical performance of a matrix of interest. ZnO QDs, MWCNTs, and PA are selected as model fillers due to the available dispersion methods, commercial relevancy, cost, and geometry. Epoxy is chosen due to its widespread use in the aerospace and automotive industry.

The objectives of this proposed work are to: 1) utilize a newly developed in-situ functionalization process and characterize the morphology and dispersion of ZnO/P-MWCNTs and ZnO/O-MWCNTs in an organic solvent or epoxy matrix, 2) investigate the thermal, electrical, and mechanical properties of the nanocomposites as a function of surface functionalization and use of PA, and 3) investigate the fracture properties and fracture mechanisms of the nanocomposites as a function of surface

functionalization and use of PA. The morphology and exfoliation state of the nanofillers will be observed with optical and electron microscopy, UV-Vis-NIR, and XRD. XPS will be used to monitor the functionalization chemistry. Thermal characterization of hybrid epoxy nanocomposites will be conducted via DSC and TGA. The mechanical response and properties will be investigated with DMA and tensile testing. Ternary systems will be fabricated and subjected to fracture tests to determine the effect of PA toughening on ZnO/P-MWCNT and ZnO/O-MWCNT epoxy nanocomposite systems.

Three different particles have been chosen for the proposed work based on availability and cost, solubility in organic solvents, ability to exfoliate MWCNTs in epoxy, and potential commercial application. ZnO QDs can be synthesized in organic solvents with a controlled diameter of ≈5 nm and dispersed in epoxy [62, 75-80]; MWCNTs with outer diameters of ≈10 nm can be dispersed in epoxy with organic solvents and functionalized using previously developed method [62, 81]; PA microparticles with a diameter of ≈10 μm have been observed to improve the fracture toughness of epoxy nanocomposites [29, 73, 74, 82]. The fillers will be mixed into an aerospace grade epoxy resin, D.E.R.™ 354, with low viscosity and broad commercial use in adhesives, composites, and coatings.

The first specific objective will be to characterize the morphology and dispersion of ZnO/P-MWCNTs and ZnO/O-MWCNTs in an organic solvent or epoxy matrix. The primary variables are surface functionalization, level of oxidation, and dispersion medium. The morphologies will be characterized via UV-Vis-NIR, x-ray diffraction (XRD), x-ray photoelectron spectroscopy (XPS) transmission optical microscopy (TOM), and transmission electron microscopy (TEM).

The second specific objective will be to investigate the thermal stability, electrical conductivity, and tensile properties of epoxy nanocomposite thin films containing ZnO/P-MWCNTs or ZnO/O-MWCNTs. The primary variables are surface functionalization, level of oxidation, and use of PA. Differential scanning calorimetry (DSC), dynamic mechanical analysis (DMA), and thermogravimetric analysis (TGA) will be used to measure the thermal stability of the thin films. A custom built four-point probe will be used to measure their electrical conductivity. The tensile response of the hybrid thin films will be monitored with a universal testing machine equipped with a laser extensometer.

The third specific objective will be to investigate the fracture toughness and fracture mechanisms of epoxy nanocomposite thin films containing ZnO/P-MWCNTs or ZnO/O-MWCNTs with or without PA. The primary variables are surface functionalization, level of oxidation, and use of PA. The fracture toughness of the epoxy nanocomposite films will be measured by using a three-point bending fixture on a universal testing machine equipped with a laser extensometer. Fracture toughening mechanisms will be observed with a laser confocal microscope (LCM) and TEM.

The approach of the proposed work is to mix surface-decorated MWCNTs and PA to transfer their beneficial mechanical, electrical, and toughening properties to an epoxy matrix. PA particles were selected for this work because of their commercial availability in narrow size distributions, low moisture uptake, and strong interfacial bonding with epoxy. Thermoplastic toughening particles such as PA have been studied in response to the poor thermomechanical performance of rubber-toughened epoxies and were observed

to effectively toughen without compromising the T_g or strength of the matrix [29, 64, 65, 73, 74, 83-87].

1.3 Organization of the dissertation

A comprehensive literature review on the recent advances in surface functionalization of CNTs, epoxy nanocomposites containing CNTs, and toughening of epoxy will be presented in Chapter II. Detailed information regarding the different types of surface functionalization methods is described in this chapter. A brief review of the current and potential applications of functionalized CNTs and toughening particles in epoxies is also provided.

Based on Chapter II, Chapters III-VI develop a new non-covalent functionalization method for CNTs, based on physical adsorption via electrostatic interactions. Due to their opposite surface charges, CNTs exhibit a negative charge, while ZnO QDs exhibit a positive charge, ZnO QDs are selectively anchored to the CNT surface via an electrostatic interaction. This physical functionalization method overcomes the traditional challenges associated with preparing well-integrated ZnO/CNT composites. After functionalization, the ZnO/CNTs are dispersed into epoxy with and without PA microparticles for improved mechanical properties, toughness, and electrical conductivity.

Finally, a summary of the findings of this dissertation and concluding remarks are given in Chapter VII along with the future research plans.

CHAPTER II

LITERATURE REVIEW

2.1 Introduction

Polymeric materials, and specifically epoxies, are widely used in various industries such as automotive, commodity, sports, medicine, aerospace, etc., but recent research has been driven by the desire to incorporate nano and micro fillers into polymer matrices for improved performance. This is due to their outstanding potential to enhance the mechanical, electrical, thermal, and fracture behavior of neat matrices. However, as higher concentrations of fillers are used to drive the improved behavior, cost and processibility are usually negatively affected.

In this chapter, the fundamental knowledge, problems, and recent advances concerning epoxy nanocomposites with improved mechanical, electrical, and fracture performance will be reviewed. The morphological and structural characterization of epoxy nanocomposites will also be reviewed.

2.2 MWCNT functionalization

Sumio Iijima is traditionally attributed as having been the first researcher to discover CNTs in 1991 [88]. SWCNTs are one dimensional materials that can be conceptualized as a sheet of graphene consisting of sp^2 hybridized C-C bonds that is wrapped up with a particular chiral vector [56, 57, 89, 90]. A pair of indices can be defined for the joined ends of a graphene sheets as (n,m). The indices n and m indicate the number of unit vectors along the graphene lattice and are used to define whether a CNT is zigzag

(m=0), armchair (n=m), or chiral [56, 57, 90]. Owing to the three different tube types, three different conductive natures are observed in CNTs. CNTs are considered metallic conductors when n=m, semiconductive with a slight band gap when n-m is a multiple of 3, and a moderately semiconductive when the other two cases are not satisfied [56, 57, 90].

MWCNTs, while geometrically similar to SWCNTs, they consist of multiple (concentric) cylinders of graphene. The typical intertube spacing is around 3.4 Å, which coincidentally is close to the interlayer spacing in graphite [90]. Even though MWCNTs can be thought of as concentric metallic or semiconducting SWCNTs, they usually behave as zero-gap metals [88]. The sp^2 C-C lattice and tunable physical properties (chirality, surface functionalization, diameter, and length) afford CNTs a wide range of electrical properties that are attractive for polymer matrices [7, 11-13, 23, 26, 29-31, 34, 40, 56-58, 61, 91-108].

MWCNTs, due to their diverse set of exceptional properties, have been extensively studied since their initial discovery [2-39]. Depending on the application, it may or may not be advantageous to disperse individually exfoliated CNTs into a polymer matrix of interest rather than an assembly of aggregated entanglement [109]. However, the numerous synthesis procedures tend to yield bundles and entanglements that are composed of hundreds or thousands of single CNTs due to the large vdW forces typically of high aspect ratio MWCNTs. Furthermore, because CNTs are insoluble in organic solvents, integrating them into a polymer matrix via solution is a challenge. These problems are the reason why the majority of research is not as fruitful as expected, since the amount of

usable material tends to be very low, if at all. For example, CNTs have been dispersed in polymers with the intent of improving their mechanical properties. However, without functionalizing the tube sidewall, the polymer matrix is unable to effectively bond to the atomically smooth surface, leading to inefficient load transfer from the matrix to the CNT [110]. Furthermore, depending on the functionalization route, the inherently strong and conductive sp^2 hybridized C-C lattice is irreparably damaged, rendering the CNTs insulative and more prone to premature fracture [44, 60, 62, 109, 111-122].

To overcome the processing and solubility challenges associated with MWCNTs, many novel approaches have been developed in recent years to functionalize the CNT surface to promote better adhesion with the matrix, stable and individual exfoliation, and alter their surface properties for various applications as seen in Table 1 [9, 15, 18, 26, 33, 44, 59, 60, 62, 114, 123-129].

Table 1. Pros and cons of commonly used CNT functionalization methods [60].

Method		Principle	CNT Damage	Easy to use	Particle-matrix interaction[a]	Re-agglomeration of CNTs in matrix
Chemical	Sidewall	sp2 → sp3 hybridization of C	✓	✗	S	✓
	Defect	Defect transformation	✓	✓	S	✓
Physical	Polymer wrapping	vdW force, π-π stacking	✗	✓	V	✗
	Surfactant adsorption	Physical adsorption	✗	✓	W	✗
	Endohedral method	Capillary effect	✗	✗	W	✓

[a]S: Strong; W: Weak; V: Variable according to miscibility between matrix and polymer on CNT.

In the subsequent sections, two different surface functionalization approaches will be presented and summarized. The methods that will be described are: 1) covalent functionalization and 2) physical functionalization.

2.2.1 Covalent functionalization

The first approach to functionalizing the surface of CNTs is covalent functionalization. This results in a chemical change of the original C-C lattice of the tube surface to something that now includes other functional groups that are connected via chemical bonds. Two unambiguous regions of reactivity are available for chemical functionalization: graphitic structure and defect sites as seen in Figure 1 [4, 18, 34, 44, 60, 62, 89, 109, 111, 113-116, 121, 123-126, 129-137].

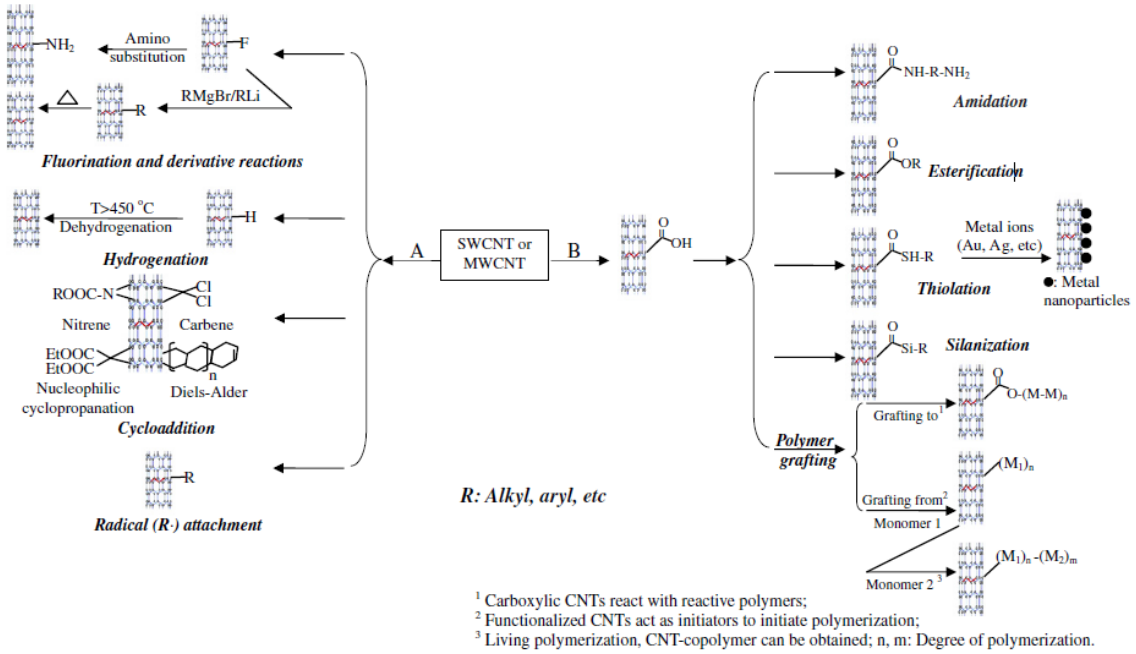

Figure 1. Various routes to covalently functionalize CNTs (A: sidewall functionalization; B: defect functionalization). Reprinted from [60].

In MWCNTs, the caps of the tubes are composed of five-membered rings that results in a relatively high reactivity compared to the sidewalls, which are composed of π-π bonded structures. Once functionalized, the CNT surface is irreparably changed, without further modification(s).

2.2.1.1 Graphitic structure

MWCNTs are made up of sp^2 hybridized C atoms that arrange themselves into a hexagonal honeycomb lattice. Chemical changes to the C-C double bonds of the lattice result in a change from sp^2 to sp^3 hybridized C, causing them to change from trigonal to

tetrahedronal geometry. This type of chemical alteration damages the CNT surface leading to reduced electrical and mechanical properties [18, 44, 60, 62, 109, 111, 113, 115, 116, 121, 124, 126].

Fluorination and derivative reactions, hydrogenation, and cycloaddition are three different strategies for sidewall functionalization that cause amino, nitrene, carbene, and radical groups to be directly functionalized to the CNT surface [59, 60]. One example of a fluorination and derivative reaction is the fluorination of CNTs followed by amino substitution as studied by Stevens and Gu et al. [138, 139]. Purified HiPco SWCNTs (amorphous carbon and catalyst Fe particles were removed) were directly fluorinated with C_2F moieties at 150 °C in a He-purged furnace whereby a gaseous mixture of He-diluted F_2 flowed over the CNTs at a specified flow rate for ≈2 hr [138]. The fluorinated SWCNTs (F-SWNCTs) were then pyrolyzed in Ar_2 at 1000 °C and monitored in situ via fourier transform infrared spectroscopy (FTIR). Raman and attenuated total reflection FTIR (ATR-FTIR) spectroscopy were used to characterize the formation and removal of C-F bonds on the sidewalls of SWCNTs. The Raman spectrum of the F-SWCNTs exhibits an increased intensity of the disorder mode (≈1292 cm^{-1}), which indicates that there has been a significant increase in sp^3 hybridized C (Figure 2).

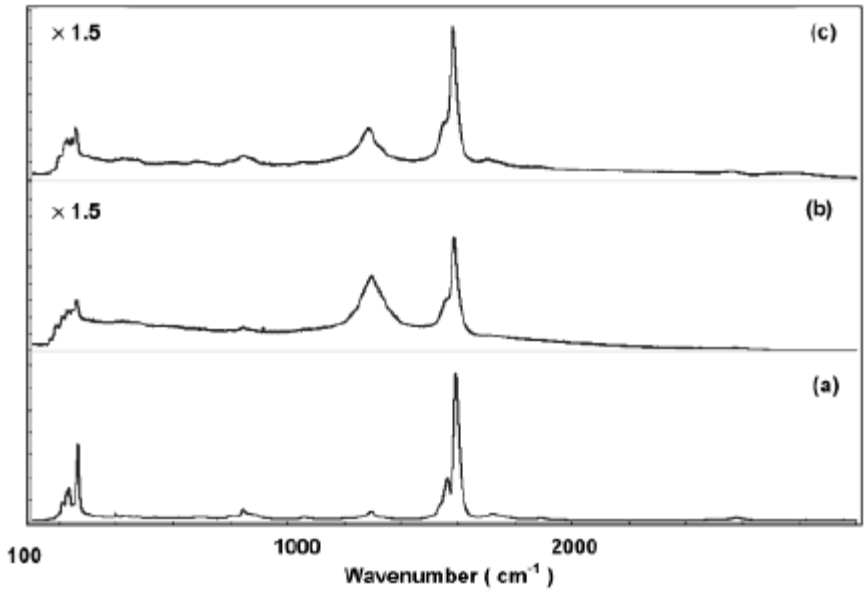

Figure 2. Raman spectra of SWCNTs. (a) Purified HiPco SWCNTs; (b) F-SWCNTs; (c) cut-SWCNTs. Reprinted from [138].

This observation supports the IR spectra that exhibits the formation of C-F bonds after fluorination at ≈1111 cm^{-1} and ≈1221 cm^{-1} (Figure 3).

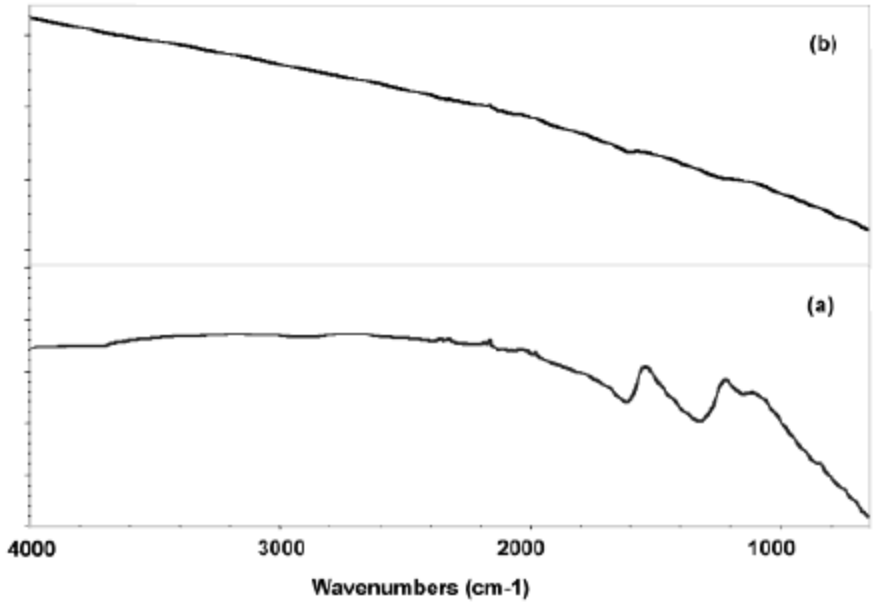

Figure 3. ATR-FTIR spectra of SWCNTs. (a) F-SWCNTs; (b) cut-SWCNTs. Reprinted from [138].

After fluorination, the F-SWCNTs were heated with terminal alkylidene diamines (ethylene, propylene, butylene, and hexamethylenediamine) in solution by stirring the precursors at 70-170 °C in the presence of pyridine (Py), which was used as a catalyst [139]. During this process, HF was eliminated, which led to the formation of amino-functionalized SWCNTs (Figure 4).

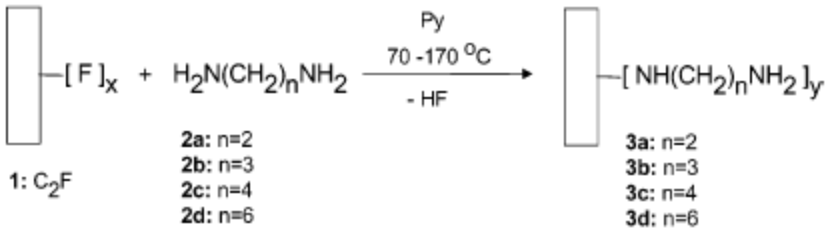

Figure 4. Schematic of functionalization chemistry for fluorination and amine substitution reactions. Reprinted from [139].

Raman, FTIR, and UV-Vis-NIR spectroscopy were used to confirm that fluorination and subsequent amino-substitution had taken place, in that order. The typical peaks observed for HiPco SWCNTs via Raman were identified as breathing (200-263 cm^{-1}) and tangential (1591 cm^{-1}) mode peaks. For F-SWCNTs, the HiPco peaks associated with breathing and tangential modes decreased and increased, respectively, due to the overwhelming presence of sp^3-hybridized C in C_2F (Figure 5).

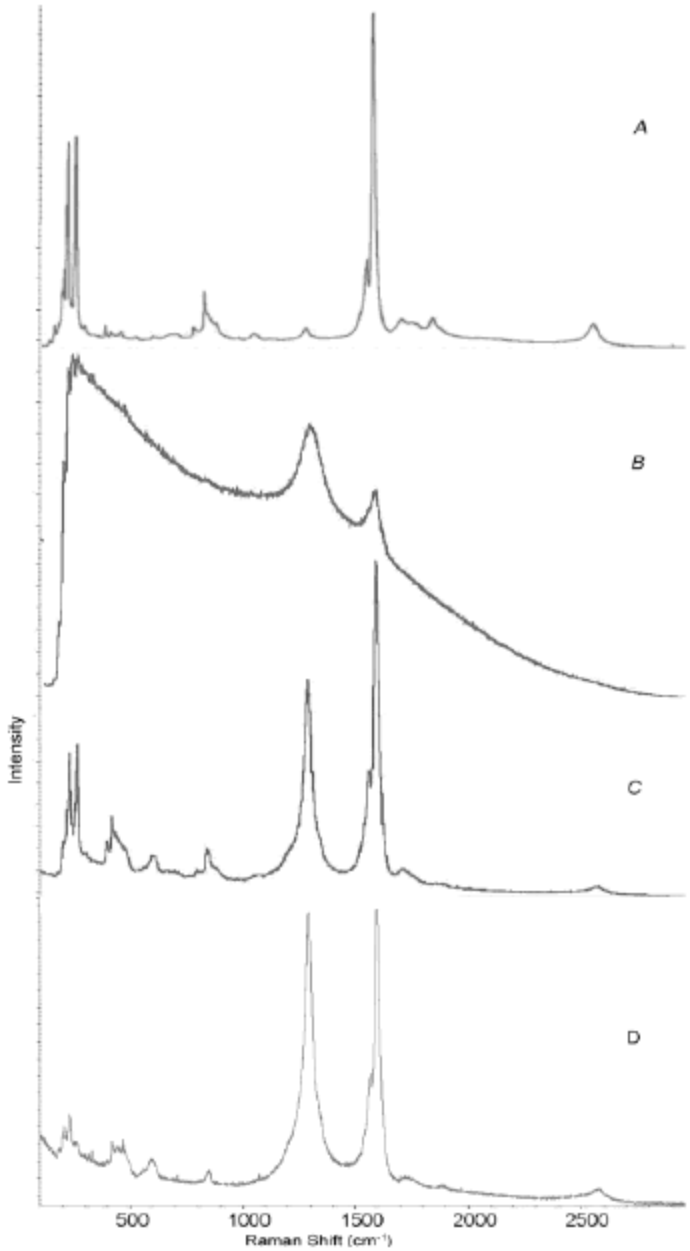

Figure 5. Raman spectra of (A) F-SWCNTs; (B) N-alkylidene amino-functionalized SWCNTs 3a; (C) nylon-SWCNT polymer derivative; (D) reaction product of 3a with adipyl chloride. Reprinted from [139].

The van Hove absorption bands typically observed for purified HiPco SWCNTs via UV-Vis-NIR disappeared when amino groups were substituted for the fluorinated C bonds (Figure 6).

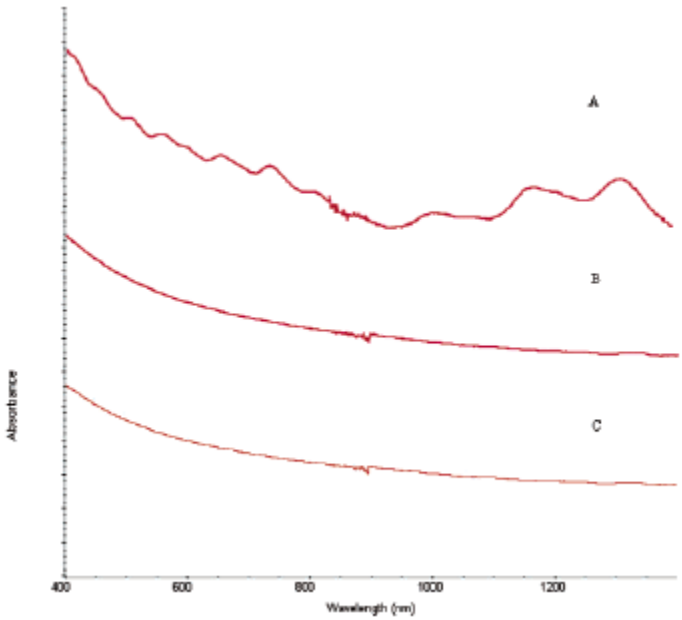

Figure 6. UV-Vis-NIR spectra of (A) Purified HiPco SWCNTs; (B) N-alkylidene amino-functionalized SWCNTs 3a; (C) 3d. Reprinted from [139].

In the ATR-FTIR spectra, two peaks at 1214 cm^{-1} and 1102 cm^{-1} were observed for the F-SWCNTs, which are characteristic of the C-F bond stretching mode (Figure 7).

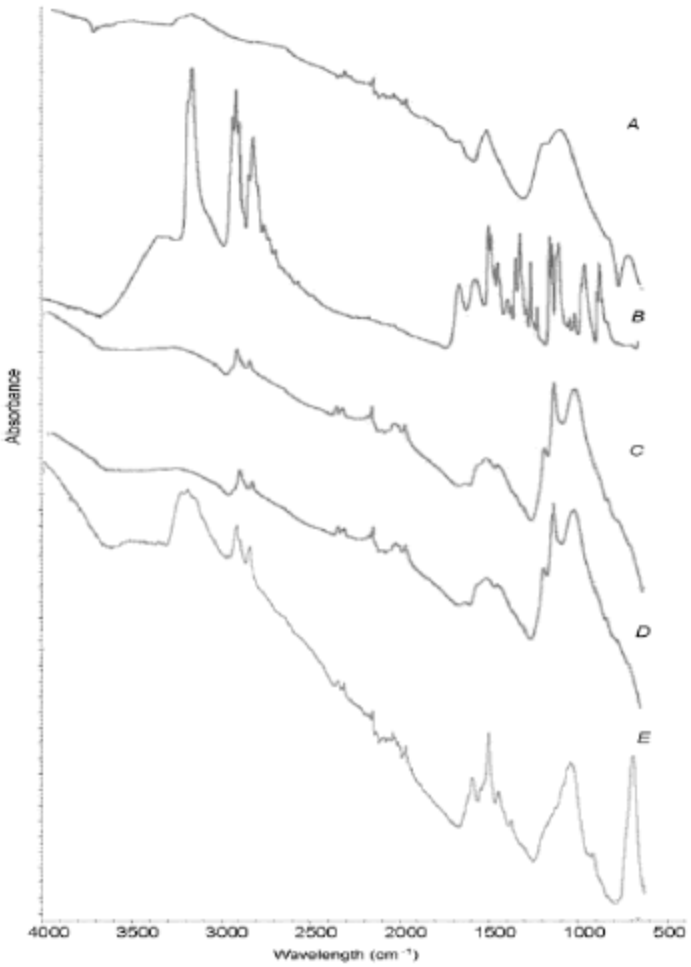

Figure 7. ATR-FTIR spectra of (A) F-SWCNTs; (B) N-alkylidene amino-functionalized SWCNTs 3a; (C) 3b; (D) 3c; (E) 3d. Reprinted from [139].

After amino groups are substituted, those peaks disappear and a number of new peaks are observed at 3400-3100 cm^{-1}, 3000-2800 cm^{-1}, and 1250-1000 cm^{-1}, which are attributed to N-H, C-H, C-N stretching, respectively, indicated that N-Alkylidene amino groups have been successfully attached to the sidewalls of SWCNTs.

With this type of functionalization, the surfaces of atomically smooth and chemically inert CNTs may be made more compatible with epoxies, and may be able to

participate in the crosslinking reaction, due to the reactive amine (NH_2) groups, resulting in CNTs that are chemically linked to the epoxy network.

2.2.1.2 Defect site

The presence of defects, usually in the form of oxygen moieties, are used for functionalization to minimize the damage that the sidewalls experience. It is generally understood that CNTs, while composed mostly of C, still have trace catalytic elements after they are synthesized. The observed defects can be grouped into four different classes: dopants, rehybridization ($sp^2 \rightleftharpoons sp^3$), topological defects (rings of smaller or larger size than hexagons), and incomplete bonding (vacancies or dislocations) [140]. At the caps of MWCNTs, fullerene-like structures with five- or seven-member rings with higher reactivity than 6-member rings may be observed. These more highly reactive tube ends are an attractive starting point to develop new covalent chemistries. Unfortunately, research efforts into developing covalent functionalization approaches using defect sites are sparse.

Oxygen functional groups are another defect type that is commonly used for functionalization. Every production methodology yields CNTs with impurities such as amorphous C (carbon black) and residual catalyst particles. Therefore, purification processes such as oxidation via acid treatment are used to remove said impurities from the raw material [120]. The oxidation step opens the tube caps and causes holes to appear due to the formation of oxygen functional groups on the surface [59, 60, 111, 116-122]. The produced CNTs are observed to have tube ends and sidewalls that are decorated with mainly carbonyl and carboxylic groups. These chemical groups have been well-studied

and used for functionalization in recent years, specifically through amidation reactions with amine groups [73, 123, 124]. For example, Sun et al. developed a functionalization technique to covalently bond polyamidoamine generation-0 (PAMAM-0) dendrimers and sulfanilamide (SAA) to the surface of oxidized SWCNTs (Figure 8) [124].

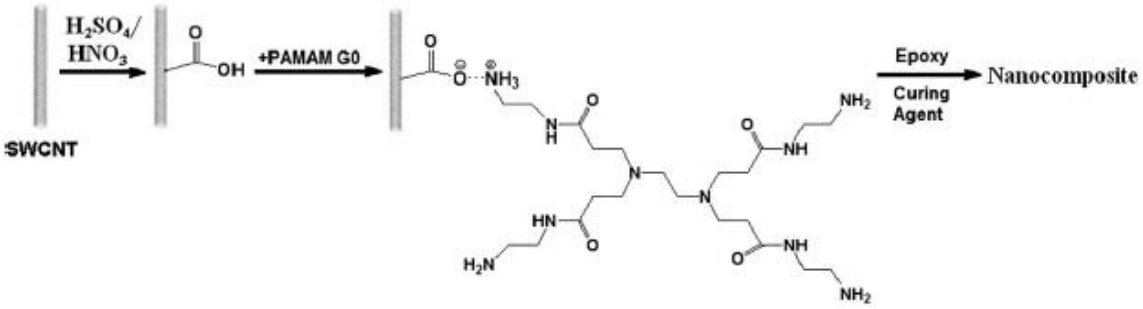

Figure 8. Schematic of surface functionalization of SWCNTs by PAMAM-0. The PAMAM-0 molecules contain extra amine groups that participate in crosslinking reaction with epoxy monomer. Reprinted from [124].

PAMAM-0 was observed to effectively exfoliate the SWCNTs and improve their adhesion to the epoxy matrix. This led to enhanced modulus, tensile strength, and ductility as well as improved fracture toughness. The rubbery plateau modulus of the epoxy composite with PAMAM-0-functionalized SWCNTs also increased, while its T_g dropped ≈5 °C. This is likely due to the stoichiometric ratio of the amines to epoxide groups in the composite system being off. Sulfanilamide (SAA) was also used by Sun et al. to functionalize the surface of previously oxidized SWCNTs [73]. SAA-functionalized SWCNTs also exhibited an improved level of exfoliation in epoxy as well as enhanced modulus, tensile

strength, ductility, and fracture toughness. However, the T_gs of the nanocomposite systems containing oxidized or SAA-functionalized SWCNTs decreased compared to the neat epoxy system as seen in Figure 9.

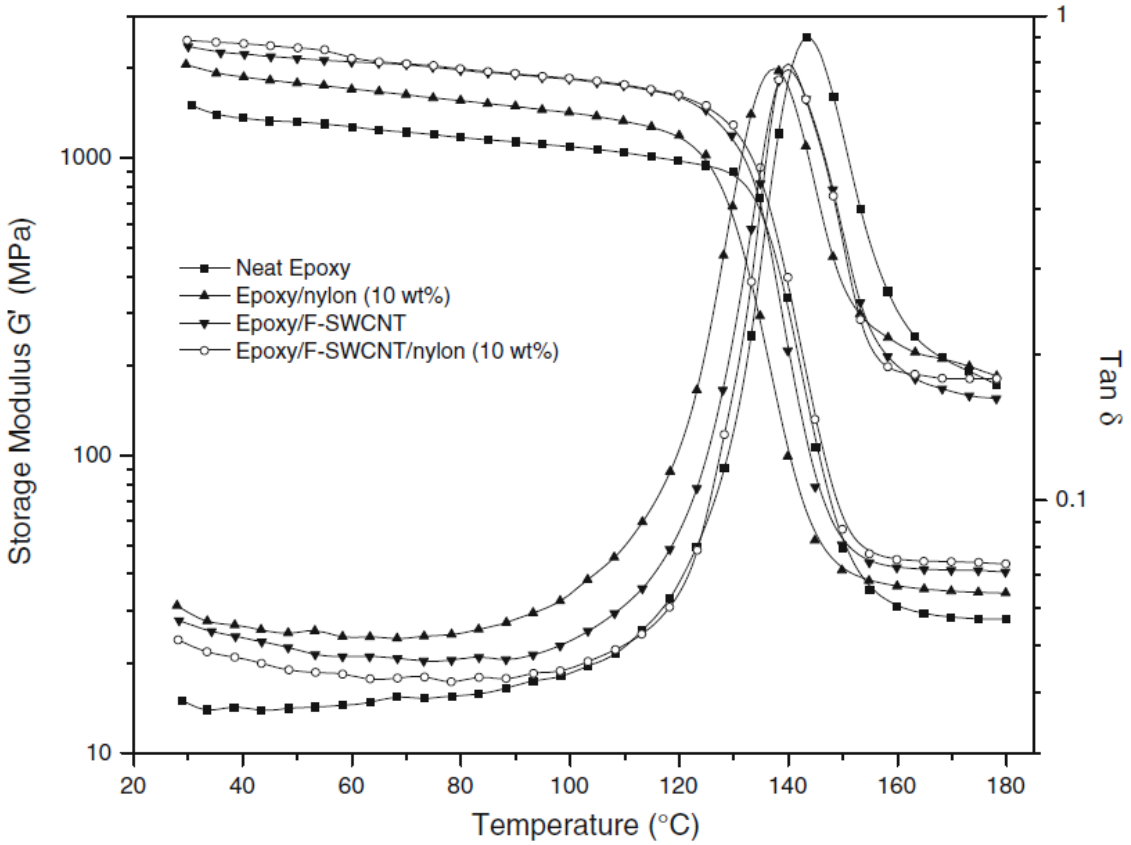

Figure 9. DMA spectra of epoxy composites containing 0.5 wt. % SWCNTs. Reprinted from [73].

The aforementioned defects are an attractive area to develop new covalent functionalization approaches while preventing further damage to the CNT chemical structure.

2.2.2 Physical functionalization

The second approach for functionalizing CNTs is physical, or noncovalent, functionalization. In this respect, the tube sidewalls are modified via vdW forces, π-π interactions, adsorption of nanoparticles, aromatic compounds, surfactants, polymers, and even short chain oligomers, or electrostatic interactions as seen in Figure 10 [59, 60].

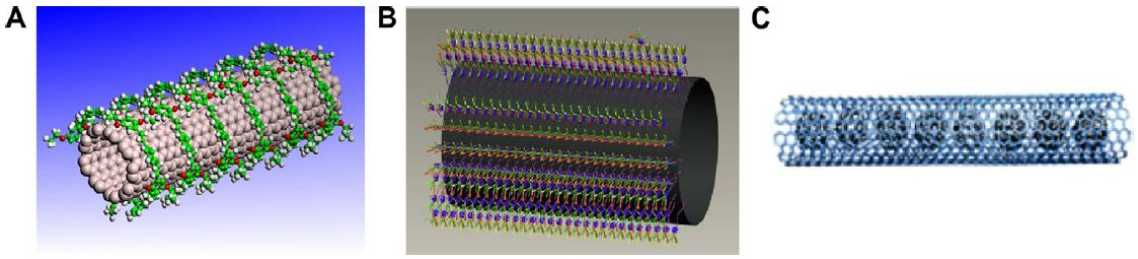

Figure 10. Various routes to physically functionalize CNTs (A: polymer wrapping; B: surfactant adsorption; C: endohedral method) . Reprinted from [60].

In stark contrast to chemical functionalization methods, the physical methods of functionalizing MWCNTs are easy, reversible, and have a much lower probability of permanently destroying the original C-C bonds in the CNT lattice resulting in functionalized MWCNTs that retain their exceptional mechanical and thermal properties.

Surfactants, polymers, and short chain oligomers have been successfully used to physically functionalize CNTs (Figure 11) [59, 60, 62].

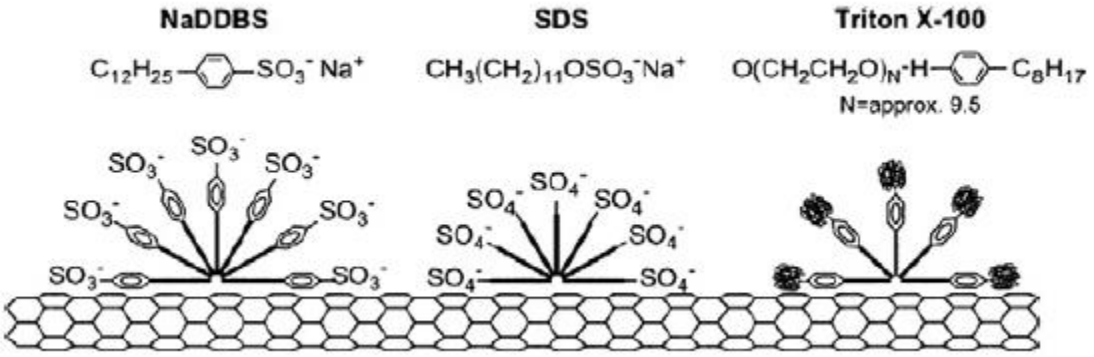

Figure 11. Schematic of surfactant adsorption on CNT surface. Reprinted from [59].

Ionic surfactants such as cetyltrimethylammonium bromide (CTAB), and sodium dodecyl sulfate (SDS) are able to stabilize a dispersion of CNTs by promoting electrostatic repulsion between formed micellar domains [59]. Triton X, a nonionic surfactant, has been observed to influence the dispersion of CNTs by forming a solvation shell from the hydrophilic groups, which assemble around the CNTs due to a thermodynamic driving force whereby the hydrophobic interface is eliminated [59]. The wrapping of the CNT surface with polymers is another attractive route to functionalize the CNT surface by taking advantage of π-π interactions, specifically by polymers that are soluble in organic solvent or aqueous solutions.

The attachment of metallic particles to the surface of MWCNTs has also been studied for the past couple of decades as another physical solution to functionalizing CNTs without destroying their structure [62, 130, 133, 134, 136, 141-172]. Unfortunately, even though MWCNTs contain significant surface and structural defects, they are still minimally reactive. Therefore, decoration by metallic quantum dots (QDs) is unlikely

without oxidation to improve their chemical reactivity [111, 112, 117, 118, 120, 133, 141]. It has been suggested in previous reports that when MWCNTs are oxidized prior to metallic QD decoration, the final morphology is more uniform compared to a pristine tube that has been decorated. Furthermore, they may be used for catalytic applications as well as providing improved interfacial bonding in a given matrix to obtain the maximum possible improvement in mechanical properties [141]. Many experimental efforts have since been pursued with some limited success [151-153, 155, 158, 168]. For example, Satishmukar et al. oxidized CNT surfaces and decorated them with gold, platinum, or silver by using a reducing agent to reduce a metal compound [142]. Li et al. functionalized the surface of CNTs with aminopyrene, which acted as a catalyst for Pt, CdS, silica growth [149]. Daneshvar-Fatah et al. developed a non-covalent functionalization method to disentangle MWCNTs by electrodepositing Ni on their surfaces and observed improved dispersion. An anti-corrosive coating containing Ni-MWCNTs exhibited increased hardness and elastic modulus [170, 172]. Xin et al. integrated Ag-decorated CNTs into PP and PS via melt compounding and solution mixing and observed a large improvement in electrical conductivity above the percolation threshold [168]. The tensile modulus and tensile strength of the polymer composites were only marginally improved compared to the systems with only CNTs. In almost all cases, the individual exfoliation of functionalized MWCNTs was not realized and as a result, the mechanical properties were either unaffected or reduced, if studied at all. In contrast, however, the presence of decorated CNTs promotes the formation of an electrically conductive network that may exhibit higher conductivities than previously reported for CNT/epoxy composites [158].

2.2.3 Summary

As stated in the previous two sections, MWCNTs may be functionalized with various molecular groups, molecules, short chains, etc. to form a multitude of MWCNT hybrids for a wide breadth of applications such as: capacitors, transistors, sensors for health and structural monitoring, functional and multifunctional composites, etc. [7, 13, 43, 45, 47, 48, 50, 54, 56-58, 60, 93, 95, 101, 109, 173-177]. However, with each approach there are advantages and disadvantages that make one or more of them a more likely candidate for effectively functionalizing CNTs and introducing them into a solvent/matrix of interest.

2.3 MWCNT/epoxy composites

Epoxies are a class of thermosetting polymers that are commonly used in the aerospace, automotive, electronics, and adhesives/sealants industries [29, 39, 54, 66, 74, 178-190]. They are mechanically strong and stiff, electrically and thermally insulative, and resistant to corrosion, solvents, and chemicals due to their crosslinked network structure [29, 54]. Unfortunately, for aerospace and electronics applications, the insulative nature of the matrix and its tendency to fracture in a brittle and catastrophic manner, with insignificant warning and energy absorption/dissipation make it challenging for epoxy nanocomposites to be fabricated and used within the demanding regimes necessary for the aforementioned industries [29, 39, 74, 105, 191-197]. In order to save on weight, composites are traditionally thought of as the silver bullet, the perfect replacement. However, in practice, the ability of epoxy nanocomposites to perform with the same level of toughness, stiffness, strength, and electrical conductivity has not been observed.

Numerous research efforts have been conducted with the purpose of developing an epoxy with dispersed fillers for improved stiffness, strength, toughness, or electrical conductivity [198]. Unfortunately, true epoxy nanocomposites are rarely reported in the literature, especially when multifunctionality is desired. In order to replace a tough and conductive material such as aluminum, the epoxy nanocomposites need to have one or two fillers dispersed into its matrix to impart better toughening and the formation of a conductive network.

2.3.1 Electrically conductive epoxy composites

Carbon black, CNTs, graphene, and hybrid carbon fillers are typically dispersed into epoxy to enhance its electrical conductivity [11, 12, 19, 29, 31, 38, 99, 105, 158, 199-206]. The expectation for improved electrical conductivity is that if a conductive filler is dispersed into an insulative matrix at a high enough concentration, a percolative network will form, a three-dimensional network that is interconnected in such a way so as to allow for the conduction of electrons through the bulk of a material. In practice, however, this is not an easy task to accomplish given the challenges associated with effectively integrating CNTs into polymer matrices as summarized in the previous section. CNTs are typically used because of their ability to be surface functionalized and their low densities.

For example, graphene and CNTs have been observed to percolate at very low concentrations [10, 96, 98, 100]. Kim et al. studied the effect of oxidized MWCNTs on the electrical conductivity of epoxy nanocomposites [11]. MWCNTs were oxidized in solutions of nitric acid or a mixture of water and ammonium hydroxide under a number of different conditions (Table 2).

Table 2. MWCNT oxidation conditions. Reprinted from [11].

Solution	Conc. [%]	$T_{treatment}$ [°C]	$T_{treatment}$ [hr]	pH
HNO_3	28.5	RT	4	3.5
HNO_3	40.0	100	1	2.5
HNO_3	40.0	100	2	2.5
HNO_3	40.0	100	4	2.5
H_2O_2/NH_4OH	28.5	RT	4	10.5

The O-MWCNTs exhibited increasingly negative zeta potential values as a function of stronger oxidative treatment. The electrical conductivity and percolation thresholds of the epoxy nanocomposites were observed to decrease and increase, respectively, as a function of oxidation strength due to extensive damage to the tube sidewalls. Moisala et al. also studied the electrical conductivity of epoxy nanocomposites containing MWCNTs and observed that a system containing MWCNTs exhibited a percolation threshold at <0.005 wt.% (much lower than expected from theory) with an electrical conductivity of ≈0.5 S/m at 0.6 wt.% MWCNTs [12]. Saw et al. fabricated MWCNT/epoxy nanocomposite thins films with short and long MWCNTs that were optically transparent, flexible, and electrically conductive. However, the system containing short MWCNTs exhibited an earlier percolation threshold and higher conductivity compared to the one with long MWCNTs as seen in Figure 12 [31].

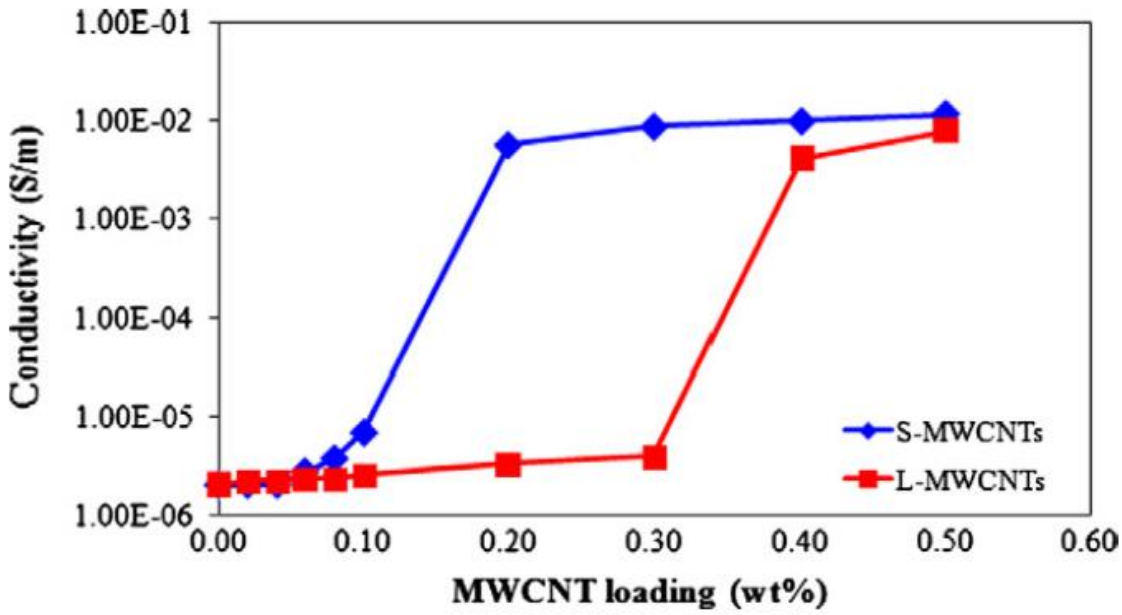

Figure 12. Electrical conductivity of epoxy nanocomposite films as a function of MWCNT concentration. Reprinted from [31].

Tang et al. studied the influence of MWCNTs and either soft submicron-rubber or rigid nano-silica on the electrical conductivity of a conventional epoxy resin [105]. The systems with the best improvement with respect to the neat epoxy matrix were those that contained MWCNTs. In fact, the system that exhibited the highest value of electrical conductivity was that which contained MWCNTs and rigid nano-silica at 1.0 wt.% and 10.0 wt.%, respectively. The reason given is that the nano-silica helps reduce the size of MWCNTs aggregates by breaking them apart to a degree, in contrast to the systems containing rubber. White et al. studied the percolation behavior of MWCNT/epoxy nanocomposites containing preformed nylon microparticles [29]. The percolation threshold of the MWCNT/epoxy system occurred at ≈0.01-0.05 wt,% MWCNTs and a final electrical

conductivity of ≈0.05 S/m was obtained at 1.0 wt.% MWCNTs. However, the system containing both nylon and MWCNTs exhibited a delayed percolation threshold at around 0.7 wt.% MWCNTs and a final electrical conductivity of ≈0.001 S/m at 1.0 wt.% MWCNTs (Figure 13).

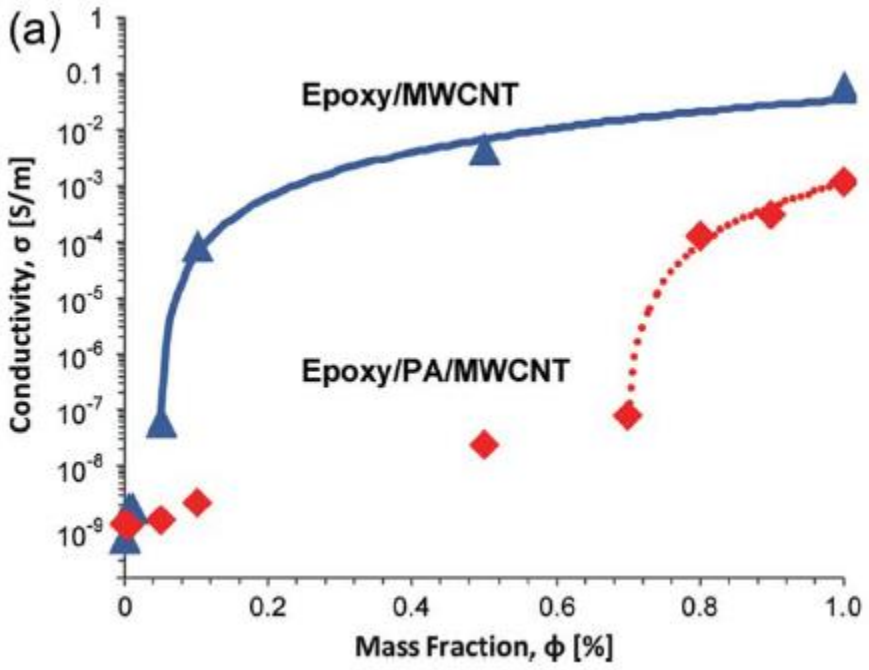

Figure 13. Electrical percolation behavior of MWCNT and nylon filled epoxy. (a) Semi-log plot of electrical conductivity as a function of wt.% MWCNTs. Reprinted from [29].

When P-MWCNTs are dispersed into epoxy, they form aggregates that are randomly oriented and distributed throughout the matrix. This random dispersion of CNTs more effectively promotes the formation of an electrically conductive network, rather than a

well-dispersed system of CNTs as observed in the system containing nylon and P-MWCNTs.

Ma et al. introduced silver-decorated MWCNTs (Ag-MWCNTs) into epoxy to improve its electrical conductivity [158]. This was achieved through ball milling in the presence of ammonium bicarbonate, followed by the reduction of Ag ions in N, N=dimethylformamide (DMF) as seen in Figure 14.

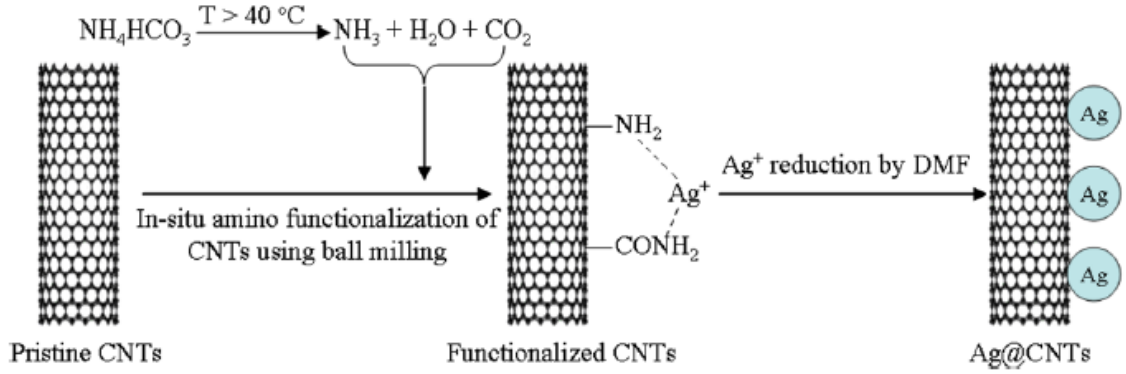

Figure 14. Schematic of Ag decoration of MWCNT sidewall. Reprinted from [158].

The surface of the MWCNTs were observed to be decorated with Ag QDs and the peak around 3 keV in the energy dispersion x-ray (EDX) spectrum confirms that the QDs are indeed Ag (Figure 15).

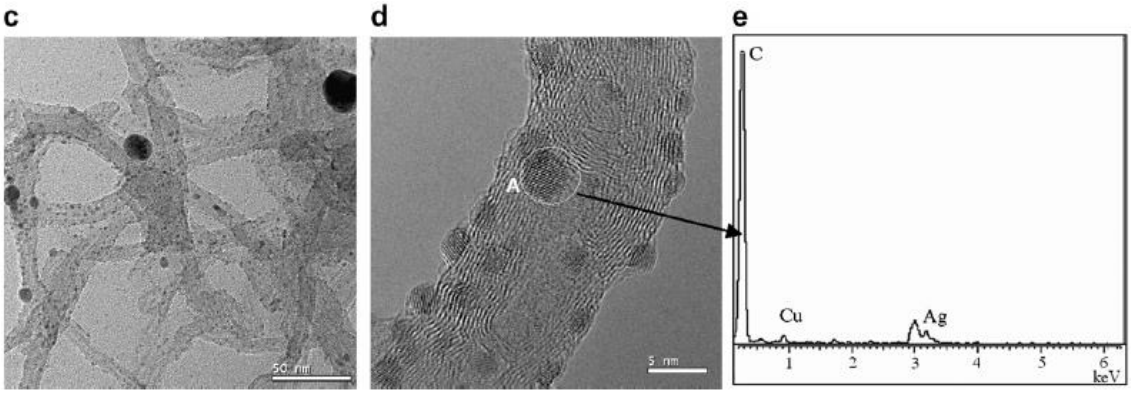

Figure 15. TEM of Ag-decorated MWCNTs with prior functionalization. (c) low resolution; (d) high resolution; (e) EDX spectrum. Reprinted from [158].

The percolation behavior of P-MWCNTs, F-MWCNTs, and Ag-MWCNTs was measured as a function of wt.% MWCNTs. All three systems exhibited a percolation threshold at ≈0.5 wt.% MWCNTs as seen in Figure 16.

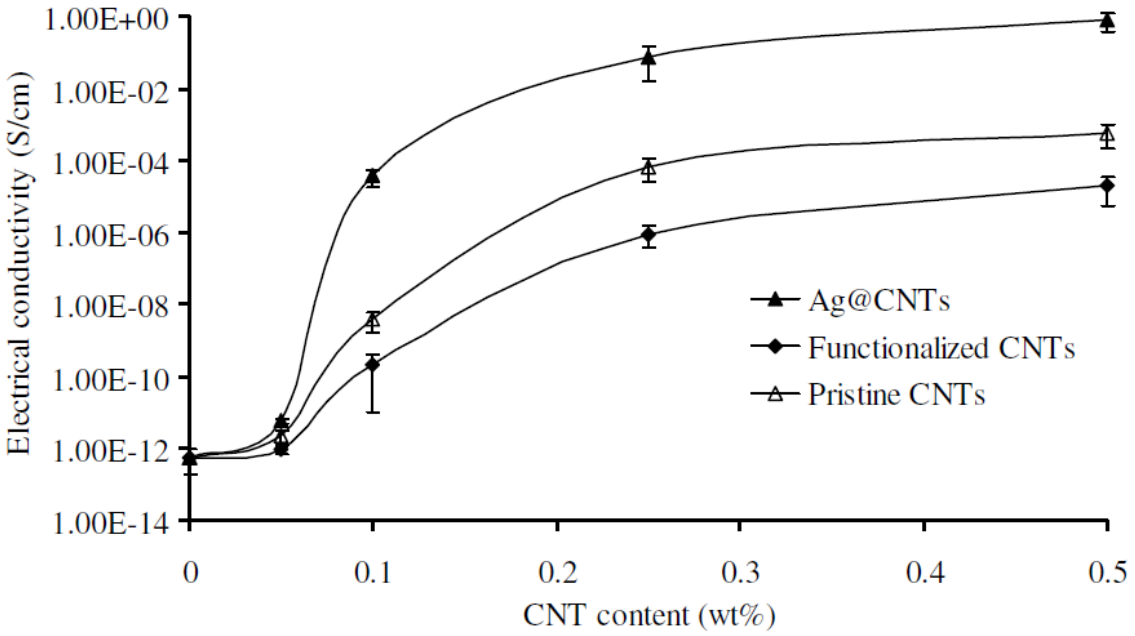

Figure 16. Electrical percolation of epoxy nanocomposites containing P-, F-, and Ag-MWCNTs. Reprinted from [158].

The electrical conductivity of the epoxy nanocomposites containing Ag-MWCNTs was expected to increase due to the inherent electrical conductivity of Ag (σ_{Ag}≈6.30x10^5 S/cm), which is much higher than the conductivity of the MWCNTs used in the study. At 0.5 wt.% Ag-MWCNTs, the epoxy nanocomposite exhibited a dramatic increase in electrical conductivity, approximately twelve orders of magnitude, from 2.2x10^{-13} S/cm to 0.81 S/cm. An increase of that magnitude at that low of a concentration is almost unheard of in the MWCNT/epoxy literature.

2.3.2 Stiff, strong epoxy composites

As previously mentioned, CNTs and graphene are typically dispersed into epoxy to enhance its electrical conductivity. They are also used to enhance the modulus and

tensile strength of epoxies [7, 8, 13, 39, 41, 44, 45, 50, 56-58, 204-234]. In contrast to the previous section, the functionalization of the tube sidewalls, while damaging the surface and potentially reducing the inherent strength and stiffness, is not necessarily detrimental to the efficacy of the tubes to enhance the modulus and strength of epoxy.

Allaoui et al. studied MWCNT/epoxies that were cured with an over-aged hardener to determine if the MWCNTs had a better reinforcing effect compared to a newly synthesized hardener [97]. While the modulus of the composites doubled and quadrupled with the addition of 1 wt.% and 4 wt.% MWCNTs, the absolute values are much less than expected for a highly crosslinked thermoset, such as epoxy (Figure 17).

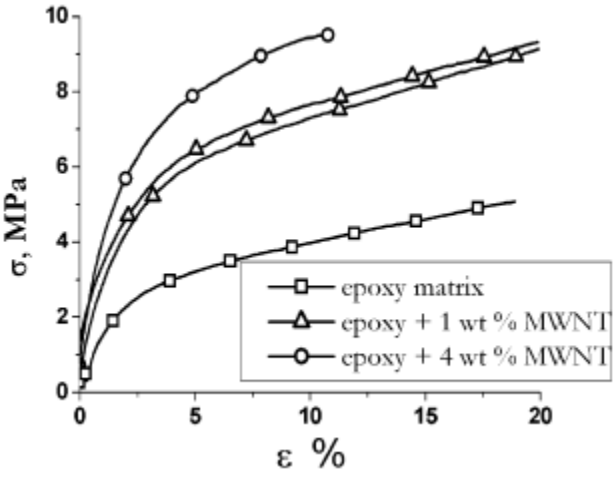

Figure 17. Tensile stress-strain curves of neat matrix and MWCNT composites. Reprinted from [97].

This is due to the fact that the hardener that was used was overaged, yielding a more loosely crosslinked network. In light of this observation, it should be noted that the MWCNTs are able to enhance the Young's modulus of the epoxy, rather significantly.

Hernandez-Perez et al. studied the mechanical properties of an epoxy containing two different types of MWCNTs (1.0 wt.%), which had significantly different aspect ratios [14]. Contrary to what is to be expected, the system with low aspect ratio MWCNTs exhibited a lower modulus than that of the neat matrix while the original tensile strength was more or less maintained. Moreover, the system containing high aspect ratio MWCNTs exhibited an even larger drop in modulus while no change in the tensile strength was observed. However, the reason behind these drops is not explained and the dispersion of the MWCNTs in these systems is not presented well. In both systems, the ductility was improved compared to the neat matrix.

Sun et al. studied the effect that surface functionalization has on the mechanical properties of SWCNT/epoxy composites [124]. PAMAM-0 was used to surface functionalize the SWCNTs before integrating them into an epoxy matrix. Four systems were studied: neat epoxy, P-SWCNT/epoxy, F-SWCNT/epoxy, and PAMAM-0/epoxy, to better understand the effectiveness of each filler. Uniaxial tension tests and DMA were conducted to determine if the MWCNTs had improved the tensile behavior and T_g, respectively (Figure 18 and Figure 19).

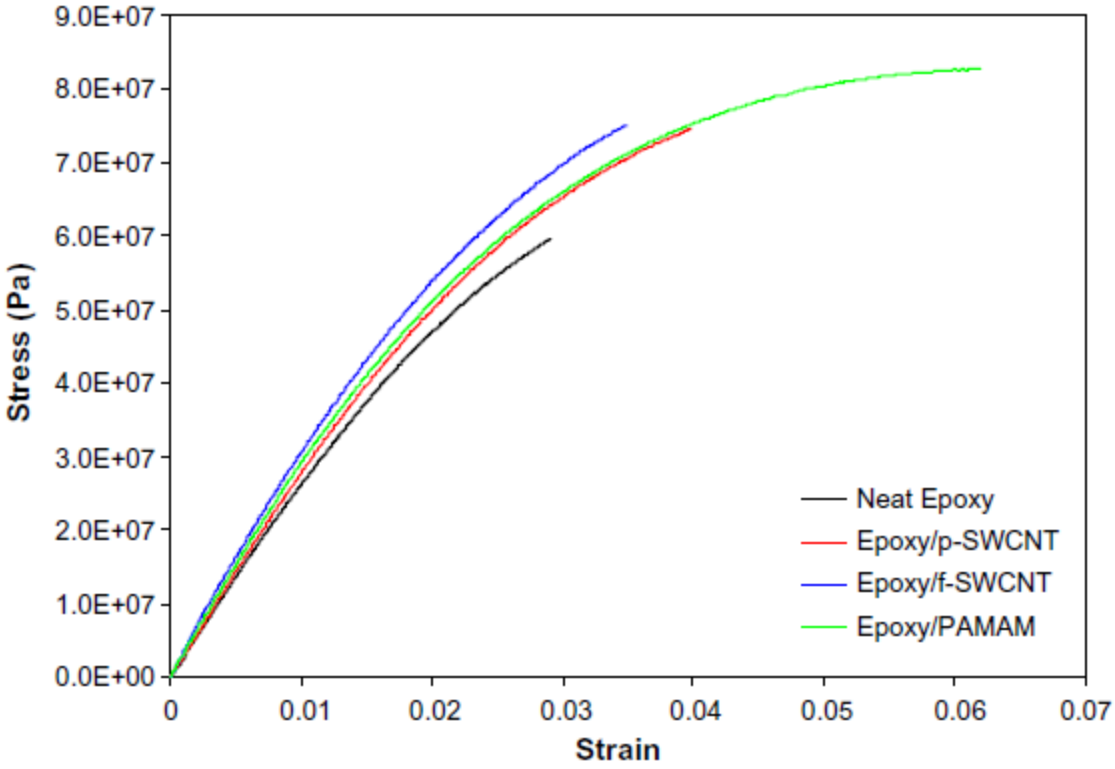

Figure 18. Tensile stress-strain curves for neat epoxy and SWCNT composites. Reprinted from [124].

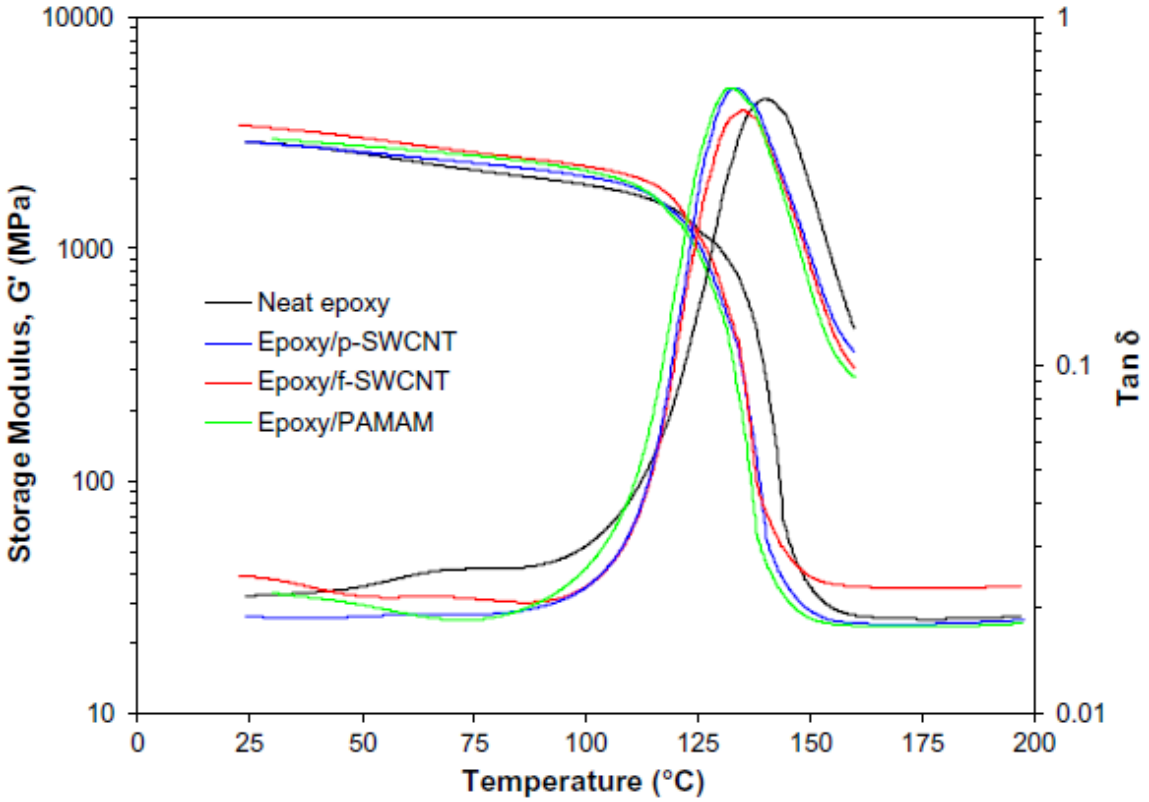

Figure 19. Dynamic mechanical behavior of neat epoxy and SWCNT composites. Reprinted from [124].

Surprisingly, not only did the composites exhibit improved moduli, but also enhanced tensile strength compared to the neat resin. Although the functionalization of SWCNTs leads to improve mechanical properties in this system, the level of enhancement is still only about half of the value that is predicted via Halpin-Tsai. It is stated that this is likely due to the observed curvature of the SWCNTs. The non-uniform dispersion of the SWCNTs and the potential side reaction between the epoxy and PAMAM-0 may also contribute to the subpar improvement. Furthermore, the T_g of the composites containing P-SWCNTs, and F-SWCNTs drops by ≤5 °C, which is not insignificant, and may be due

to partial adsorption of the curing agent onto the P-SWCNT surface leading to a change in the stoichiometric ratio. In the case of F-SWCNT, the presence of excess amines may be the reason for the observed drop in T_g.

P-MWCNTs and O-MWCNTs were dispersed into an epoxy matrix via ultrasonication by Montazeri et al. to investigate their effect on the mechanical properties of the resin [22]. The modulus and tensile strength of the composites was observed to increase as a function of centration, with the P-MWCNTs exhibiting the highest modulus while O-MWCNTs exhibited the highest tensile strength (Table 3).

Table 3. Tensile properties of MWCNT/epoxy composites. Reprinted from [22].

Property	MWCNT	0.0 wt.%	0.1 wt.%	0.5 wt.%	1.0 wt.%	1.5 wt.%	2.0 wt.%	3.0 wt.%
E [MPa]	Pristine	3430	3458	3705	3951	4138	4225	4365
	Oxidized		3465	3680	3860	4050	4100	4200
σ_{TS} [MPa]	Pristine	64	67	69	71	74	75	71
	Oxidized		67	71	74	77.5	78.5	71
ε_B [%]	Pristine	6.1	5	4.45	4.2	3.96	4.26	4.1
	Oxidized		5.2	5.5	5.15	5.8	7.52	6

The improved modulus is suggested to be due to the trapping of polymer in the voids within MWCNT aggregates, which reduces the effective volume fraction of the matrix. The improved tensile strength is suggested to be due to the shortening of O-MWCNTs due

to acid-treatment. Ayatollahi et al. observed a similar trend for MWCNT/epoxies containing up to 1.0 wt.% MWCNTs [24].

Sun et al. developed a simple functionalization method to disentangle and debundle O-MWCNTs via electrostatic tethering of positively charged inorganic nanoclay [81]. The method entails oxidizing the surface of MWCNTs in acid to induce a negative surface charge and exfoliating α-zirconium phosphate (α-ZrP) nanoplatelets in aqueous solution with a basic molecule to exfoliate them and induce a positive surface charge. The two solutions are subsequently mixed and sonicated the debundle the O-MWCNTs. The solution of well-exfoliated MWCNTs is then transferred into organic solvent, mixed with epoxy and a specific hardener and degassed, and finally cured. The composites exhibit significantly enhanced modulus and tensile strength at a very low loading of MWCNTs (Figure 20).

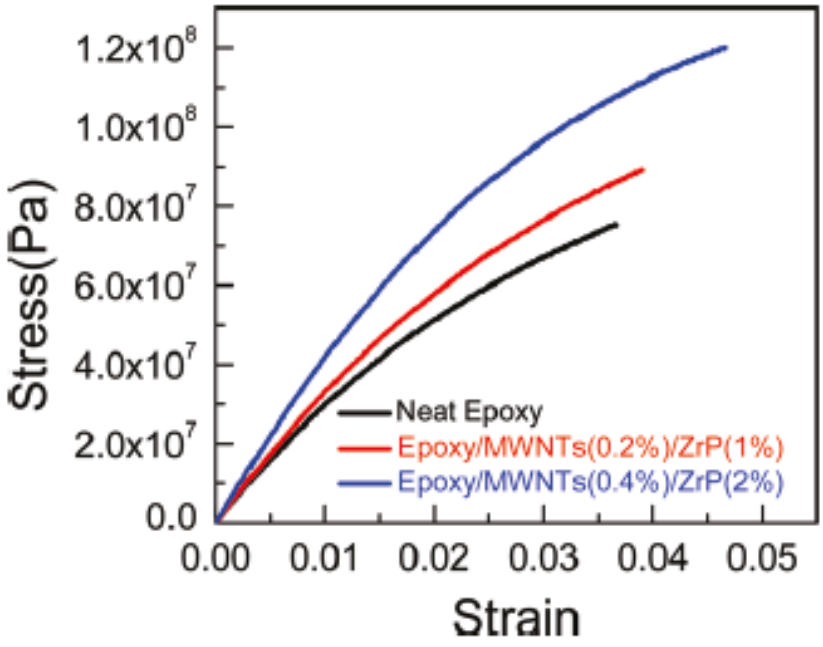

Figure 20. Tensile stress-strain curves of neat epoxy and ZrP/MWCNT/epoxy composites. Reprinted from [81].

Long-range electrostatic interactions are given as the reason for the improved tensile strength and ductility, whereas the individual dispersion of MWCNTs is given in support of the improved modulus. This observation, that nanoclays are able to individually exfoliate MWCNTs, has never been previously reported. However, attention should be drawn to the fact that the T_g of these samples was not reported and that it is also likely that they are not electrically conductive due to the surface of the MWCNTs being oxidized.

White et al. dispersed PA microparticles into a matrix containing MWCNTs to improve the fracture toughness of the brittle matrix [29]. However, the introduction of PA caused the modulus of the ternary composite to drop by ≈15% as seen in Table 4.

Table 4. Summary of tensile properties of neat epoxy and composites. Reprinted from [29].

System	E [GPa]	σ_{TS} [MPa]	ε_B [%]	K_{IC} [MPa·√m]
Neat Epoxy	2.79 ± 0.09	64.0 ± 2.9	3.2 ± 0.3	0.52 ± 0.05
Epoxy/PA	2.48 ± 0.08	69.6 ± 1.9	9.2 ± 1.9	0.85 ± 0.08
Epoxy/MWCNTs	2.79 ± 0.09	76.3 ± 1.2	6.2 ± 1.4	0.74 ± 0.31
Epoxy/PA/MWCNTs	2.38 ± 0.09	75.2 ± 2.0	10.9 ± 1.3	1.10 ± 0.14

While the tensile strength and ductility improve for all composite systems, the ones that contain PA exhibit reduced modulus compared to the neat resin. The reason for this is the low T_g of PA, which imparts it with a relatively low modulus compared to the epoxy matrix. Furthermore, the high concentration of PA (20 wt.%) also plays a contributing role. More importantly, and contrary to what is expected when a high concentration of low T_g filler is introduced into a high T_g matrix, no change in the T_g of the composites (according to DMA) was observed.

Yang et al. studied the effect of surface functionalization with two different chemical moieties on the tensile properties of MWCNT/epoxy nanocomposites [32]. The sidewalls of MWCNTs were covalently functionalized with 2,2'-(ethylenedioxy)-diethylamine and 1,8-diamineooctane to form liquid-like (L-MWCNTs) and solid MWCNTs (S-MWCNTs), respectively. Unmodified and modified MWCNTs were introduced into an epoxy matrix at 0.5 wt.% via a solvent-less process. L-MWCNTs were observed to form a homogeneous dispersion, while

s-MWCNTs were observed to be poorly dispersed even though they possess a similar chemical structure as l-MWCNTs. A system of P-MWCNTs was also dispersed into epoxy for comparison. The tensile and dynamic mechanical behavior of the composites was characterized and reported Table 5.

Table 5. Tensile properties and T_g (according to DMA) of neat epoxy and MWCNT/epoxy composites. Reprinted from [32].

System	E [GPa]	σ_{TS} [MPa]	ε_B [%]	T_g [°C]
Neat Epoxy	2.39	80.4	5.4	118.5
Epoxy/P-MWCNTs	2.47	76.9	4.9	119.8
Epoxy/S-MWCNTs	2.63	89.3	5.8	121.6
Epoxy/L-MWCNTs	3.07	98.8	6.7	124.1

The system containing P-MWCNTs exhibited slightly improved modulus, but reduced tensile strength and ductility, which is likely due to the aggregated state of the P-MWCNTs diminishing the ability of the MWCNTs to effectively transfer stress throughout the matrix and acting as stress concentrations for stress buildup. The S-MWCNT/epoxy system exhibits enhanced modulus, tensile strength, and ductility, although these are moderated at best. A more significant improvement in the modulus, tensile strength, and ductility is observed for the system containing L-MWCNTs and this is likely due to the fact that the interaction between the functionalized surface and epoxy

is stronger and they are better dispersed than S-MWCNTs. The T_g of the composites is observed to increase, albeit slightly, when MWCNTs are dispersed into epoxy. The MWCNT/epoxy composite systems exhibit larger glassy and rubbery storage moduli due to the stiffening effect of MWCNTs on the surrounding matrix. The system containing S-MWCNTs exhibits higher T_g, which is suggested to be a result of the free amine groups on the S-MWCNT surface that are able to crosslink with the epoxide groups leading to higher crosslink density. However, due to the partially exfoliated state of the S-MWCNTs, fewer amine groups are free to react with epoxide groups, unlike for well-exfoliated L-MWCNTs, which have a much larger number of free amine groups resulting in a denser network structure.

2.3.3 Toughened epoxy composites

A number of different approaches have been developed over the years to toughen epoxy such as: 1) rubber toughening, 2) molecular flexibilization, 3) thermoplastic particle toughening, and 4) nanofiller toughening. The efficacy of a particular toughening approach to improve the fracture toughness of epoxy rests on its ability to promote various toughening mechanisms that absorb energy such as: shear band formation (with and without particle interaction), croiding and crazing, microcracking, crack bridging, and crack bifurcation, pinning, etc. [235]. The level of improvement that can be expected for the toughening mechanisms mentioned is as follows: shear banding and croiding may result in an order of magnitude improvement in K_{IC}, crazing may result in a several fold increase in K_{IC}, microcracking and multiple cracking may double the K_{IC}, cracking bridging may result in an incremental improvement in K_{IC}, and crack bifurcation, crack

pinning, crack segmentation, etc. may result in a fractional enhancement of K_{IC}. For the case of thermoplastic-toughened epoxies, the most likely observed toughening mechanism is crack bridging, whereby the particle is of a comparable size to that of the natural crack tip radius and is able to bridge the crack and undergo severe plastic deformation up to failure [29, 64-71, 73, 236, 237].

Rubber toughening, whether by reactive or non-reactive rubbers, is accomplished by the introduction of a liquid rubber phase that phase separates upon the crosslinking of the epoxy matrix [66, 84-87, 173, 191, 192, 238-253]. The theory behind carboxyl-terminated butadiene and acrylonitrile (CTBN) rubber toughening of epoxy is that the CTBN reacts with the carboxyl groups of the epoxy. Upon curing, the molecular weight of the matrix increases leading to phase separation of the epoxy and rubber. Even though the toughening ability of reactive and non-reactive rubbers is exceptional, as previously evidenced, they decrease the overall strength and T_g of the matrix due to the large concentration of relatively soft fillers that are introduced and also increase the viscosity of matrix making it less processable [173, 251].

Toughening via the introduction of preformed thermoplastic particles such as polyetherimide (PEI), polyethersulphone (PES) and polyamide, into an epoxy matrix has been extensively studied since the 1980s [29, 64-71, 73, 254-256]. The earliest reported studies on thermoplastic-toughened epoxies were conducted by Bucknall and Partridge in 1983 [257, 258]. A commercial PES was used to toughen various thermoset resins and the resulting composites exhibited little improvement in toughness. Later studies using PES and PEI particles concluded that while significant toughness enhancement was possible,

it would only be observed if phase separation occurred and good interfacial adhesion was achieved [69].

Studies involving the dispersion of preformed PA microspheres into an epoxy to: improve the fracture toughness of the matrix and to introduce toughened interleaves into carbon fiber-reinforced (CFR) polymers, have been conducted in recent years [29, 73, 74, 82, 183, 197, 259]. PA is expected to be able to toughen epoxy via crack bridging whereby as the crack propagates and new fracture surfaces are created, PA particles are of a comparable size as the natural crack tip radius of epoxy that they are able to bridge the crack and resist further propagation by absorbing fracture energy and plastically deforming.

Sun et al. introduced PA at 5 wt.% and 10 wt.% into an epoxy matrix containing pristine, oxidized, or sulfanilamide- (SAA) functionalized SWCNTs at 0.5 wt.% [73]. The tensile, fracture, and dynamic mechanical properties were investigated to determine the reinforcement efficiency of the nylon with respect to the SWCNT/epoxy composites. It was generally observed that the introduction of nylon reduced the modulus of the ternary systems (those containing SWCNTs and nylon) as a function of concentration due to the lower modulus of the PA compared to the epoxy. However, the tensile strength and ductility improved in every ternary system with the exception of the ones containing SAA-functionalized SWCNTs due to adsorption of the curing agent resulting in a change in the stoichiometric ratio. The fracture toughness of the SWCNT/epoxy systems is only marginally improved because SWCNTs alone are unable to promote effective toughening mechanisms in epoxy. In contrast, the systems containing PA exhibit improved fracture

toughness compared to not only the neat resin, but also the systems containing SWCNTs. This is due to the promotion of crack bridging by the PA microparticles during fracture, whereas in the ternary system the presence of SWCNTs and PA promote crack bifurcation, deflection, and microcracking. Unfortunately, the T_gs of the composite systems containing PA, F-SWCNTs, and PA/SWCNTs were reduced compared to the neat resin by ≈5 °C.

White et al. introduced PA microparticles at 20 wt.% into an epoxy matrix with and without pristine MWCNTs at 1.0 wt.% to improve the fracture toughness of epoxy [29]. The Mode I fracture toughness and critical strain energy release rate of the composites was characterized via SEN-3PB tests. To prepare the samples for testing, a notch was introduced with a v-notch cutter to ≈1-2 mm. Subsequently, a jeweler saw was used to make a much smaller notch into which a liquid nitrogen-chilled and fresh razor blade would be placed into. A natural crack was introduced into the samples by tapping once or twice on the top of the razor blade. The samples were then loaded into a three-point-bending configuration and the load versus deflection data was collected. As seen in Table 4 and Figure 21, the fracture toughness is enhanced by the presence of PA and MWCNTs. However, the presence of MWCNTs alone, is insufficient to promote effective toughening mechanisms aside from very large clusters interacting with the crack tip, whereas PA alone is able to bridge the crack as it propagates through the sample.

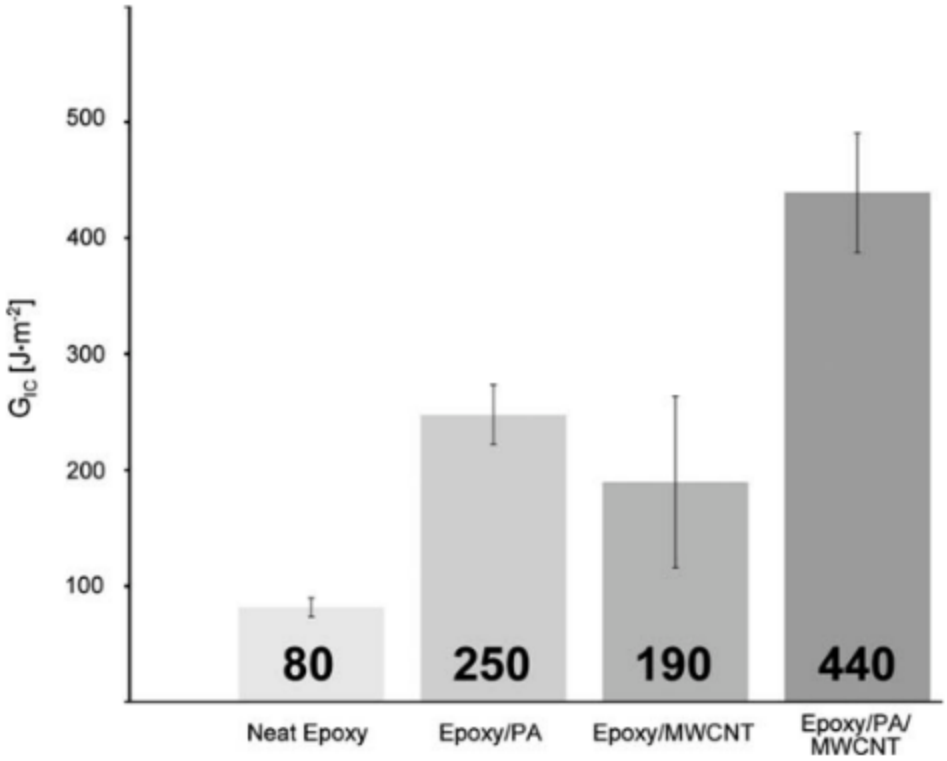

Figure 21. Mode I critical strain energy release rate, G_{IC}, of neat epoxy and the composite systems. Reprinted from [29].

The ternary system containing PA microparticles and P-MWCNTs exhibits the highest fracture toughness compared to the neat matrix. It is suggested that the presence of MWCNTs and PA promotes more effective crack bridging by the heterogenous distribution of MWCNT clusters near PA that results in further plastic deformation around the crack tip. The same explanations were given for the observed improvement in the Mode I critical strain energy release rate. Of note, the T_gs of the composite systems exhibited no change compared to the neat matrix, which contradicts previous work [73].

Nanoparticle toughening of epoxies (nano silica, CNTs, graphene, block-copolymer micelles, and nanoclay) has also been extensively studied, but has been met with varying degrees of success [2, 24, 29, 39, 41, 43, 49, 55, 73, 105, 195, 196, 199, 201, 208, 220, 225, 260-283] Unfortunately, only moderate improvements were observed for CNT toughening of epoxy matrices [39]. It should be pointed out that in these cases, the CNTs were agglomerated, rather than well-dispersed. The two previously mentioned studies are of importance because they confirm that SWCNTs and MWCNTs, when aggregated or partially exfoliated, are unable to effectively improve the fracture toughness of epoxy [29, 73].

As mentioned in an earlier section, Hernandez-Perez et al. studied the effect of aspect ratio on the mechanical properties of MWCNT/epoxy composites with 1.0 wt.% MWCNTs [14]. The impact on fracture toughness was also characterized and the results were consistent with what is to be expected for composites containing two distinct groups of MWCNTs that have a large difference in aspect ratio. The K_{IC} of the system containing long MWCNTs increased by ≈33% compared to the neat matrix, while the system containing short MWCNTs exhibited no change at all (Figure 22).

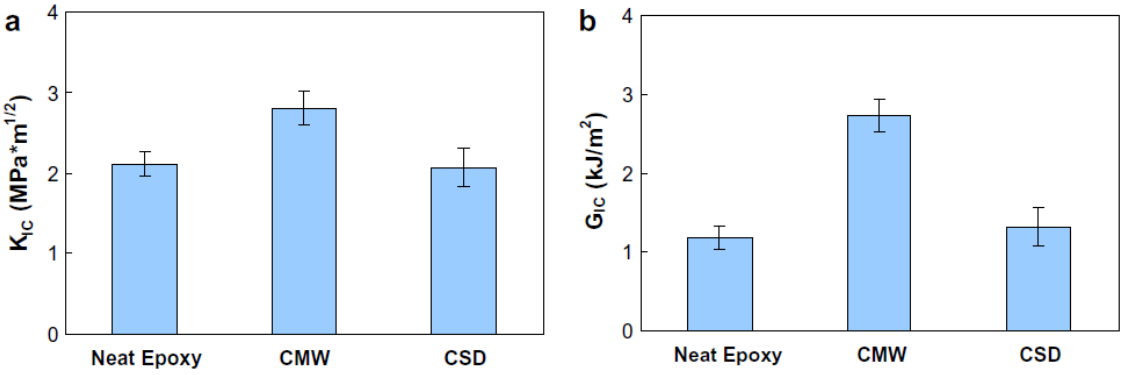

Figure 22. Fracture behavior of neat epoxy and composites containing high aspect ratio (CMW) and low aspect ratio (CSD) MWCNTs. Reprinted from [14].

The G_{IC} of the system containing high aspect ratio MWCNTs improved by a factor of 2.3 compared to the neat matrix, while the system containing low aspect ratio MWCNTs exhibited a moderate increase (≈12.5%). The fracture surfaces of the neat and composite samples were imaged via SEM to explain the observed change in the fracture toughness. The fracture surface of neat epoxy is flat and smooth, indicative of a brittle fracture. However, the fracture surfaces of the composite systems exhibited higher surface roughness compared to the flat surface of the neat epoxy. Tube pullout was observed, which indicates poor particle-matrix adhesion, and is given as the reason for the enhanced fracture toughness in the composite systems. The T_g of the systems was characterized via DMA and it was observed that the presence of the MWCNTs drove the T_g to higher temperatures.

Zhou et al. dispersed 0.0-0.4 wt.% MWCNTs into a conventional aerospace-grade epoxy resin (EPON 862) with a commonly used hardener (EPICURE W) to determine if MWCNT aggregates could be reduced via ultrasonication, and if so, would this enhance

the mechanical or fracture behavior of the composites [16]. SEN-3PB tests were conducted on bulk samples to determine the effect of MWCNT loading on the fracture toughness of epoxy. A slight increase in the fracture toughness was observed (Figure 23) up to 0.3 wt.% MWCNTs, but it decreased upon further loading (0.4 wt.%).

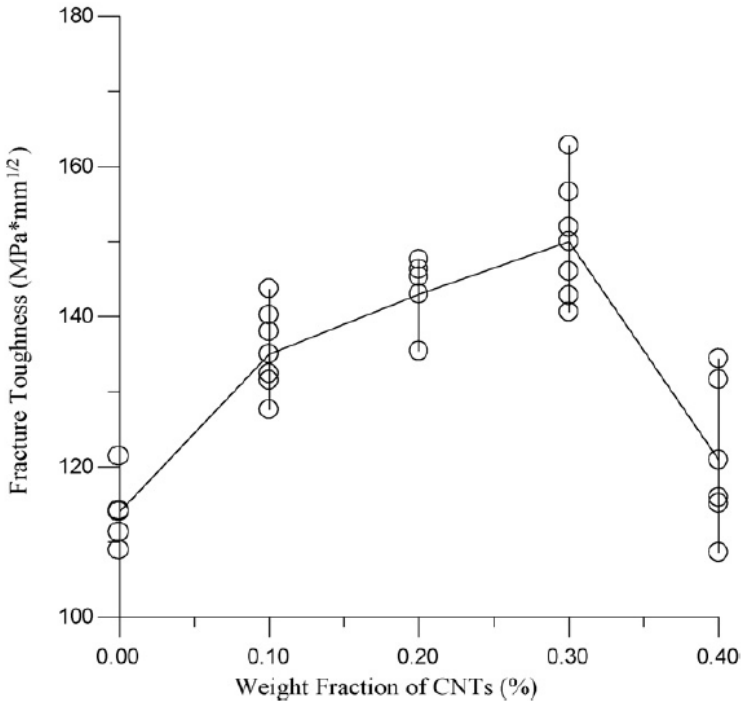

Figure 23. Critical stress intensity factor, K_{IC}, as a function of MWCNT concentration. Reprinted from [16].

The fracture surfaces of the neat epoxy and composites were investigated with SEM to identify the mechanism(s) responsible for this observed behavior. In the composite systems with concentrations below 0.4 wt.%, the crack was observed to have changed

direction as it crossed MWCNTs, indicating that crack bridging had taken place. This explanation does not follow from intuition, it's more likely that the MWCNTs are aggregated and rather than bridging the crack, they deflect it. The T_g of the neat matrix and composite systems was not evaluated. Ayatollahi et al. also studied the effect of MWCNT concentration on the tensile properties and fracture toughness of MWCNT/epoxy composite systems and observed similar trends [24, 25].

A number of studies on ternary epoxy composites containing rubber, PES, graphene, and CNTs were also studied with varying degrees of improvement [39, 105, 194, 201, 272, 275, 277-279, 281, 282, 284].

2.3.4 Summary

A large number of studies have been done over the years to determine the efficacy of MWCNTs in forming an electrically conductive network in epoxy and have mostly focused on filler concentration and surface chemistry only. The studies rarely take into account the aspect ratio, dispersion, and alignment of the nanotubes. The next section will detail epoxy composites containing MWCNTs for improving their stiffness and strength.

Numerous studies have also been conducted to deduce the effect of introducing MWCNTs, whether functionalized or not, on the tensile properties of epoxies. The studies show that in general, the introduction of MWCNTs does moderately improve the modulus regardless of surface chemistry. However, if the dispersion of the MWCNTs is observed to improve as a result of surface functionalization, then the modulus is generally observed to increase more significantly than for a system of aggregated P-MWCNTs. However, for the tensile strength and ductility of the composites, not only does the presence of

aggregates play a role, but the level of damage to the tube sidewalls as a result of surface functionalization is crucial. If the damage is too severe, the inherently high tensile strength of the MWCNTs is severely diminished resulting in premature fracture of the epoxy. Furthermore, depending on the surface chemistry of the MWCNTs and the concentration that is dispersed into the matrix, the change in T_g, if observed at all, is inconclusive.

In this section, the history of the toughening of epoxies with thermoplastic particles, specifically nylon, and MWCNTs was summarized and discussed. The importance of the particle-matrix interface, dispersion state, concentration, and size were discussed. Rubber-toughening of epoxies has been met with the most success, whereas CNT-toughening has been met with little success. Furthermore, the toughening of epoxies with thermoplastic particles has its advantages and disadvantages when it comes to the drawbacks associated with rigid and soft particles. In the case of PA, its introduction into a relatively stiff and high-T_g matrix result in a composite with reduced modulus and T_g, even in the presence of very stiff CNTs.

Finally, it should be noted that in the aforementioned studies and a majority of what has been published in the literature, little to no care is taken to carefully examine the morphology and dispersion of the CNTs in a matrix/solvent of interest and how that effects the final properties of the composite.

2.4 Hybrid epoxy thin films

Epoxies are typically used in industries that require low gas/water permeability, low electrical conductivity, low viscosity for easy processability, high strength and stiffness, and optical clarity. Notwithstanding adhesives and coatings, freestanding films

of epoxy have not been well-studied, particularly for multifunctional applications. The Studies on thermoset thin films have been conducted over the years to determine if various fillers could improve the mechanical properties, gas barrier resistance, corrosion resistance, fracture toughness, and electrical and thermal conductivities [5, 31, 178-180, 184, 285-301]. The study of epoxy, a commonly used thermoset polymer in the aerospace, automotive, and coatings/sealants industries, in thin film composite form has only been studied on a handful of occasions [5, 31, 178-180, 285-297, 302].

The fracture toughness of thin, brittle polymeric films has been studied since the 1980s, but has not reached a level of understanding as in the case of bulk composites, even though thin films are used in a number of applications [293, 297, 298, 300, 301, 303-307]. In short, the number of publications that report the mechanical behavior of free-standing epoxy thin films is low. A few studies have shown that the stiffness and strength of epoxy films are able to be enhanced with the introduction of a dispersion of nanofillers . The number of publications that report the multifunctional behavior of free-standing epoxy thin films is even lower. Therefore, a more concerted effort is needed to better understand the processing-structure-property relationships in epoxy thin films for various applications.

2.5 Concluding remarks

The previously detailed literature review highlighted the history, problems, and recent advances associated with MWCNT functionalization, epoxy nanocomposites containing MWCNTs for improved stiffness, strength, and electrical conductivity, epoxies toughened with thermoplastic particles and MWCNTs, and thin film epoxies and their

composites. Several systems were presented, including unfunctionalized and functionalized MWCNTs in epoxy, epoxies toughened with nylon, and multifunctional epoxies.

The effectiveness of covalent and non-covalent functionalization techniques to effectively and efficiently disperse MWCNTs in various solvents and epoxies is strongly dependent on particle-particle interactions, particle-matrix interactions, aspect ratio, and loading level [13, 50, 56-58]. The effectiveness of MWCNTs and thermoplastic particles on enhancing the mechanical, electrical, and fracture properties of epoxy also strongly depends on aspect ratio, concentration, dispersion, particle-particle, and particle-matrix interactions [13, 29, 50, 56-58, 64, 65, 67-69, 71, 73]. In the case of nanotube reinforced epoxy nanocomposites, the level of dispersion of the nanofillers is one of the most significant factors in determining the mechanical properties, electrical properties, fracture behaviors, and toughening mechanisms of the fabricated composite. Despite extensive research efforts over the past two decades, the mechanisms by which nanoscale fillers influence the macroscale behaviors of polymer nanocomposites, let alone thin films, have yet to be completely understood and demand subsequent investigation.

CHAPTER III

DISPERSION OF FUNCTIONALIZED MWCNTS IN ORGANIC SOLVENT AND EPOXY*

3.1 Introduction

Since their discovery in 1991 by Iijima, CNTs have been extensively studied and the number of publications per year continues to grow [59, 60, 88]. Their superior electrical, thermal, and mechanical properties make them attractive candidates for polymer nanocomposites [40, 47, 50, 52, 54, 55, 59, 60, 95, 99, 101, 102, 108, 123, 126, 158, 168, 209]. In recent years, numerous studies have focused on developing new functionalization methods for CNTs to be used in varied applications without destroying the C-C lattice. For example, defects on the CNT surface have been used as templates for the adsorption of metallic and metallic oxide QDs [113, 133, 140-142, 154]. These CNT/QD hybrids have emerged as a new class of functionalized CNTs that exhibit unique catalytic, magnetic, electrical, and optical properties that may help to improve the electrical and mechanical performance of epoxies.

ZnO has recently attracted significant attention due to its wide band gap (3.37 eV), low cost, nontoxic nature, and high electron mobility [308]. The integration of CNTs and ZnO QDs may result in a hybrid material that exhibits features characteristic of the constituents and could be used in the nanotechnology industry.

---

*Reprinted with permission from "Tensile Properties and Electrical Conductivity of Epoxy Composite Thin Films Containing Zinc Oxide Quantum Dots" by S. A. Hawkins, H. Yao, H. Wang, and H.-J. Sue, 2017, *Carbon*, 115, 18-27, Copyright 2016 by Elsevier.

Previously, ZnO/CNT hybrids were prepared by thermal deposition of wet chemistry, chemical vapor deposition, sputter coating, depending on the zinc oxide precursors [144, 157, 160, 163-166, 309, 310]. Thermal deposition involves maintaining very strict control of temperature (up to 1000 °C). For example, ZnO is able to grow directly on the CNT surface via vapor-solid growth, whereby Zn atoms are provided by evaporating a foil at 500-600 °C [311]. Thermal evaporation has also been used by Chrissanthopoulos to decorate the surface of MWCNTs whereby ZnO powder, graphite powder, and MWCNTs are placed into a furnace at ≈1000 °C causing the carbothermal reduction of ZnO into Zn, which is then transferred in the gaseous phase to the surface of the MWCNTs and oxidizes [310]. Conversely, the wet chemistry approach is the preferred method due to its ease of processing and scalability. Jiang et al. synthesized ZnO/MWCNTs with a similar approach as Sun et al. by refluxing of a solution of zinc acetate dihydrate and lithium hydroxide monohydrate in anhydrous ethanol containing SDS at 80 °C for 3 hr [144, 312]. Recently, Sun et al. developed a method, similar to Meulenkamp et al., whereby colloidal ZnO QDs are synthesized by refluxing a solution of zinc acetate dihydrate and potassium hydroxide at 60 °C for 2 hr and purified by washing and filtration [77, 313]. Magnetron sputtering, microwave irradiation, thermal hydrolysis, sol chemistry, covalent coupling have also been used to fabricated ZnO/CNT hybrids with various microstructures [134, 157, 163, 166, 314].

Even though numerous studies aimed at developing ZnO/CNT hybrids were performed, the average particles sizes ranged between 10-70 nm without much control

over their polydispersity and shape [144, 160, 163, 171, 309, 310, 314, 315]. Therefore, the ability to prepare consistent ZnO/CNTs with a mean particle diameter of <10 nm at low temperature (<100 °C) remains.

In the present study, an in-situ method has been developed to prepare ZnO/MWCNT hybrids (with and without previous surface oxidation) that have an average particle diameter of ≈4-5 nm. The ZnO/MWCNT hybrids synthesized via our new functionalization approach are observed to be well-decorated, soluble and stable in methanol, and well-dispersed in methanol and a mixture of acetone/methanol/epoxy/curing agent. This is the first report to demonstrate a well-dispersed system of ZnO-functionalized MWCNTs using a simple, two-step procedure.

3.2 Experimental

3.2.1 Materials

The epoxy resin used in this work was D.E.R.™ 354, a diglycidyl ether of bisphenol F (DGEBF) liquid epoxy prepolymer, donated by DOW Chemical, with an epoxide equivalent weight of 158 g/eq. EPIKURE™ W, a diethyltoluene diamine (DETDA) curing agent, was donated by Momentive Specialty Chemicals Inc. (Columbus, OH), with an amine equivalent weight of 43.29 g/eq, was used as the curing agent. MWCNTs were donated by Arkema with reported inner and outer diameters of 2-6 nm and 10-15 nm, respectively, length of 0.1-10 μm, >90 % carbon content, and a reported density of ≈2.1 g/cm^3. Zinc acetate dihydrate and potassium hydroxide (KOH) were

purchased from Sigma-Aldrich and used as received. Acetone and methanol (MeOH) were purchased from Macron Fine Chemicals and Sigma-Aldrich and used as received. All materials were dried at ≈70 °C overnight and used as received with the exception of MWCNTs, which were subjected to mild oxidation according to previous reports [73, 81, 124, 180].

3.2.2 Pretreatment of MWCNTs

About 250 mg of P-MWCNTs were added to a concentrated mixture of sulfuric (45 mL) and nitric acid (15 mL) at a 3:1 volume ratio and ultrasonicated in a sonication bath (Branson 2510) for 2 h at 25 °C. Next, 190 mL of deionized water (DI-H_2O) was added to hinder further oxidation and the solution was sonicated for another 1 h at 25 °C. After oxidation, the MWCNTs were isolated with a polyvinylidine fluoride (PVDF) filter membrane (Millipore, Durapore, 0.45 μm pore size) under vacuum. The O-MWCNTs were washed four times with DI-H_2O during the filtration process to remove any trace of acid residue. Then, the solution was washed with MeOH four times, and the O-MWCNTs were collected and resuspended in MeOH at a concentration of 1 mg/mL using ultrasonication for 1 h.

3.2.3 Synthesis of ZnO/MWCNTs

The synthesis of ZnO nanoparticles in MeOH is reported elsewhere [77, 313]. The procedure to prepare ZnO-functionalized MWCNTs is similar to the above method. P-MWCNTs (160 mg) or O-MWCNTs (160 mg) in MeOH were added to a flask and sonicated for 30 min to obtain a homogenous solution. Next, KOH (1 g) was added to the

flask and dissolved via sonication for 10 min. Concurrently, zinc acetate dihydrate (1.96 g) was added to a separate flask with MeOH and dissolved via sonication for 5 min. After both reactants were completely dissolved, the solutions were mixed at 60 °C while stirring at 300 RPM to initiate the reaction. Then, the solution was refluxed at 60 °C for 2 h to promote the growth of ZnO QDs. After initiation and growth, the ZnO/P-MWCNTs and ZnO/O-MWCNTs were filtered through a PVDF membrane (0.45 μm pore size) under vacuum with MeOH four times and then redispersed in MeOH via ultrasonication for 1 h. Their concentrations were determined by pipetting a predetermined amount of solution into an aluminum weighing dish and the weight recorded. Next, the solution was left in an oven overnight at 60 °C to slowly evaporate the solvent. Finally, the pan with dry ZnO/P-MWCNTs was weighed and the difference was divided by the initial solution volume to determine the concentration of ZnO/P-MWCNTs in MeOH.

3.2.4 Dispersion of ZnO/MWCNTs into solvent/matrix

A predetermined amount of ZnO/MWCNTs was pipetted into a glass flask at a specific concentration. Acetone was added to the solution at a 1:2 ratio by volume and the solution was homogenized via ultrasonication for 30 min. Then, the solution was pipetted into a glass cuvette for observation with an optical microscope in transmission mode to observe the current level of dispersion. UV-Vis-NIR spectroscopy was used to characterize the dispersion state, stability, and morphology of ZnO/MWCNTs in solution.

3.2.5 Characterization

UV-Vis absorbance spectra of ZnO/MWCNT solutions were acquired with a UV-Vis-NIR spectrophotometer (Shimadzu, UV-3600). Thermogravimetric analysis (TGA) was performed with a TGA Q500 (TA Instruments) on ≈5 mg samples in oxygen purging at 40 mL/min at a heating rate of 10 °C from room temperature to 900 °C with a 15 min isotherm to determine the concentration of ZnO and MWCNTs present in the composite systems. The difference in weight after decomposition at ≈300 °C and 500 °C was defined as the wt.% of MWCNTs present in the ZnO/MWCNT solution. For the purposes of this paper, all wt.%/wt.% ratios between ZnO/MWCNTs were held at 2:1. Zeta potential of the MWCNT and ZnO/MWCNT solutions was measured with a Delsa^{TM} Nano Submicron particle analyzer (Beckman Coulter, Inc.). The solutions were diluted to 0.1 mg/mL in MeOH for various measurements.

X-ray photoelectron spectroscopy (XPS) was obtained from a Kratos Axis Ultra using a non-monochromatic MgK_α photon source (1486 eV). UV-Vis absorbance spectra were acquired with a UV-Vis-NIR spectrophotometer (Shimadzu, UV-3600) on 25 μm thick liquid samples before curing. X-ray diffraction (XRD) spectra of ZnO and ZnO/MWCNTs were generated using a Bruker D8 Advanced Powder XRD with CuK_α incident radiation (k = 1.5418 Å). Transmission optical microscopy (TOM) images of filler dispersion were obtained by pipetting a predetermined amount of ZnO/MWCNTs in solution at a specific concentration into a glass cuvette and observing it under an Olympus BX60 microscope with a Canon Mark 2 Digital Camera.

3.3 Results and discussion

3.3.1 MWCNT functionalization

The synthesis of ZnO QDs using zinc acetate and potassium hydroxide in MeOH was previously reported in the literature [77-79]. The high dielectric constant of MeOH compared to other solvents results in high solubility of zinc acetate and quicker formation of ZnO QDs [316]. The *in situ* preparation of ZnO/P-MWCNTs as seen in Figure 24 is similar to the synthesis of ZnO QDs with a slight alteration.

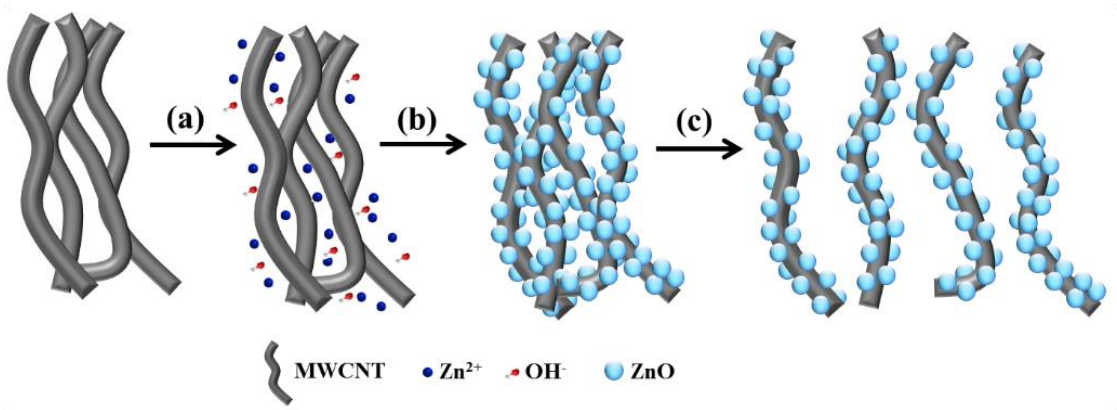

Figure 24. Schematic of ZnO/P-MWCNT synthesis. (a) Zinc acetate and potassium hydroxide are added into a sonicated P-MWCNT/MeOH solution; (b) ZnO QDs are grown on the surface of CNTs by refluxing for 2 h at 60 °C; (c) Homogeneously exfoliated ZnO/P-MWCNTs in MeOH [302].

P-MWCNTs are disentangled by ultrasonication coupled with electrostatic repulsion between ZnO QDs and steric hindrance effects. Functional groups or defects on the CNT surface have been theoretically confirmed to act as binding and reactive sites for

nanoparticle nucleation, and the nucleation energy of metal oxides can be reduced when additional functional groups are present on the surface of MWCNTs [59, 130, 133, 134, 141-143, 150, 154, 155, 317, 318]. Therefore, it is energetically more favorable for ZnO to nucleate on O-MWCNTs, leading to accelerated nucleation. Several oxygen-containing functional groups are commonly observed on the surface of O-MWCNTs *via* FTIR: hydroxyls, carboxyls, and epoxides [30, 62, 81, 111, 112, 116-122, 319, 320]. It is believed that carboxyl groups are the most likely anchoring sites for ZnO nanoparticles to interact with because it is the most polar and has a stronger negative charge compared to the other oxygen functional groups.

The morphologies of the functionalized P-MWCNTs and O-MWCNTs were characterized via TEM to provide direct evidence of ZnO QDs surface decoration. As seen in Figure 25, P-MWCNTs exhibit an outer diameter of 10-20 nm and tend to curl due to kinking and buckling in the graphitic structure (Figure 25a) [34].

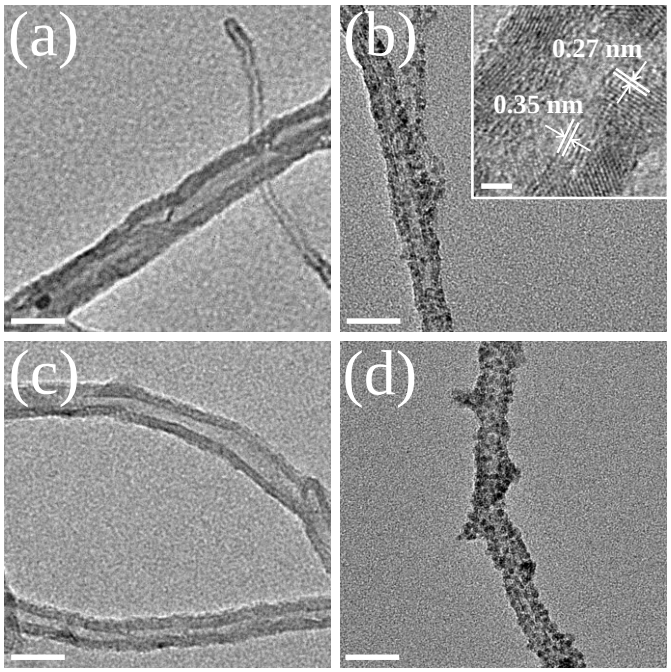

Figure 25. TEM of (a) P-MWCNTs, (b) ZnO/P-MWCNTs, (c) O-MWCNTs, and (d) ZnO/O-MWCNTs with scale bars = 25 nm. Inset in (b) shows high magnification TEM of ZnO/P-MWCNT surface with scale bar = 2 nm [302].

ZnO QDs appear to be directly attached to the surface of P-MWCNTs and O-MWCNTs and increases their effective diameters to 20-28 nm. TEM micrographs of the functionalized P-MWCNTs clearly exhibit well-packed QDs with spherical shape and nearly uniform size on the surface (Figure 25b). Spherical ZnO QDs can be clearly seen on the surface of a P-MWCNT in Figure 26.

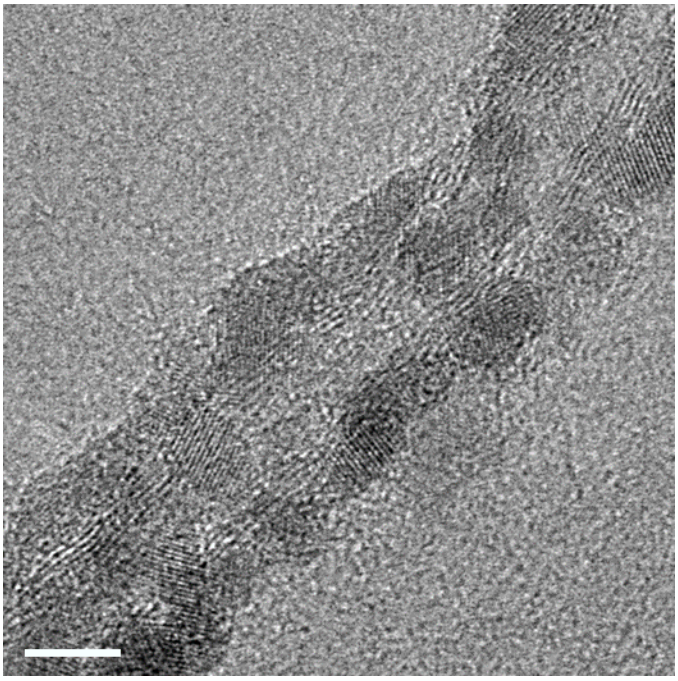

Figure 26. High resolution TEM micrograph of ZnO/P-MWCNT after functionalization with scale bar = 5 nm [302].

ZnO/O-MWCNTs are observed to have uneven surfaces with some clustering of QDs as compared to ZnO/P-MWCNTs (Figure 25d). In Figure 27, ZnO QDs can also be clearly observed on the surface of an O-MWCNT; however, there appears to be some clustering in the upper portion of the tube.

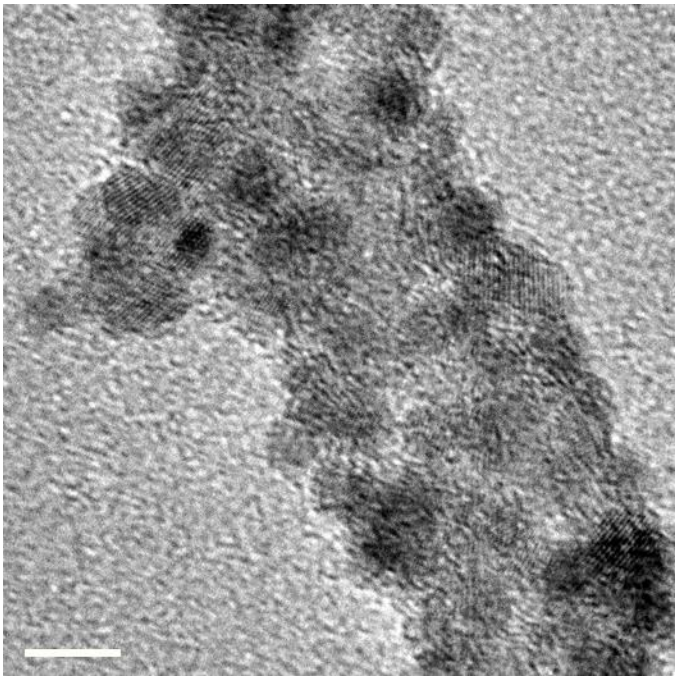

Figure 27. High resolution TEM micrograph of ZnO/O-MWCNT after functionalization with scale bar = 5 nm [302].

XRD spectra of ZnO, ZnO/P-MWCNTs, and ZnO/O-MWCNTs exhibit various peaks associated with ZnO and P-MWCNTs as seen in Figure 28. The diffraction peaks at $2\theta = 31.7°$, 34.3°, 36.1°, 47.4°, 56.4°, 62.91°, and 67.9°match with (100), (002), (101), (102), (110), (103) and (112) reflections of the Wurtzite ZnO structure [77]. The characteristic peaks for CNTs are observed at $2\theta = 25.9°$ (002) and 43.2° (100) [321]. The interplanar spacing of ZnO was measured as 0.27 nm, which corresponds well with the (002) plane of ZnO with a hexagonal structure. P-MWCNTs exhibited an interlayer distance of 0.35 nm (Figure 25b).

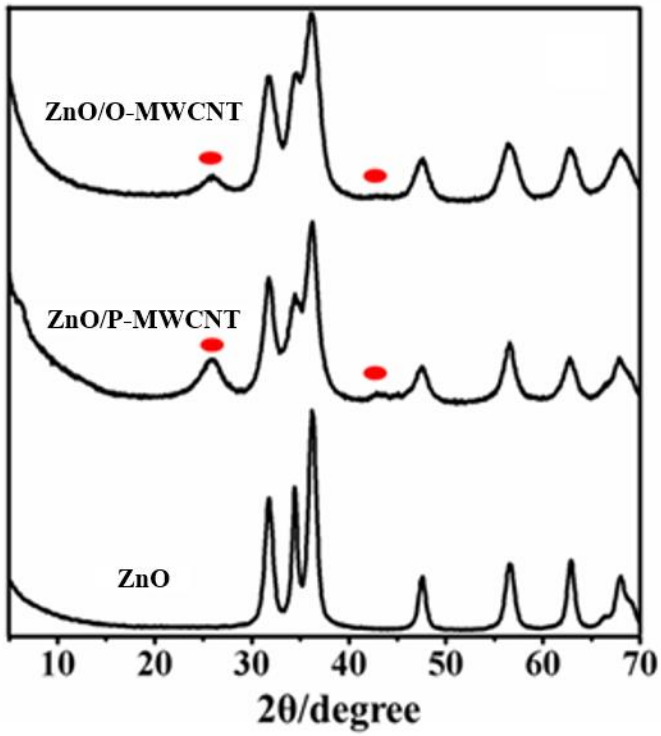

Figure 28. XRD spectra of ZnO QDs, ZnO/P-MWCNTs, and ZnO/O-MWCNTs. Peaks characteristic of CNTs are marked by red dots [302].

XPS was used to determine the carbon to oxygen (C/O) ratio, which is indicative of the surface characteristics of the MWCNTs with oxygen-containing functional groups. Figure 29a represents a typical XPS spectrum of ZnO/P-MWCNTs; zinc, oxygen, and carbon are the dominant species. The results indicate that the P-MWCNTs and O-MWCNTs have a C/O ratio of 25 and 12, respectively. This indicates that more oxygen-functional groups are present on the O-MWCNT surface. XPS was also used to measure the electronic coupling between ZnO and the P-MWCNT surface.

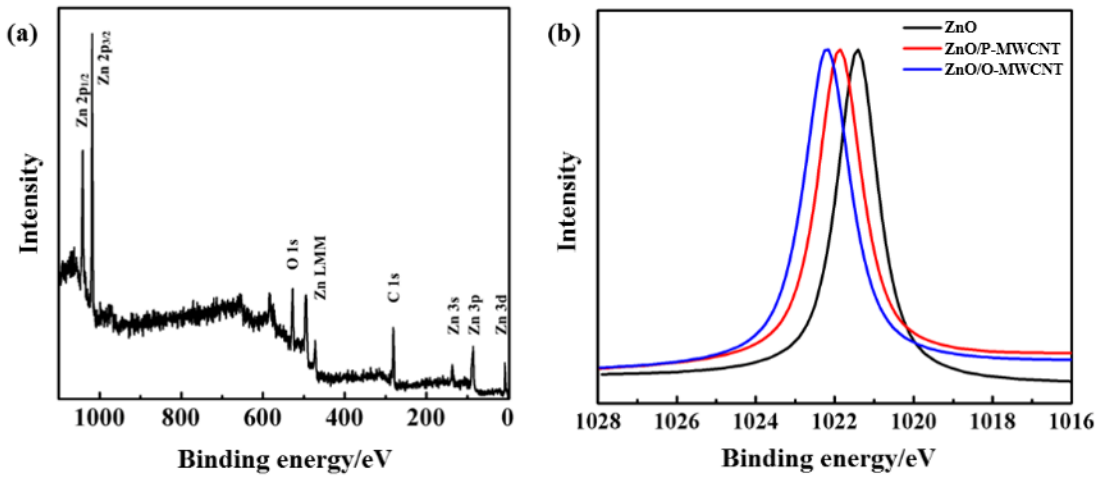

Figure 29. (a) XPS spectrum of ZnO/MWCNTs, and (b) XPS spectra of Zn $2p_{3/2}$ on ZnO, ZnO/MWCNTs, and ZnO/O-MWCNTs [302].

The high-resolution spectra of Zn $2p_{3/2}$ for ZnO, ZnO/P-MWCNTs, and ZnO/O-MWCNTs are shown in Figure 29b. The Zn $2p_{3/2}$ peak is positioned at 1021.4 eV with high symmetry for ZnO, indicating the presence of Zn^{2+} [309]. However, the peaks for ZnO/P-MWCNTs and ZnO/O-MWCNTs exhibit a shift to higher binding energy by 0.46 eV and 0.79 eV, respectively. This shift signifies increased oxidation of Zn due to their proximity to the electronegative MWCNTs [322]. The presence of an electronegative MWCNT surface creates a strong dipole moment with ZnO QDs. Therefore, strong coupling between ZnO QDs and MWCNTs exists on the surface between them, not merely physisorption. This lends more credence to the TEM images in which the ZnO crystallites are observed to firmly attach to the MWCNT surface [116].

The wt.%/wt.% ratios between ZnO QDs and MWCNTs in functionalized MWCNTs were calculated from the initial solution concentration and the difference in

weight percent at 370 °C and 650 °C, the loss of acetate ions, similar to purified ZnO, and the degradation of MWCNTs, respectively, as seen from the TGA curves shown in Figure 30 [77]. For ZnO/P-MWCNTs and ZnO/O-MWCNTs, the wt.%/wt.% ratios were calculated to be ≈1.5/1.

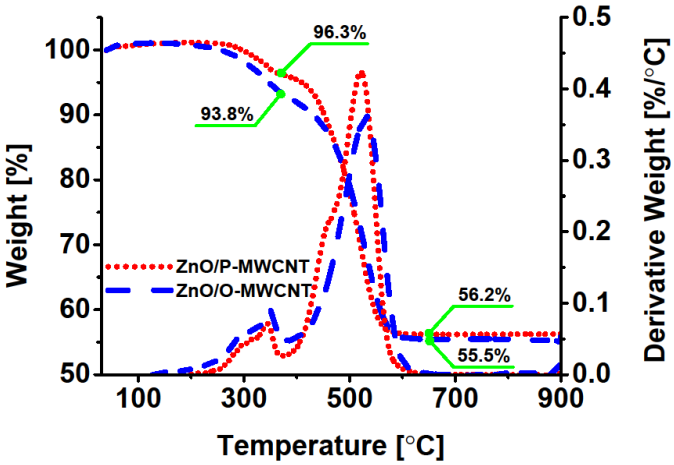

Figure 30. Weight loss and derivative weight loss curves of ZnO/MWCNTs and ZnO/O-MWCNTs as a function of temperature with residual weight at 370 °C and 650 °C marked [302].

Given the calculated wt.%/wt.% ratios are equal, the systems can be compared in terms of their morphology and effect on the electrical and tensile properties. The observed initial weight increase (≤1%) is attributed to the buoyancy effect commonly reported for vertically aligned TGAs. In short, as the furnace begins to heat, the walls become hotter than the center, causing vertical circulation throughout the chamber. The hot air near the walls rises, while the cold air is pushed down resulting in a drag force on the sample that

increases the apparent weight %. It is also possible that slight oxidation of the MWCNTs occurs during the TGA run in air [116].

3.3.2 ZnO/MWCNT stability in solvent/matrix

The UV-Vis absorption spectra of ZnO QDs, P-MWCNTs, and ZnO/P-MWCNTs were quantified in MeOH at a concentration of ≈ 3mg/mL (Figure 31).

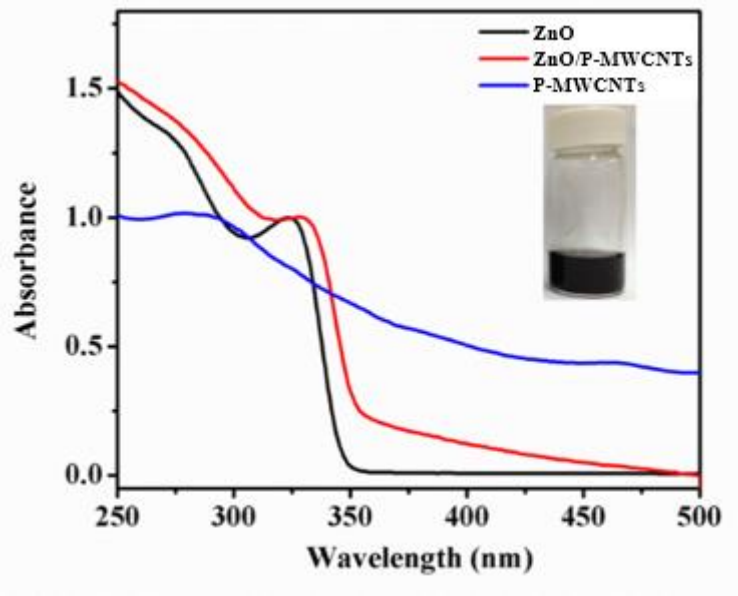

Figure 31. UV-Vis absorption spectra of ZnO, P-MWCNTs, and ZnO/P-MWCNTs. Reprinted from [323].

The P-MWCNT solution exhibits a large absorption range from ≈250-500 nm. The ZnO absorption spectrum exhibits a well-defined onset at ≈359 nm, characteristic of ZnO QDs. The absorption spectrum of ZnO-functionalized P-MWCNTs exhibits characteristics of

both individual spectra. It is likely that the absorption spectrum of ZnO/O-MWCNTs is very similar to that of ZnO/P-MWCNTs and it, therefore, was not measured.

Concentrated solutions (≈3 mg/mL) demonstrate good stability and solubility in methanol for several months (Figure 32a).

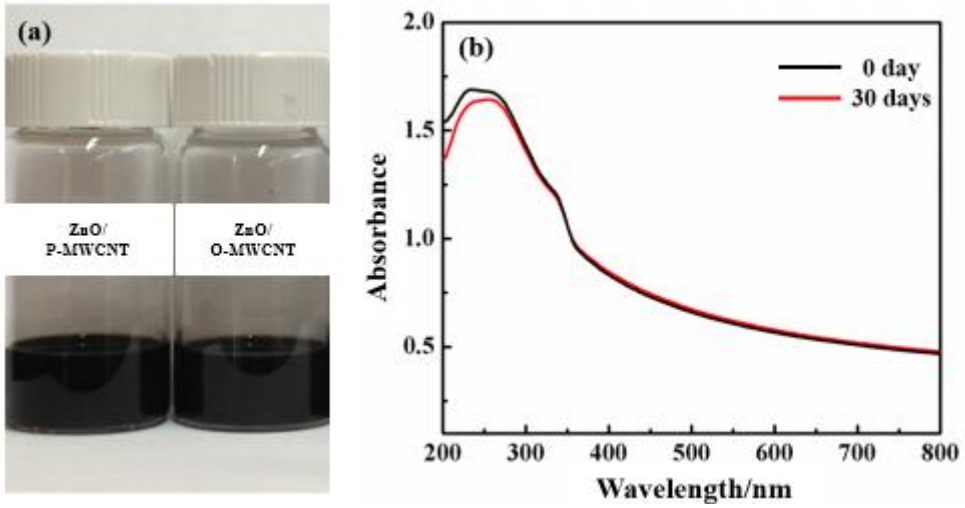

Figure 32. (a) Photograph of ZnO methanol solution with different types of CNTs, and UV-Vis absorption spectra of the soluble ZnO/P-MWCNT suspension in MeOH after standing for (b) 0 days and (c) 30 days. Reprinted from [323].

UV-Vis spectroscopy was conducted to quantify the stability of the suspensions as a function of time (Figure 32). As seen in Figure 32, the absorption spectra of ZnO remains relatively unchanged over the course of a month. Similarly, the absorption spectra of ZnO/O-MWCNTs as a function of time is expected to exhibit similar behavior as ZnO/P-MWCNTs given their zeta potential values are similar.

The stability of the solutions was characterized by their zeta potentials in MeOH. In general, nanoparticles with a zeta potential magnitude |Z| greater than 30 mV are expected to be stable from electrostatic repulsive forces [62]. Zeta potential values for ZnO QDs, P-MWCNTs, O-MWCNTs, and their functionalized counterparts are listed in Table 6. ZnO QDs have a measured zeta potential value of +44 mV in MeOH, while P-MWCNTs and O-MWCNTs exhibit negative values of -15 mV and -28 mV, respectively. After *in situ* decoration of ZnO QDs on the tube surface, the zeta potential values of P-MWCNTs and O-MWCNTs shift to positive values of +41mW and +34 mV, respectively.

Table 6. Zeta potential values of ZnO QDs, MWCNTs, and ZnO/MWCNTs in MeOH [302].

Samples	**ZnO**	**P-MWCNT**	**ZnO/P-MWCNT**	**O-MWCNT**	**ZnO/O-MWCNT**
Zeta potential (eV)	+44	-15	+41	-28	+34

3.3.3 ZnO/MWCNT dispersion in solvent/matrix

The dispersion state of ZnO QDs in the presence of P-MWCNTs and O-MWCNTs was monitored before and after curing via UV-Vis spectroscopy. The absorption onset of individually dispersed colloidal ZnO nanoparticles was observed to be 359 nm as reported in previous work [77, 79]. Absorbance spectra of glass, DGEBF and DETDA were

acquired to compare the absorbance spectra of ZnO/MWCNT hybrids in DGEBF+DETDA. DGEBF, DETDA, and the mixture of the two were observed to have absorption onsets of 306 nm, 325 nm, and 320 nm. Furthermore, the glass slides used to create a custom cuvette with a slot thickness of 25 μm were observed to have an absorption onset of 285 nm. Therefore, the materials used will not alter the absorption onset characteristic of colloidal ZnO. However, due to the strong absorbance of MWCNTs around 300-325 nm, the dispersion state of ZnO QDs cannot be conclusively determined based on their recorded absorbance spectra. It appears that the dissociation of ZnO QDs from the P-MWCNT surface likely occurs during the curing procedure. This implies that the change in solubility and/or thermal energy released during cure is sufficient to overcome the stability of ZnO QDs on the P-MWCNT surface leading to subsequent partial aggregation of ZnO QDs.

3.4 Conclusions

Stable solutions of ZnO/MWCNTs were successfully prepared via a simple two-step approach whereby ZnO QDs were grown *in situ* in a MeOH solution containing MWCNTs by refluxing at elevated temperature. Various characterization techniques (XRD, UV-Vis-NIR, XPS, TOM, TEM, TGA, and zeta potential) were used to determine the morphological structure, stability, and dispersion of the hybrid MWCNTs after functionalization. The MWCNT hybrid exhibited large positive zeta potential values after functionalization with ZnO QDs and this led to the observed stability of ZnO/MWCNT solutions over the course of 30 days by UV-Vis-NIR. Furthermore, the structure of the hybrid MWCNTs was investigated with TEM, XRD, TGA, and XPS. TEM images

revealed the presence of a decorated MWCNT containing spherical QDs with a narrow size-distribution of ≈5 nm in diameter. Furthermore, the QDs were identified as ZnO and having a wurtzite crystal structure via XRD based on the peaks observed for ZnO QDs alone. Moreover, TGA spectra revealed that the MWCNTs were decorated with ZnO QDs at a wt.%/wt.% ratio of ZnO/MWCNTs of ≈2:1. Finally, the dispersion level of the ZnO/MWCNTs was observed to be exceptional when in MeOH, even after the epoxy and curing agent were dissolved in solution.

CHAPTER IV

EFFECT OF MWCNT FUNCTIONALIZATION ON MECHANICAL AND ELECTRICAL PROPERTIES OF EPOXY NANOCOMPOSITE THIN FILMS*

4.1 Introduction

Epoxy resins have seen widespread use in the aerospace and automotive industries due to their excellent chemical resistance, thermal stability, and mechanical properties. However, when used in applications where electrical conductivity is required, such as electromagnetic interference (EMI) shielding, a secondary phase consisting of conductive fillers is necessary. Conductive fillers such as aluminum, gold, silver, graphite, or carbon black have commonly been used to increase the electrical conductivity of a particular polymer matrix, but mechanical strength and ductility are significantly reduced at the filler concentrations necessary to achieve conductivity [185]. The discovery of carbon nanotubes (CNTs), which have high aspect ratios and excellent electrical and mechanical properties, has been favorably linked to the development of conductive and multifunctional composites [11, 12, 23, 25, 26, 29-31, 40, 49, 56, 88, 92, 94, 97-100, 102, 103, 105-108, 209, 324, 325]. In this work, a new method is introduced to physically functionalize multi-walled (MWCNTs) and disperse them in an aerospace grade epoxy resin to prepare an electrically conductive, strong composite for potential use as a B-staged interleave in carbon fiber reinforced composites (CFRCs) using vacuum assisted resin transfer molding (VaRTM) [74, 178-180].

---

*Reprinted with permission from "Tensile Properties and Electrical Conductivity of Epoxy Composite Thin Films Containing Zinc Oxide Quantum Dots" by S. A. Hawkins, H. Yao, H. Wang, and H.-J. Sue, 2017, *Carbon*, 115, 18-27, Copyright 2016 by Elsevier.

Single-walled CNTs (SWCNTs) have among the highest values of modulus, strength, electrical conductivity, and thermal conductivity of all known materials [326-329]. However, they are expensive and tend to bundle into ropes with adjacent tubes due to high van der Waals (vdW) interactions, thus limiting their effectiveness at reinforcing mechanical and conductive properties in polymer composites [81]. MWCNTs, on the other hand, have inherently lower modulus and conductivity compared to SWCNTs, but are able to more significantly enhance those properties in polymer composites [330]. MWCNTs in epoxy have been observed to form electrically percolated networks at low volume fractions [10, 98, 100, 331]. Previous experimental work has shown that MWCNT treatment via functionalization, ultrasonication, etc., causes an increase in the percolation threshold, while mechanical properties are not affected [99]. In order to improve the mechanical properties of a matrix, MWCNTs need to be well-dispersed and have strong mechanical adhesion to the matrix [42]. Surface functionalization has been shown to exhibit well-dispersed CNTs with improved chemical bonding, commonly done through exposure to a mixture of sulfuric and nitric acids [8, 111-113, 117-119, 121].

Sun and Warren et al. studied the tensile properties of SWCNTs in epoxy composites and as interleaves in CFRCs [73, 81, 124, 178, 180, 181, 319]. It was observed that SWCNT oxidation followed by covalent surface functionalization with polyamido-amine generation-0 (PAMAM-0) resulted in improved dispersion and adhesion in an epoxy matrix. These improvements led to enhanced modulus, but only marginal improvement in tensile strength to the epoxy composite [124]. A newly developed functionalization method whereby oxidized MWCNTs are electrostatically

tethered to exfoliated zirconium phosphate nanoplatelets was developed by Sun et al. [81, 319, 332]. When ternary composites were fabricated by dispersing these nanoparticles in epoxy at low concentration (0.2 wt.% and 0.4 wt.% MWCNTs), the composites exhibited exceptionally improved modulus and strength without any reduction in ductility [81].

Here, we present a new approach to synthesize functionalized MWCNTs via *in situ* growth of positively charged zinc oxide (ZnO) QDs, resulting in a system of well-exfoliated MWCNTs in epoxy matrices. ZnO, a semiconductor, has garnered attention due to its wide band gap, low cost, high electron mobility, and environmental friendliness [308]. The large surface area-to-volume ratio and exceptional electrical conductivity of MWCNTs make them a good candidate for ZnO decoration [144, 157, 160, 162-166, 171, 309, 310, 314, 333]. Ideally, ZnO nanoparticles would decorate individually exfoliated MWCNTs without aggregating on the surface. If achieved, the interfacial contact between MWCNTs and ZnO would facilitate electron conductivity among MWCNTs in an epoxy matrix. Our approach takes advantage of the electronegative nature of MWCNTs to electrostatically deposit positively charged ZnO QDs, which overcome the attractive vdW forces between tubes to achieve individual dispersion in organic solvents and in epoxy [62, 323]. In this work, we present the tensile properties and electrical conductivity of epoxy composite thin films containing ZnO-functionalized pristine MWCNTs (P-MWCNTs) and oxidized MWCNTs (O-MWCNTs). We demonstrate that the above approach can greatly improve tensile properties without decreasing the T_g of the epoxy or the electronic state of the P-MWCNTs

in epoxy as compared to relevant experimental findings in the literature. The usefulness of the present study for multifunctional application of epoxy composites is discussed.

4.2 Experimental

4.2.1 Materials

The epoxy resin used in this work was D.E.R.™ 354, a diglycidyl ether of bisphenol F (DGEBF) liquid epoxy prepolymer, donated by DOW Chemical, with an epoxide equivalent weight of 158 g/eq. EPIKURE™ W, a diethyltoluene diamine (DETDA) curing agent, was donated by Momentive Specialty Chemicals Inc. (Columbus, OH), with an amine equivalent weight of 43.29 g/eq, was used as the curing agent. MWCNTs were donated by Arkema with reported inner and outer diameters of 2-6 nm and 10-15 nm, respectively, length of 0.1-10 μm, >90 % carbon content, and a reported density of ≈2.1 g/cm^3. Zinc acetate dihydrate and potassium hydroxide (KOH) were purchased from Sigma-Aldrich and used as received. Acetone and methanol (MeOH) were purchased from Macron Fine Chemicals and Sigma-Aldrich and used as received. Release paper composed of a cellulose-based paper coated with polydimethylsiloxane (PDMS) was donated by Experia Specialty Solutions. Epofix^{TM} Cold-Setting Embedding Resin and Hardener were purchased from Electron Microscopy Sciences and used to embed thin films for electron microscopy observation. All materials were dried in a vacuum oven at ≈70 °C overnight and used as received with the exception of MWCNTs, which were subjected to mild oxidation according to previous reports [73, 81, 104, 124, 332].

4.2.2 Pretreatment of MWCNTs

Around 250 mg of P-MWCNTs were added to a concentrated mixture of sulfuric (45 mL) and nitric acid (15 mL) at a 3:1 volume ratio and ultrasonicated in a sonication bath (Branson 2510) for 2 h at 25 °C. Next, 190 mL of deionized water (DI-H_2O) was added to hinder further oxidation and the solution was sonicated for another 1 h at 25 °C. After oxidation, the MWCNTs were isolated with a polyvinylidine fluoride (PVDF) filter membrane (Millipore, Durapore, 0.45 μm pore size) under vacuum. The O-MWCNTs were washed four times with DI-H_2O during the filtration process to remove any trace of acid residue. Then, the solution was washed with MeOH four times, and the O-MWCNTs were collected and resuspended in MeOH at a concentration of 1 mg/mL using ultrasonication for 1 h.

4.2.3 Synthesis of ZnO/MWCNTs

The synthesis of ZnO nanoparticles in MeOH is reported elsewhere [77, 313]. The procedure to prepare ZnO-functionalized MWCNTs is similar to the above method. P-MWCNTs (160 mg) and O-MWCNTs (160 mg) in MeOH were added to a flask and sonicated for 30 min to obtain a homogenous solution. Next, KOH (1 g) was added to the flask and dissolved via sonication for 10 min. Concurrently, zinc acetate dihydrate (1.96 g) was added to a separate flask with MeOH and dissolved via sonication for 5 min. After both reactants were completely dissolved, the solutions were mixed at 60 °C while stirring at 300 RPM to initiate the reaction. Then, the solution was refluxed at 60 °C for 2 h to promote the growth of ZnO QDs. After initiation and growth, the ZnO/P-MWCNTs and ZnO/O-MWCNTs were filtered through a PVDF membrane (0.45 μm pore size) under

vacuum with MeOH four times and then redispersed in MeOH via ultrasonication for 1 h. Their concentrations were determined by pipetting a predetermined amount of solution into an aluminum weighing dish and the weight recorded. Next, the solution was left in an oven overnight at 60 °C to slowly evaporate the solvent. Finally, the pan with dry ZnO/P-MWCNTs was weighed and the difference was divided by the initial solution volume to determine the concentration of ZnO/P-MWCNTs in MeOH.

4.2.4 Thin film composite preparation

DGEBF and DETDA were used as the matrix and hardener, respectively, to fabricate epoxy composite thin films. DGEBF (3.92 g) and DETDA (1.18 g) were added to a flask and degassed at 60 °C on a rotary evaporator under vacuum at 60-120 RPM for 30 min. The epoxy mixture was then B-staged in a preheated oven at 121 °C for 45 min to increase its viscosity for thin film processing. Once B-staged, the solution was poured onto an Elcometer 4340 Thin Film Coater preheated to 80 °C and cast at 5 mm/s to a thickness of 100-200 μm. Then, the film was placed in a preheated oven at 121 °C and cured for 2 h followed by a post-cure at 177 °C for 3 h. Composite films were fabricated according to the same procedure with a slight alteration. A ZnO/P-MWCNT composite film was prepared by sonicating a predetermined amount of ZnO/P-MWCNTs in MeOH in a flask for 30 min. DGEBF and DETDA were dissolved in acetone via sonication for 5 min and were subsequently added to the ZnO/P-MWCNT MeOH solution with a final MeOH/acetone vol.%/vol.% of 2/1. The mixed composite solution was then sonicated for 15 min followed by removal of the solvent using a rotary evaporator at 60 °C for 15 min at 60-120 RPM. Next, the viscous resin was degassed in a vacuum oven at 80 °C for 2 h

to ensure the complete removal of solvent. Then, the resin was carefully removed with a spatula and placed on a thin film coater preheated to 80 °C and cast at 5 mm/s to a thickness of 100-200 μm. For the O-MWCNT systems, the thin film coater was preheated to 100 °C due to their increased viscosity compared to the P-MWCNT systems. Once cast, the films were placed in an oven and cured at 121 °C for 2.75 h followed by a post cure at 177 °C for 3 h. The curing time and temperature were held constant at 2.75 h at 121 °C followed by 3 h at 177 °C to ensure the same degree of cure for all systems.

4.2.5 Characterization

Differential scanning calorimetry (DSC) was conducted with a DSC Q20 (TA Instruments) from 30 °C to 180 °C with a ramp rate of 10 °C/min to determine the glass transition temperature (T_g) of the epoxy systems. The T_g was defined as the point of inflection during the second heating cycle. Dynamic mechanical analysis (DMA) in tension was conducted on an RSA-G2 DMA (TA Instruments) in the linear viscoelastic region of each sample at a strain amplitude of 0.05%, frequency of 1 Hz, and at a heating rate of 10 °C/min from room temperature to 180 °C. T_g was reported as the peak in the tan δ curve and was compared to the T_g measured via DSC to check for any differences in the observed behavior. The values were consistent for all systems and differed by ≈10 °C which is typical between the two tests. The storage modulus in the glassy region was compared to the measured elastic modulus for all films.

Transmission electron microscopy (TEM) images of MWCNT dispersion and morphology were obtained by microtoming cured samples (80-100 nm) and observing them using a JEOL JSM7500F and a JEOL JEM-2010 operated at 60-200 kV.

Transmission optical microscopy (TOM) images of filler dispersion were obtained by polishing cured samples (100-200 μm) and observing the thin sections under an Olympus BX60 microscope with a Canon Mark 2 Digital Camera.

Four-point-probe conductivity measurements were performed on free-standing P-MWCNT and ZnO/P-MWCNT films with an Agilent Digital Multimeter (Agilent Technology, US) with a tip spacing of 1.6 mm. The electrical conductivity of epoxy composite thin films was measured using a four-point-probe (Signatone, SP4-40045TBY) on a resistive stand (Signatone, Model 302), which is lowered onto the film and a high impedance current source (Keithley 6221) was connected to the outer two probes. A voltmeter (Keithley 2000) was used to measure the voltage drop across the inner two probes. The conductivity was calculated by using the formula:

$$\sigma = \frac{1}{\frac{\pi}{ln\,2} \cdot \frac{V}{I} \cdot t \cdot k} \tag{1}$$

where σ is the electrical conductivity (S/m), V is the voltage drop measured across the inner two probes, I is the current through the outer two probes, t is the thickness of the film being measured, and k is a correction factor that depends on the diameter and thickness compared to the probe spacing. The thickness of the films was measured with a micrometer (Mitutoyo, 293-340) at the location of contact.

Tensile tests were conducted on a screw-driven Instron 4411 test fixture with a 2.5 kN load cell (MTS) at a loading rate of 5 mm/min under ambient test conditions according to ASTM D638-14 [334]. Thin film tensile samples were prepared by punching out dogbones with a cutting die that conforms to the geometry specified in ASTM D1708-13

[335]. The linear displacement during testing was measured via a laser extensometer (MTS LX1500) that measures the distance between two pieces of reflective tape. The recorded load and displacement values were normalized by the initial cross-sectional area and gage length, respectively, and then plotted as engineering stress versus engineering strain. Young's modulus was defined as the slope of the initial linear portion of the curve. Tensile strength and percent elongation were reported as the maximum stress experienced and the strain at break, respectively. Average values with standard deviations were reported from at least 5 specimens per sample tested.

4.3 Results and discussion

4.3.1 Dispersion characterization in cured epoxy

TOM and TEM were used to observe the dispersion state of P-MWCNT, O-MWCNT, ZnO/P-MWCNT, and ZnO/O-MWCNT epoxy composite thin films at different length scales to ensure a homogenous dispersion is truly representative of the bulk as seen in Figure 33 and Figure 34.

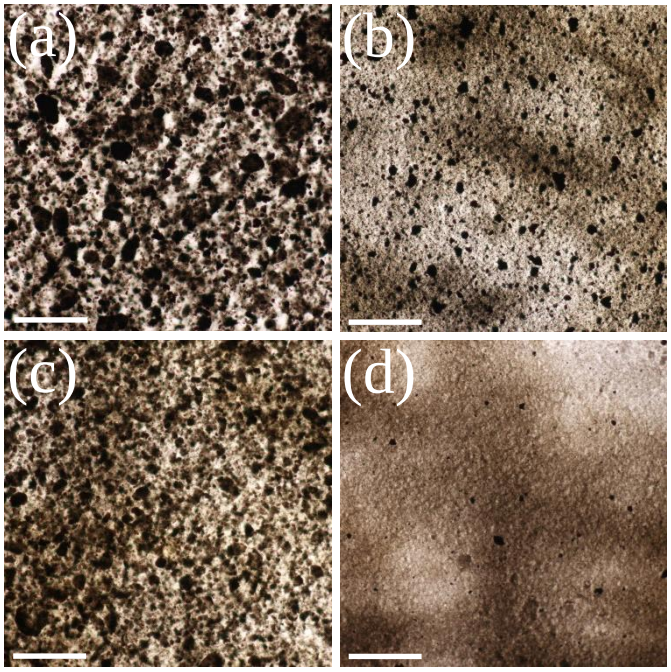

Figure 33. TOM of polished thin sections (≈50-75 μm) of cured epoxy composites containing (a) P-MWCNTs, (b) ZnO/P-MWCNTs, (c) O-MWCNTs, and (d) ZnO/O-MWCNTs with scale bars = 125 μm [302].

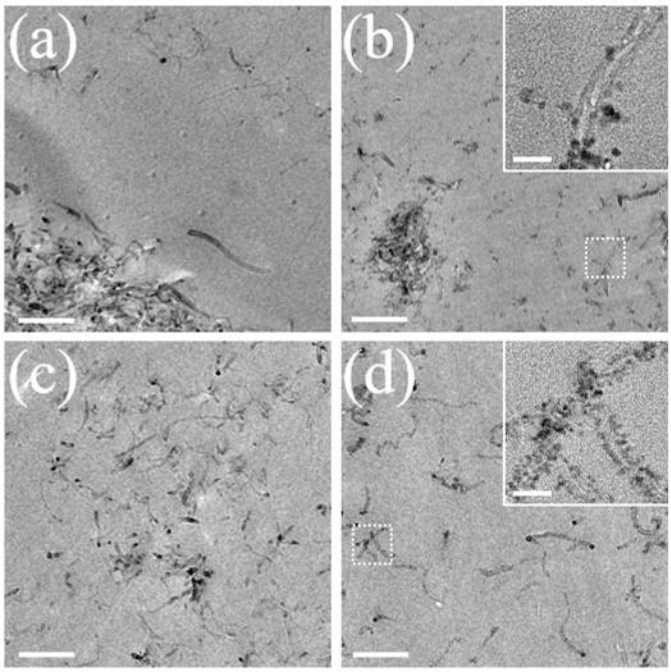

Figure 34. TEM of microtomed thin sections (≈60-80 nm) of epoxy composites with (a) P-MWCNTs, (b) ZnO/P-MWCNTs, (c) O-MWCNTs, and (d) ZnO/O-MWCNTs with scale bars = 250 nm. Insets in (b) and (d) show high magnification TEM of ZnO/P-MWCNTs with dissociated ZnO QDs and ZnO/O-MWCNTs with surface-bound ZnO QDs, respectively, with scale bars = 25 nm [302].

In the epoxy systems containing P-MWCNTs, O-MWCNTs, and ZnO/P-MWCNTs, MWCNT aggregation can be clearly seen in the TOM micrographs. At a smaller length scale, the TEM micrographs reveal that for the P-MWCNT system, aggregated, resin-rich, and exfoliated regions are present (Figure 34a). In the O-MWCNT system, they appear to be much better exfoliated to a greater degree than the P-MWCNT system when looking at the TEM micrograph (Figure 34c). However, when the TOM image is observed, aggregation, albeit to a lesser degree and size, is apparent (Figure 33a and Figure 33c). For the ZnO/P-MWCNT system, the aggregates present in the TOM

observation are smaller and less concentrated than those in the unfunctionalized systems (Figure 33b). However, under TEM, the ZnO QDs that previously decorated the surface of the P-MWCNTs when in MeOH have dissociated from the surface and coalesced to form large agglomerates in epoxy (Figure 34b), which are likely the particles seen in the TOM image. Upon closer inspection, the P-MWCNTs do not appear to have aggregated in epoxy and are still partially decorated by ZnO QDs (Figure 35 and Figure 36).

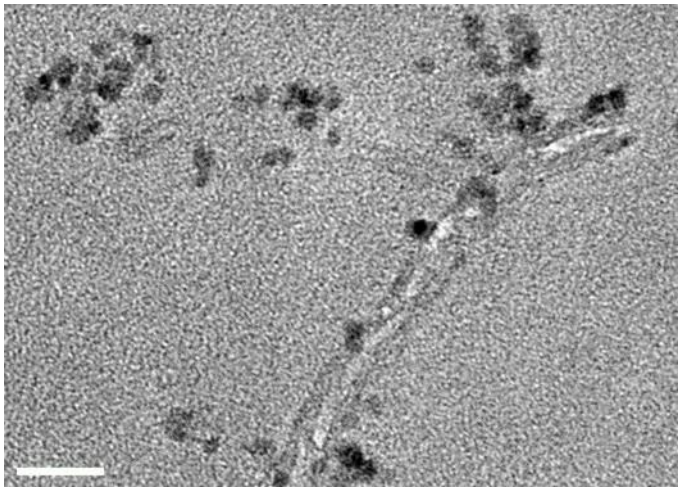

Figure 35. High resolution TEM micrograph of ZnO/P-MWCNT in cured epoxy with scale bar = 25 nm. Note the poor decoration of ZnO QDs on the P-MWCNT surface and the clusters of ZnO QDs in the surrounding matrix [302].

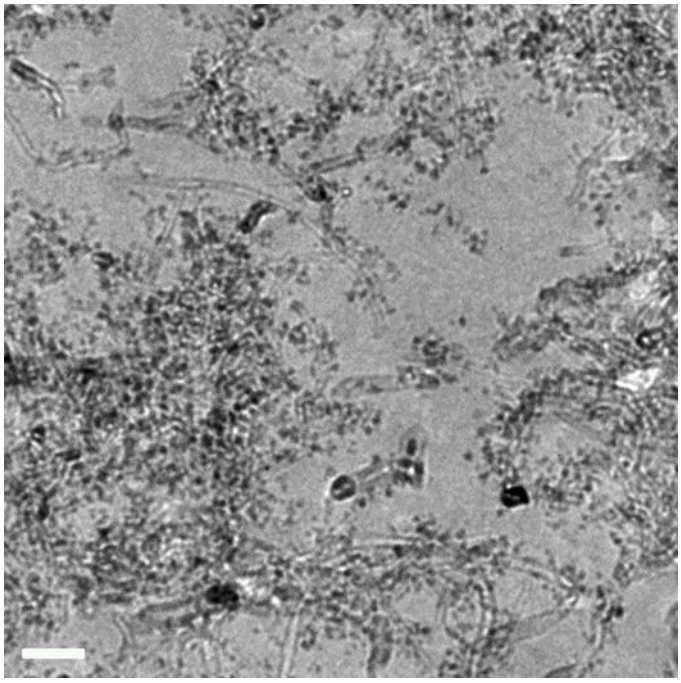

Figure 36. High magnification TEM micrograph of ZnO/P-MWCNTs in cured epoxy with scale bar = 50 nm. Note the large clusters of ZnO QDs in the surrounding matrix [302].

For the epoxy/ZnO/O-MWCNT system, very few aggregates are visible in the TOM image (Figure 33d). Under TEM, the ZnO/O-MWCNTs are clearly well-exfoliated compared to the other three systems (Figure 34d). More importantly though, the ZnO QDs are still bound to the surface of the O-MWCNTs and have not disassociated as in the epoxy/ZnO/P-MWCNT case (Figure 37 and Figure 38).

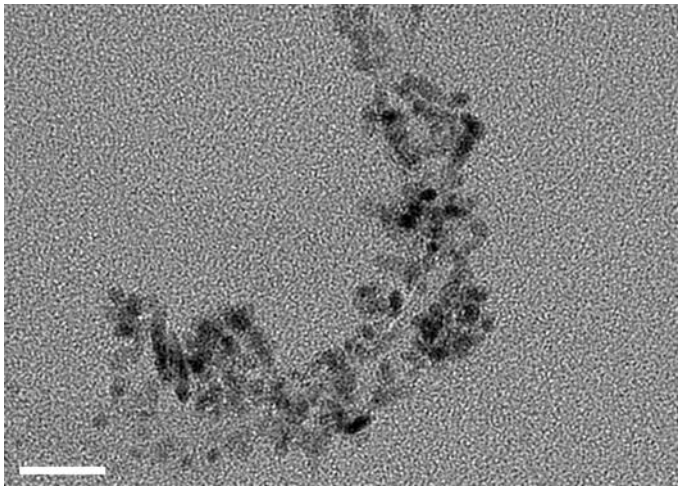

Figure 37. High resolution TEM micrograph of ZnO/O-MWCNT in cured epoxy with scale bar = 25 nm. Note the decoration of ZnO QDs on the O-MWCNT surface with no observable clustering of ZnO QDs in the surrounding matrix [302].

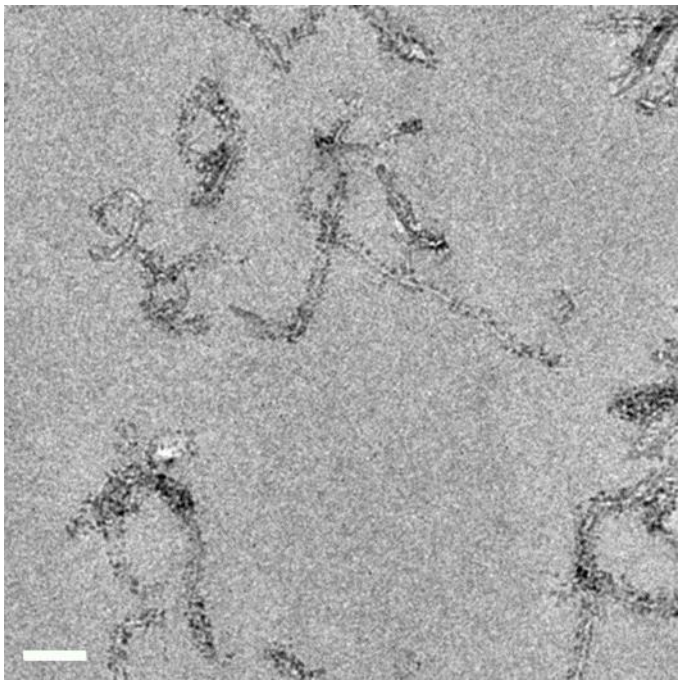

Figure 38. High magnification TEM micrograph of ZnO/O-MWCNTs in cured epoxy with scale bar = 50 nm. Note the well-decorated O-MWCNTs and the absence of ZnO QDs clusters [302].

4.3.2 Thermal and dynamic mechanical behavior

DSC and DMA were conducted on the neat and epoxy systems to ensure that the films were processed to the same degree of cure and maintained a consistent T_g. The T_g of the films was reported as the inflection point on the 2nd heating cycle with DSC and the peak of the tan δ curve with DMA on the 1st heating cycle. It is desirable that the T_g remain unaffected by the introduction of functionalized P-MWCNTs. Based on the tabulated DSC values in Table 7, the films appear to exhibit nearly the same T_g. However, the values from DMA suggest that the epoxy/O-MWCNT system did not completely cure or had an improper stoichiometric ratio.

Table 7. T_g of neat and epoxy composite thin films reported from DSC and DMA measurements [302].

Samples	T_g [°C by DSC]	T_g [°C by DMA]
Neat Epoxy	135	155
Epoxy/P-MWCNT	136	145
Epoxy/O-MWCNT	133	139
Epoxy/ZnO/P-MWCNT	134	144
Epoxy/ZnO/O-MWCNT	134	150

The most likely reason for this drop in T_g is an improper stoichiometric ratio between epoxide and amine groups due to the absorption of curing agent onto the O-MWCNT surface during the curing process, resulting in lower crosslink density. This phenomenon may also occur in the other MWCNT-containing systems, however, to a lesser degree than for the O-MWCNT system. The DSC curves in Figure 39 indicate that there is no difference, thermally, between the samples.

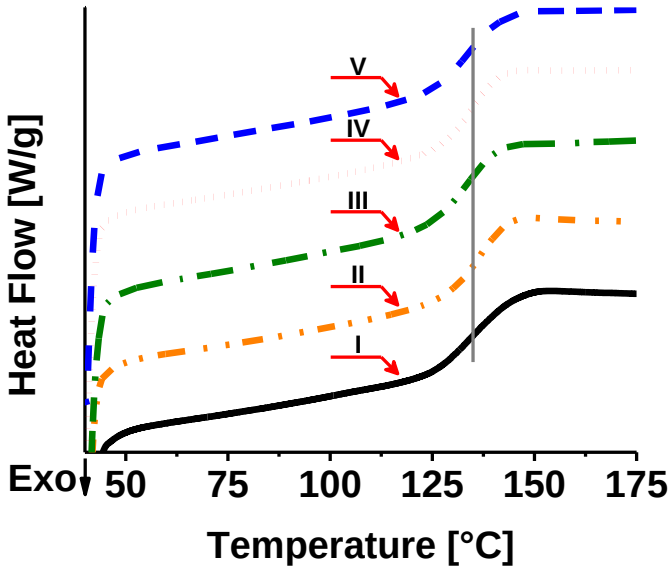

Figure 39. Second heating cycle of neat and epoxy composite thin films via DSC at a ramp rate of 10 °C/min. (I) Neat epoxy, (II) Epoxy/P-MWCNT, (III) Epoxy/O-MWCNT, (IV) Epoxy/ZnO/P-MWCNT, (V) Epoxy/ZnO/O-MWCNT [302].

The storage modulus and tan δ of the neat and epoxy composite thin films, which are defined as the ability of a material to store elastic energy and its dampening ability, respectively, are plotted versus temperature in Figure 40. The reported T_g values of the

films are less consistent than the DSC values, likely due to the aforementioned mechanism.

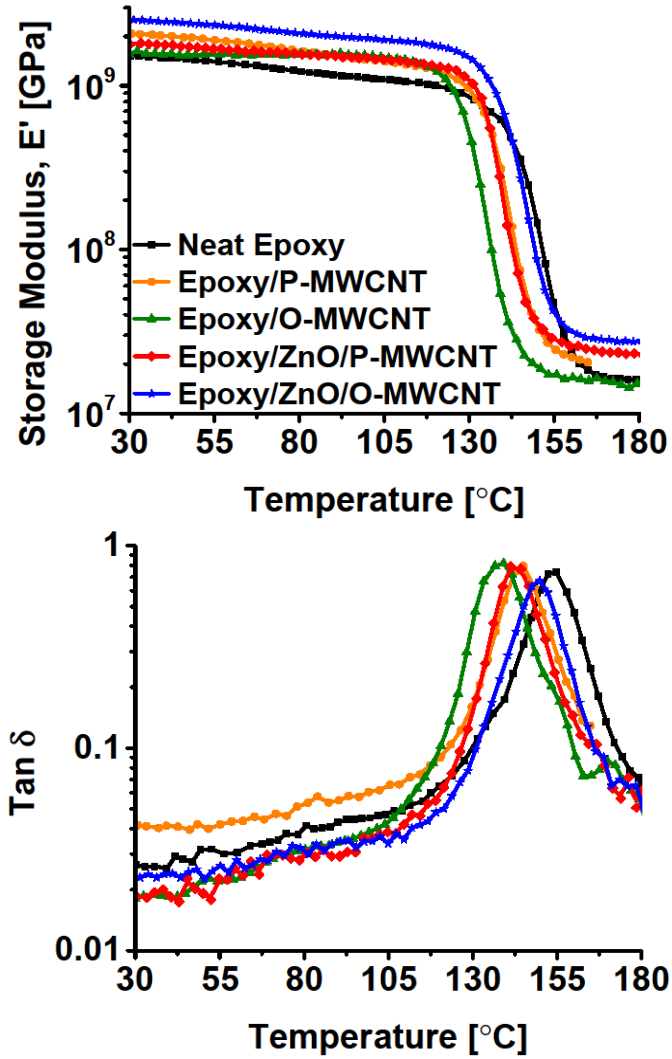

Figure 40. DMA spectra (E' and tan δ) of neat and epoxy composite thin films at a ramp rate of 3 °C/min [302].

It should be noted that the rubbery plateau modulus of the epoxy/O-MWCNT system is lower than those of the other samples, lending further credence that curing agent is absorbed by O-MWCNTs during cure. Furthermore, the system with P-MWCNTs exhibits a glassy storage modulus above and a T_g below that of the neat epoxy, which are likely due to frictional forces or mechanical interlocking between P-MWCNTs resulting in improved stress transfer and the absorption of curing agent resulting in incomplete cure.

4.3.3 Electrical conductivity

To understand the electrical conductivity behavior of the epoxy composites, it is important to first learn about the intrinsic conductivity values of P-MWCNT and ZnO/P-MWNCT first. The sheet conductivity versus thickness of spin-coated P-MWCNT and ZnO/P-MWCNT thin films was measured with a four-point probe and is plotted in Figure 41. In general, sheet conductivity increases as film thickness increases.

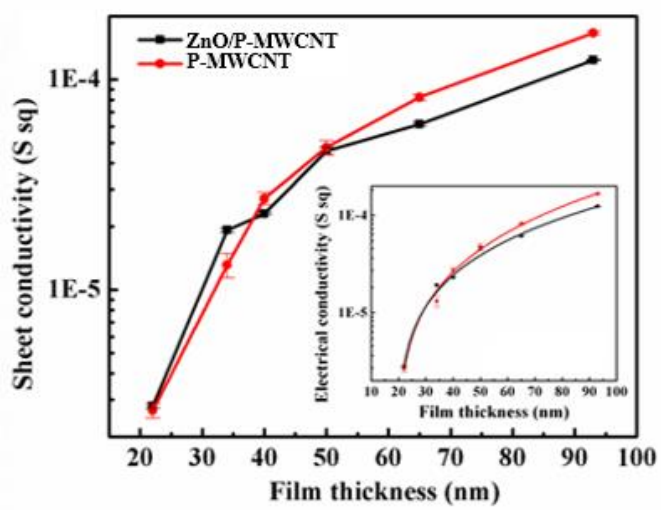

Figure 41. Sheet conductivity of P-MWCNT and ZnO/P-MWCNT thin films before and after the removal of ZnO nanoparticles [302].

Electrical percolation is observed at around the same critical thickness for both films (inset in Figure 41). At a film thickness up to twice the diameter of a MWCNT (<50 nm) the sheet conductivity of the P-MWCNT thin films is slightly lower than that of the ZnO/P-MWCNT film. This is likely due to incomplete formation of a percolated network by P-MWCNTs alone. When thicker films are tested, as expected, the P-MWCNT thin films exhibit higher sheet conductivity than ZnO/P-MWCNT films because of reduced cross-junction resistance [336]. At a thickness of 90 nm, the DC conductivities of P-MWCNTs and ZnO/P-MWCNTs are 1,790 S/m and 1,340 S/m, respectively. As anticipated, the DC conductivity of O-MWCNTs (66 S/m) is around 30x lower than P-MWCNTs (1,790 S/m). The small reduction in conductivity for ZnO/P-MWCNTs suggests that they are still able to form an electrically percolated network in epoxy.

The electrical conductivities of the neat and composite thin films were measured with a four-point probe. A current source was used to supply various levels of DC current through the two outer probes in the four-point probe, which the voltage drop across the two inner probes was measured with a multimeter. The recorded values were used to calculate the conductivity (S/m) according to Equation (1. The electrical conductivity values of the epoxy composite thin films are presented in Figure 42 along with other reported literature values for MWCNTs above their percolation thresholds [29, 99, 158].

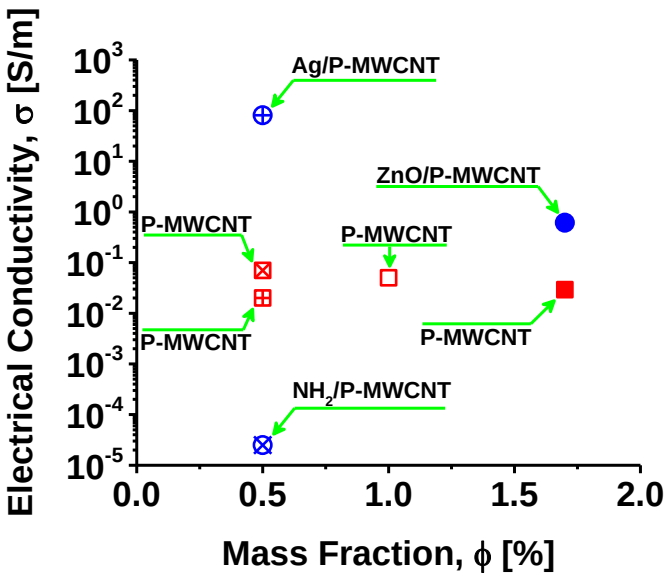

Figure 42. Electrical conductivities of P-MWCNT and ZnO/P-MWCNT composite films, along with other literature values [302].

The films containing O-MWCNTs were observed to be non-conductive; their conductivity is likely at or below the limit of our instruments. However, the films containing P-MWCNTs were observed to be conductive. In particular, the film containing

ZnO/P-MWCNTs exhibits an electrical conductivity that is an order of magnitude greater than previous systems studied. The other films exhibit conductivities comparable to those in the literature [29]. The significant increase in the electrical conductivity for the ZnO/P-MWCNT system may be due to the presence of semi-conductive ZnO QDs bound to the P-MWCNT surface as compared to the plain P-MWCNTs. CNTs are known to have defects present in their structure that act as scattering sites, which reduce the mean free path of electrons and the number density of charge carriers, leading to decreased electrical conductivity. Tightly bound ZnO QDs on the surface of P-MWCNTs may reduce the contact resistance of P-MWCNT junctions and increase the number density of charge carriers in epoxy by suppressing the effect of surface defects on electron scattering, resulting in improved electrical conductivity [62, 158]. When P-MWCNTs, which act as electron conductors, are hybridized with ZnO QDs, which suppress the scattering of electrons at surface defects, fast and efficient interfacial charge transfer is possible as evidenced by a decrease in the semicircle size in electrochemical impedance spectroscopy [62]. Furthermore, the decoration of P-MWCNTs with ZnO QDs may facilitate ballistic transport of electrons between adjacent tubes by increasing their mean free path [337]. The increased electrical conductivity of films containing ZnO/P-MWCNTs compared to P-MWCNTs may also be due to the improved dispersion whereby the percolation threshold is significantly reduced, resulting in the formation of a percolated network at a much smaller concentration. Moreover, the detachment of ZnO QDs from the surface may also facilitate the earlier formation of a percolated network. The lowering of the percolation threshold compared to the P-MWCNT system allows for greater enhancement

of the electrical conductivity. Finally, it appears that any oxidation of MWCNTs, regardless of surface functionalization, results in a loss of conductivity.

4.3.4 Tensile performance

The fabricated thin films were machined to a standardized geometry with a cutting die (ASTM D1708-13) to ensure that comparisons of the mechanical behavior between film systems are valid [335]. Once machined, the specimens were subjected to tensile loading rates of 5 mm/min on a UTM with a laser extensometer to measure the gage displacement. Engineering stress vs. engineering strain curves were plotted (Figure 43) from the generated data and E, σ_{UT}, and ε_B were tabulated (Table 8) [334].

Table 8. Tensile properties (Young's modulus, tensile strength, and percent elongation) of neat and epoxy composite thin films tested on a UTM at a loading rate of 5 mm/min [302].

Samples	E [GPa]	σ_{UT} [MPa]	ε_B [%]
Neat Epoxy	2.71 ± 0.04	51 ± 5	2.7 ± 0.4
Epoxy/P-MWCNT	3.01 ± 0.04	41 ± 10	1.5 ± 0.4
Epoxy/O-MWCNT	2.53 ± 0.09	41 ± 13	1.8 ± 0.7
Epoxy/ZnO/P-MWCNT	3.59 ± 0.12	61 ± 1	3.0 ± 0.2
Epoxy/ZnO/O-MWCNT	4.10 ± 0.09	62 ± 8	3.0 ± 0.8

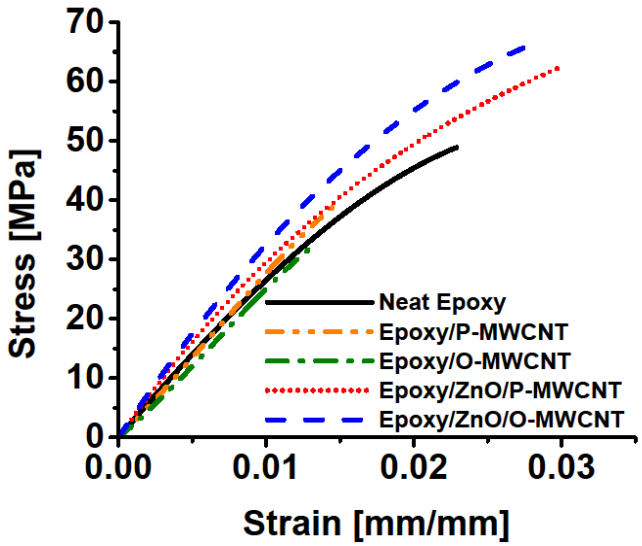

Figure 43. Tensile engineering stress vs. engineering strain curves for neat and epoxy composite thin films [302].

The concentration of MWCNTs is kept at 1.7 wt.%. The addition of P-MWCNTs improves modulus, but embrittles the composite as can be seen in the ductility reduction and large standard deviation of tensile strength. When O-MWCNTs are dispersed in epoxy, the modulus, tensile strength, and strain at break decrease. This is most likely because of O-MWCNT aggregation and undercuring of epoxy due to absorption of the curing agent during the crosslinking reaction.

For the composite samples, the Epoxy/ZnO/P-MWCNT film exhibited significantly enhanced modulus and tensile strength as compared to the Epoxy/P-MWCNT film. Even though ZnO QDs were mostly detached from P-MWCNTs, they appear to have facilitated P-MWCNT dispersion in epoxy resulting in better stress transfer and improved interfacial bonding with the epoxy matrix. As expected, when ZnO/O-MWCNTs are dispersed in epoxy, the modulus is further improved to 50% higher

than that of neat epoxy. It should be noted that the glassy storage modulus (Fig. 9) follows the trends of the tensile moduli reported here. The tensile strength is likewise improved and is likely the result of strong bonding between ZnO QDs and the O-MWCNT surface, which further promotes bonding to the epoxy matrix. The exact mechanism responsible for the significantly enhanced tensile properties in Epoxy/ZnO/P-MWCNT and Epoxy/ZnO/O-MWCNT composites is still not fully understood and is subject to future work whereby the interfacial adhesion of epoxy matrix with ZnO/P-MWCNTs and ZnO/O-MWCNTs will be determined.

As stated above, the dispersion of ZnO/P-MWCNTs via a simple and effective functionalization method in an epoxy matrix has significantly improved not only the tensile properties, but also the electrical conductivity of an epoxy composite, without compromising T_g or processability. On the other hand, the presence of O-MWCNTs in the cured system exhibited a 15 °C drop in T_g, likely due to absorption of the curing agent, leading to reduced crosslink density [124]. Furthermore, the systems with O-MWCNTs and ZnO/O-MWCNTs exhibit insulative behavior at the same content of O-MWCNTs. It appears that the favorable electrostatic interaction between ZnO QDs and MWCNTs improves their dispersion, resulting in significantly enhanced elastic modulus without a reduction in T_g. The increased tensile strength in the ZnO-functionalized systems is likely due to long-range electrostatic interactions between positively charged ZnO QDs and negatively charged MWCNTs that redistributes stress and shields pre-existing defects [37, 81, 104, 332]. During uniaxial tension testing, ZnO QDs act as an electrostatic tether,

diminishing the tendency of the MWCNTs to slip or pullout from the matrix, thereby causing an increase in tensile strength.

The *in situ* growth of such a large number of ZnO QDs significantly increases the available anchoring sites for the epoxy matrix to bond with MWCNTs to achieve better adhesion with the matrix and higher resistance to tube pullout. Furthermore, it is clearly observed that epoxy/O-MWCNT, whether ZnO-functionalized or not, are nonconductive. This is likely the result of the destruction of electron transfer between O-MWCNTs during the functionalization process. However, for epoxy/ZnO/P-MWCNT composites, the electrical conductivity is higher than that observed in previous studies by an order of magnitude at a comparable concentration. Therefore, it is evident that functionalization of P-MWCNTs by ZnO nanoparticles is favored over other known approaches to improve tensile properties and electrical conductivity of epoxy. Previous attempts at fabricating multifunctional epoxy composites without sacrificing T_g, tensile properties, or electrical conductivity have been unsuccessful. As is usually reported in the literature, when nanofillers are dispersed in the matrix only one of the aforementioned properties is improved while the others decrease. The common reasons given for this behavior are: plasticization of the matrix via the inclusion of nanofillers, reduced crosslink density of the cured system due to adsorption of the curing agent or crosslinking with the nanofillers, increased defect concentration on nanofiller surface via oxidation and chemical functionalization. In this work, we used a new physical functionalization method to fabricate multifunctional epoxy composites that exhibit none of the previously mentioned drawbacks commonly reported in the literature.

The objective of this work has been to fabricate a robust multifunctional epoxy composite system with improved tensile properties and electrical conductivity at a relatively low nanofiller concentration without sacrificing T_g. To date, most literature results only show meaningful improvement in either conductivity or tensile properties of polymers, not both, despite significant efforts. Furthermore, the improvements in electrical conductivity, while not insignificant, are sufficient for electrostatic charge dissipation (10^{-4} S/m) and EMI shielding (≈10 S/m) [40, 60]. A complete understanding of the role(s) of ZnO QDs and MWCNTs is important when designing mechanically strong and electrically conductive epoxy composites for high performance aerospace structural applications. The stiff and conductive epoxy thin films prepared here, which can be manufactured at low cost and with a simple *in situ* modification step, are ideal for structural engineering applications, especially interleaves in CFRCs using VaRTM. The films are also good candidates for service in applications requiring low-density, mechanically strong, and electrically conductive materials that can be easily processed using conventional epoxy manufacturing techniques.

Other metallic nanoparticles should be investigated in order to understand the role of QD chemistry on: 1) the interfacial adhesion with the matrix and the CNT surface, 2) the improvement of the electrical conductivity of the functionalized CNT, and 3) the participation of QD-decorated CNTs in fracture toughening through various mechanisms. The toughening mechanisms in epoxy composite thin films containing ZnO/P-MWCNTs and ZnO/O-MWCNTs with and without additional toughening particles are currently being systematically investigated and will be reported shortly.

4.4 Conclusions

The tensile properties and electrical conductivities of an epoxy resin filled with a hybrid of ZnO-functionalized P-MWCNTs or O-MWCNTs were investigated. Epoxy/ZnO/MWCNT composite thin films were successfully prepared in a robust and scalable fashion. The composite thin films containing ZnO and P-MWCNT exhibit high conductivity and significantly improved elastic modulus not generally observed in the literature, without compromising thermal stability or processability. The functionalization of P-MWCNTs and O-MWCNTs leads to a system of well-dispersed MWCNTs in epoxy. This results in improved tensile properties and also a significant improvement in electrical conductivity compared to previously reported values.

CHAPTER V

EFFECT OF PA ADDITION ON MECHANICAL AND ELECTRICAL PROPERTIES OF HYBRID EPOXY NANOCOMPOSITE THIN FILMS CONTAINING MWCNTS

5.1 Introduction

Nylon has been used in epoxies to effectively improve their ductility and toughness, while decreasing their stiffness and T_g [29, 73, 82, 256]. White and Sun et al. studied the effect of PA on the mechanical, electrical, and fracture toughness behavior of CNT/epoxy nanocomposites [29, 73, 74]. Sun et al. observed that the integration of sulfanilamide-functionalized SWCNTs with PA in an epoxy matrix synergistically improved the modulus, tensile strength, and toughness of the bulk nanocomposite [73]. The functionalized SWCNTs were observed to be well-exfoliated in the epoxy matrix, which led to the improvement in mechanical properties. White et al. dispersed pristine MWCNTs with PA in epoxy to determine if the bulk properties of PA/MWCNT/epoxy composites would be reproduced at lower cost with easier processibility [29]. MWCNTs were unable to significantly improve the fracture toughness of epoxy, however, the tensile strength, percent elongation, and electrical conductivity were significantly improved [29]. When PA microparticles were added, they were observed to help improve the dispersion of MWCNTs by breaking apart aggregates. The ternary composite exhibited a delayed electrical percolation threshold, while the fracture toughness and strain at break were synergistically improved [29].

In the present study, preformed PA microparticles are introduced to hybrid epoxy composite films containing modified or unmodified MWCNTs to improve their fracture

toughness. However, in light of recent reports in the literature, the thermal, mechanical, and electrical behaviors are investigated and reported here. The effect of PA microparticles in ternary composite thin films is presented in the subsequent chapter. This approach takes advantage of the ability of PA to undergo severe plastic deformation, this suggests that epoxy composites containing these particles should exhibit improved ductility. Furthermore, previous reports have indicated that the presence of PA microparticles actually helps to break down MWCNT aggregates in epoxy, leading to improved toughness, while still maintaining an electrically conductive network. The findings of the present study will be presented in the following subsections.

5.2 Experimental

5.2.1 Materials

D.E.R.™ 354, a diglycidyl ether of bisphenol F (DGEBF) liquid epoxy prepolymer, donated by DOW Chemical, with an epoxide equivalent weight of 158 g/eq, was used as the matrix in this work. EPIKURE™ W, a diethyltoluene diamine (DETDA) curing agent, was donated by Momentive Specialty Chemicals Inc. (Columbus, OH), with an amine equivalent weight of 43.29 g/eq, and was used as the curing agent. MWCNTs were donated by Arkema with reported inner and outer diameters of 2-6 nm and 10-15 nm, respectively, length of 0.1-10 μm, >90 % carbon content, and a reported density of ≈2.1 g/cm^3. Zinc acetate dihydrate and KOH were purchased from Sigma-Aldrich and used as received. Acetone and MeOH were purchased from Macron Fine Chemicals and Sigma-Aldrich and used as received. Release paper composed of a cellulose-based paper

coated with polydimethylsiloxane (PDMS) was donated by Experia Specialty Solutions. DGEBF and D.E.H.™ 615 were used to embed thin films for electron microcopy. All materials were dried at ≈70 °C overnight in a vacuum oven and used as received with the exception of MWCNTs, which were subjected to mild oxidation according to previous reports [73, 81, 104, 124, 332].

5.2.2 Pretreatment of MWCNTs

250 mg of P-MWCNTs were added to a concentrated mixture of sulfuric (45 mL) and nitric acid (15 mL) at a 3:1 volume ratio and ultrasonicated in a sonication bath (Branson 2510) for 2 h at 25 °C. Next, 190 mL of DI-H_2O was added to hinder further oxidation and the solution was sonicated for another 1 h at 25 °C. After oxidation, the MWCNTs were isolated with a PVDF filter membrane (Millipore, Durapore, 0.45 μm pore size) under vacuum. The O-MWCNTs were washed four times with DI-H_2O during the filtration process to remove any trace of acid residue. Then, the solution was washed with MeOH four times, and the O-MWCNTs were collected and resuspended in MeOH at a concentration of 1 mg/mL using ultrasonication for 1 h.

5.2.3 Synthesis of ZnO/MWCNTs

The synthesis of ZnO nanoparticles in MeOH is reported elsewhere [77, 313]. The procedure to prepare ZnO-functionalized MWCNTs is similar to the above method. P-MWCNTs (160 mg) and O-MWCNTs (160 mg) in MeOH were added to a flask and sonicated for 30 min to obtain a homogenous solution. Next, KOH (1 g) was added to the flask and dissolved via sonication for 10 min. Concurrently, zinc acetate dihydrate (1.96

g) was added to a separate flask with MeOH and dissolved via sonication for 5 min. After both reactants were completely dissolved, the solutions were mixed at 60 °C while stirring at 300 RPM to initiate the reaction. Then, the solution was refluxed at 60 °C for 2 h to promote the growth of ZnO QDs. After initiation and growth, the ZnO/P-MWCNTs and ZnO/O-MWCNTs were filtered through a PVDF membrane (0.45 μm pore size) under vacuum with MeOH four times and then redispersed in MeOH via ultrasonication for 1 h. Their concentrations were determined by pipetting a predetermined amount of solution into an aluminum weighing dish and the weight recorded. Next, the solution was left in an oven overnight at 60 °C to slowly evaporate the solvent. Finally, the pan with dry ZnO/P-MWCNTs was weighed and the difference was divided by the initial solution volume to determine the concentration of ZnO/P-MWCNTs in MeOH.

5.2.4 Thin film composite preparation

DGEBF and DETDA were used as the matrix and hardener, respectively, to fabricate epoxy composite thin films. DGEBF (3.92 g) and DETDA (1.18 g) were added to a flask and degassed at 60 °C on a rotary evaporator under vacuum at 60-120 RPM for 30 min. The epoxy mixture was then B-staged in a preheated oven at 121 °C for 45 min to increase its viscosity for thin film processing. Once B-staged, the solution was poured onto an Elcometer 4340 Thin Film Coater preheated to 80 °C and cast at 5 mm/s to a thickness of 100-200 μm. Then, the film was placed in a preheated oven at 121 °C and cured for 2 h followed by a post-cure at 177 °C for 3 h. Composite films were fabricated according to the same procedure with a slight alteration. A PA/ZnO/P-MWCNT composite film was prepared by sonicating a predetermined amount of ZnO/P-MWCNTs

in MeOH in a flask for 30 min. A specific amount of PA microparticles were dispersed in an acetone solution in a separate flask via ultrasonication for 15 min. Next, the two solutions were mixed together and ultrasonicated for a further 15 min. DGEBF and DETDA were dissolved in acetone via sonication for 5 min and were subsequently added to the PA/ZnO/P-MWCNT MeOH/acetone solution with a final MeOH/acetone vol.%/vol.% of 2/1. The mixed composite solution was then sonicated for 15 min followed by removal of the solvent using a rotary evaporator at 60 °C for 15 min at 60-120 RPM. Next, the viscous resin was degassed in a vacuum oven at 80 °C for 2 h to ensure the complete removal of solvent. Then, the resin was carefully removed with a spatula and placed on a thin film coater preheated to 80 °C and cast at 5 mm/s to a thickness of 100-200 μm. For the O-MWCNT systems, the thin film coater was preheated to 100 °C due to their increased viscosity compared to the P-MWCNT systems. Once cast, the films were placed in an oven and cured at 121 °C for 2.75 h followed by a post cure at 177 °C for 3 h. The curing time and temperature were held constant at 2.75 h at 121 °C followed by 3 h at 177 °C to ensure the same degree of cure for all systems.

5.2.5 Characterization

Differential scanning calorimetry (DSC) was conducted with a DSC Q20 (TA Instruments) from 30 °C to 180 °C with a ramp rate of 10 °C/min to determine the glass transition temperature (T_g) of the epoxy systems. The T_g was defined as the point of inflection during the second heating cycle. Dynamic mechanical analysis (DMA) in tension was conducted on an RSA-G2 DMA (TA Instruments) in the linear viscoelastic region of each sample at a strain amplitude of 0.05%, frequency of 1 Hz, and at a heating

rate of 10 °C/min from room temperature to 180 °C. T_g was reported as the peak in the tan δ curve and was compared to the T_g measured via DSC to check for any differences in the observed behavior. The values were consistent for all systems and differed by ≈10 °C which is typical between the two tests. The storage modulus in the glassy region was compared to the measured elastic modulus for all films.

Transmission optical microscopy (TOM) images of filler dispersion were obtained by polishing cured samples (100-200 μm) and observing the thin sections under an Olympus BX60 microscope with a Canon Mark 2 Digital Camera.

Four-point-probe conductivity measurements were performed on free-standing P-MWCNT and ZnO/P-MWCNT films with an Agilent Digital Multimeter (Agilent Technology, US) with a tip spacing of 1.6 mm. The electrical conductivity of epoxy composite thin films was measured using a four-point-probe (Signatone, SP4-40045TBY) on a resistive stand (Signatone, Model 302), which is lowered onto the film and a high impedance current source (Keithley 6221) was connected to the outer two probes. A voltmeter (Keithley 2000) was used to measure the voltage drop across the inner two probes. The conductivity was calculated by using (1 and the thickness of the films was measured with a micrometer (Mitutoyo, 293-340) at the location of contact.

Tensile tests were conducted on a screw-driven Instron 4411 test fixture with a 2.5 kN load cell (MTS) at a loading rate of 5 mm/min under ambient test conditions according to ASTM D638-14 [334]. Thin film tensile samples were prepared by punching out dogbones with a cutting die that conforms to the geometry specified in ASTM D1708-13 [335]. The linear displacement during testing was measured via a laser extensometer

(MTS LX1500) that measures the distance between two pieces of reflective tape. The recorded load and displacement values were normalized by the initial cross-sectional area and gage length, respectively, and then plotted as engineering stress versus engineering strain. Young's modulus was defined as the slope of the initial linear portion of the curve. Tensile strength and percent elongation were reported as the maximum stress experienced and the strain at break, respectively. Average values with standard deviations were reported from at least 5 specimens per sample tested.

5.3 Results and discussion

5.3.1 Dispersion characterization in cured epoxy

TOM was used to observed the dispersion state of PA, PA/P-MWCNTS, PA/O-MWCNTS, PA/ZnO/P-MWCNTS, and PA/ZnO/O-MWCNTS in cured epoxy nanocomposite films as seen in Figure 44.

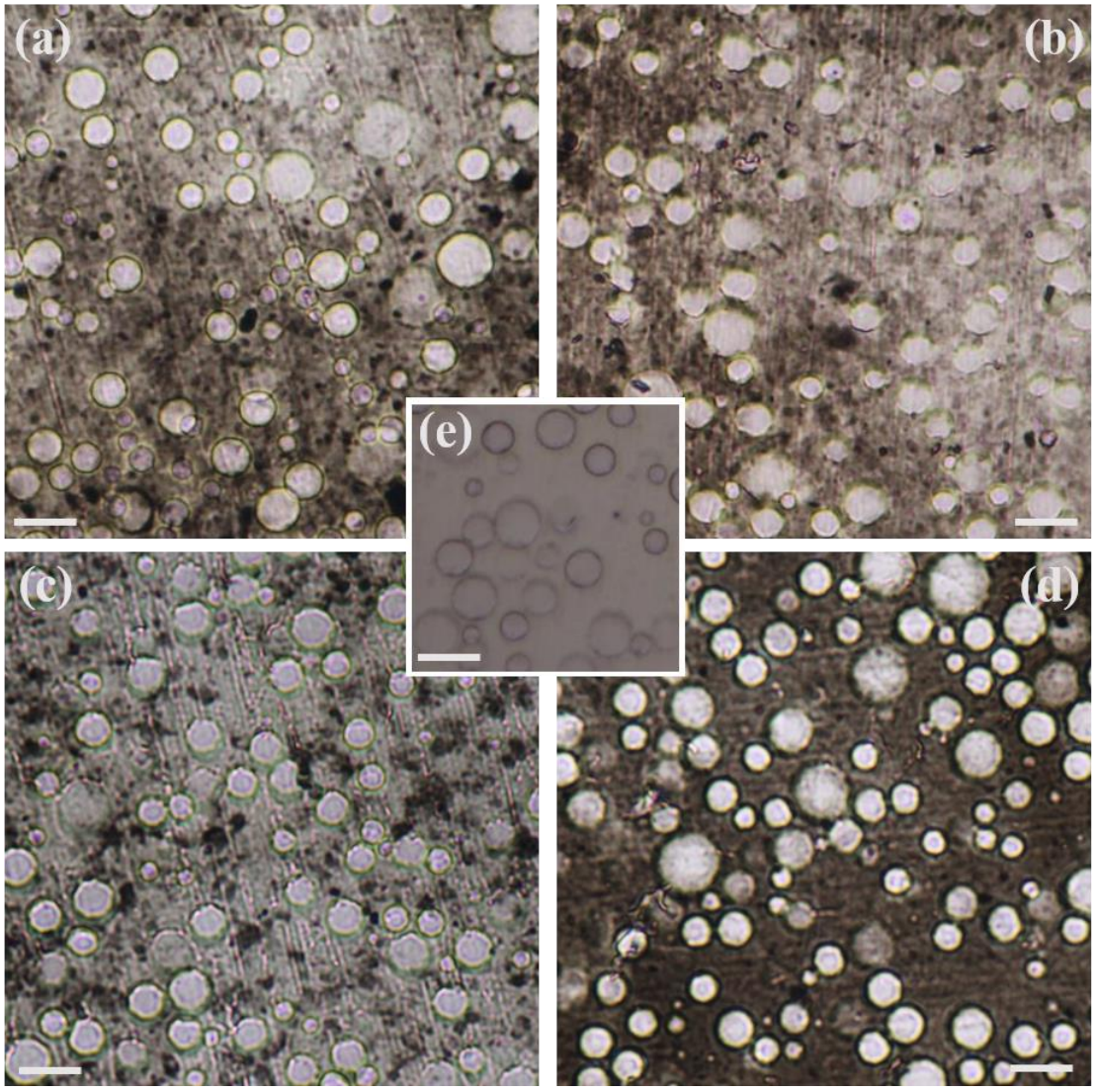

Figure 44. TOM of polished thin sections (≈50-75 μm) of cured epoxy composites containing (a) PA/P-MWCNTs, (b) PA/ZnO/P-MWCNTs, (c) PA/O-MWCNTs, (d) PA/ZnO/O-MWCNTs, (e) PA with scale bars = 10 μm.

In the PA/epoxy system (Figure 44e), the microparticles are observed to be ≈10 μm in diameter and are well-dispersed, given their extremely large size relative to the MWCNTs used in this study. However, aggregates can clearly be seen in the micrographs for the systems containing PA/P-MWCNTs (Figure 44a), PA/O-MWCNTs (Figure 44c), and to

a lesser degree for the systems containing PA/ZnO/P-MWCNTs (Figure 44b), and PA/ZnO/O-MWCNTs (Figure 44d). The aggregates appear to be reduced in size and number for the ZnO-functionalized MWCNTs as compared to the unfunctionalized MWCNTs. For comparison, Figure 45 presents the dispersion of P-MWCNTs in epoxy to illustrate the large size difference of the aggregates in the presence of PA.

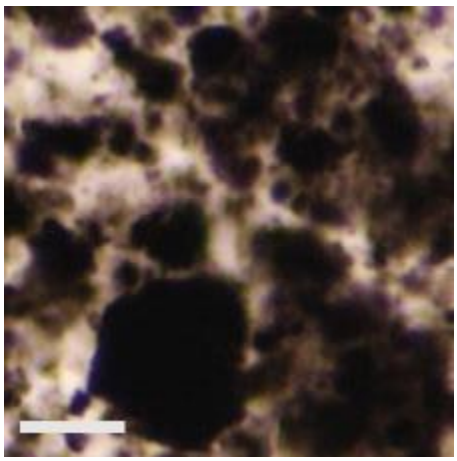

Figure 45. TOM of polished thin section (≈50-75 μm) of P-MWCNT/epoxy composite with scale bar = 10 μm.

The investigation of the morphology and dispersion of the ternary systems via TEM requires microtoming at cryogenic temperatures (cryotome) due to the relatively low T_g of PA (≈40 °C). It is expected that the presence of the PA may cause some level of hydrogen bonding between the ZnO QDs and the surface of the PA microparticles. For the case of ZnO/P-MWCNTs, ZnO QDs have been observed to dissociate from the MWCNT surface and aggregate (Figure 34, Figure 35, and Figure 36). In the presence of

PA, however, these large aggregates may be broken up and the individual QDs may be attracted to the PA surface and engage in hydrogen bonding. In the case of ZnO/O-MWCNTs where the QDs are more tightly bound to the oxidized surface, as evidenced by XPS in Section 3.3.1, the decorated tube surface may be attracted to the PA surface, rather than the QDs themselves. However, without further investigation, the above theories are pure speculation.

5.3.2 Thermal and dynamic behavior

DSC and DMA were conducted on the ternary systems to ensure that not only were the films fully cured, but that they also maintained a consistent T_g. The T_g of the films was reported as the inflection point on the 2nd heating cycle with DSC and the peak of the tan δ curve with DMA on the 1st heating cycle Table 9.

Table 9. T_g of neat and nylon-toughened epoxy films reported from DSC and DMA measurements.

Samples	T_g [°C by DSC]	T_g [°C by DMA]
Neat Epoxy	135	155
Epoxy/PA	133	NA
Epoxy/PA/P-MWCNT	132	NA
Epoxy/PA/O-MWCNT	134	NA
Epoxy/PA/ZnO/P-MWCNT	122	132
Epoxy/PA/ZnO/O-MWCNT	132	145

For the ternary systems containing PA microparticles, the T_g is expected to decrease, but surprisingly, no change is observed (Figure 46), with the exception of the system containing PA/ZnO/P-MWCNTs (according to DSC).

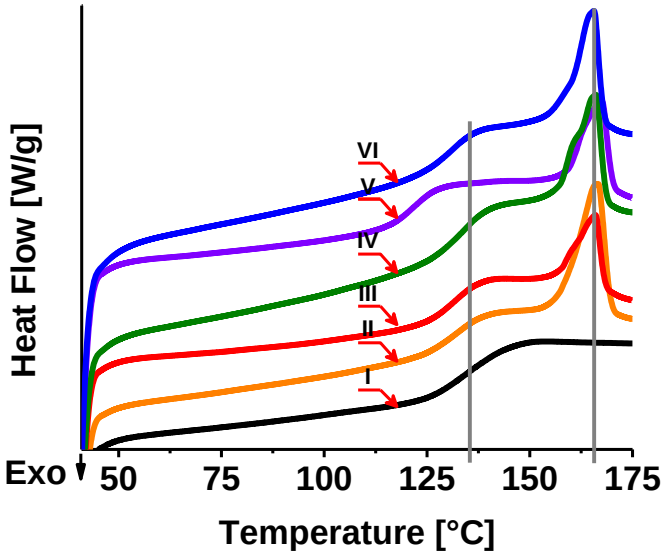

Figure 46. Second heating cycle of neat and nylon-toughened thin films via DSC at a ramp rate of 10 °C/min. (I) Neat epoxy, (II) Epoxy/PA, (III) Epoxy/PA/P-MWCNT, (IV) Epoxy/PA/O-MMWCNT, (V) Epoxy/PA/P-MWCNT, (VI) Epoxy/PA/ZnO/O-MWCNT.

Its T_g is reduced by ≈10 °C and could be due to the explanation given above, whereby the presence of PA imparts an attractive force to the ZnO QDs that have dissociated from the surface of P-MWCNTs. This attractive force may be strong enough to overcome the strong particle-particle interactions that exist between the ZnO nanoparticles causing the aggregates to break apart. The dispersed ZnO QDs may now decorate the surface of PA or remain in the epoxy matrix. The hydroxyl groups on the

ZnO surface may crosslink with the epoxide groups resulting in a change in the stoichiometric ratio resulting in reduced crosslink density and T_g.

The DMA spectra of Neat epoxy, Epoxy/PA/ZnO/P-MWCNT, and Epoxy/PA/ZnO/O-MWCNT are presented in Figure 47.

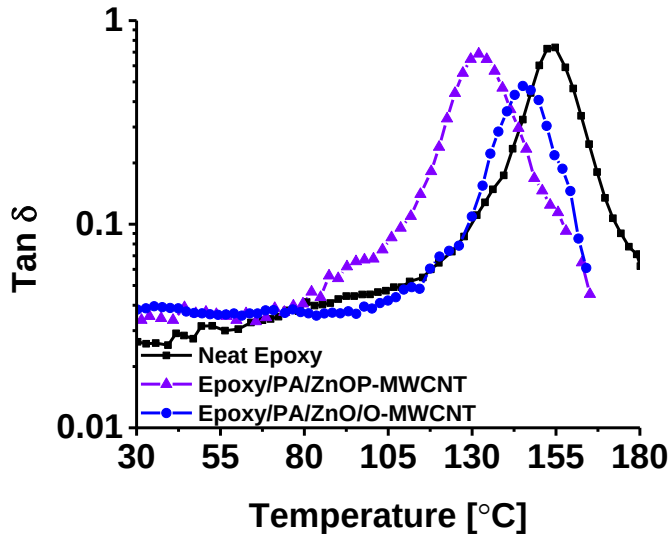

Figure 47. DMA spectra (tan δ) of neat epoxy and PA/ZnO/MWCNT/epoxy composite films at a ramp rate of 3 °C/min.

A drop of ≈10 °C is observed for the PA/ZnO/O-MWCNT/epoxy system, whereas a ≈20 °C drop is observed for the PA/ZnO/P-MWCNT/epoxy system.

5.3.3 Electrical conductivity

The electrical conductivities of the binary and ternary epoxy thin films were measured with a four-point probe, A current source was used to generate DC current

through the outer two probes in the four-point probe assembly, while the voltage drop across the two inner probes was measured with a very accurate multimeter. The recorded values were used to calculated the electrical conductivity (S/m) according to Equation (1). The conductivities of the neat epoxy and its composites are presented in Figure 48.

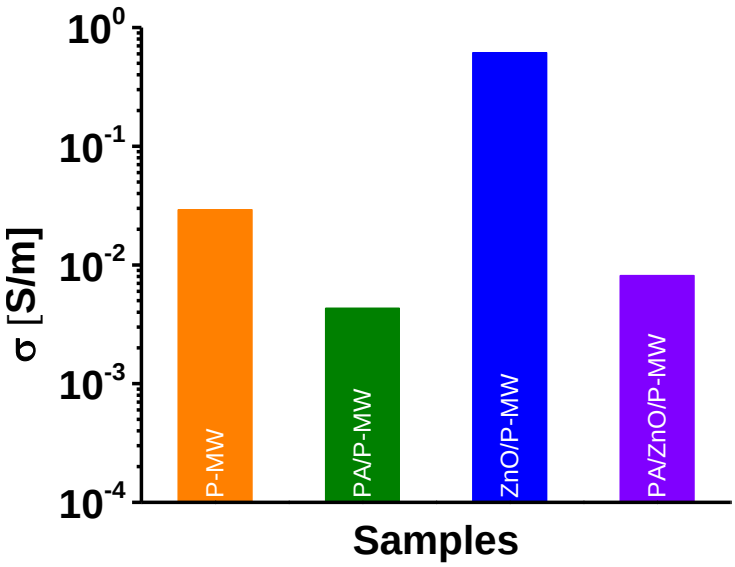

Figure 48. Electrical conductivities of conductive films. MWCNTs and PA were kept at 1.7 wt.% and 20 wt.%, respectively.

As stated earlier, the systems containing O-MWCNTs were observed to be non-conductive, based on the lower limit of the setup used. However, the films containing PA/P-MWCNTs and PA/ZnO/P-MWCNTs exhibited high electrical conductivities. While, the values are lower than that of their binary counterparts, they are nonetheless sufficient for antistatic coatings and potentially conductive thin films [60]. The reason for

the drop in electrical conductivity at when the concentration of MWCNTs is the same as in the binary systems is given as follows. It was previously reported that MWCNT aggregates were broken into smaller aggregates in the presence of PA microparticles causing a delay in the formation of a percolative network. The same argument can be made here, given the TOM micrographs presented in Section 5.3.1. The reason for the improved electrical conductivity of PA/ZnO/P-MWCNTs is again the same as stated in an earlier section, whereby the improved dispersion as a result of surface functionalization reduced the percolation threshold.

5.3.4 Tensile performance

The as-prepared thin films were machined to a standardized geometry with a steel cutting die in accordance with ASTM D1708-13 to ensure that valid comparisons between systems could be made [335]. After the microtensile specimens were prepared, they were subjected to uniaxial tension at a loading rate of 5 mm/min on a UTM with a laser extensometer for measuring the displacement in the gage section [334]. At least five specimens were tested for each sample. Engineering stress vs. engineering strain curves were plotted (Figure 49) from the generated data and E, σ_{UT}, and ε_B were tabulated (Table 10).

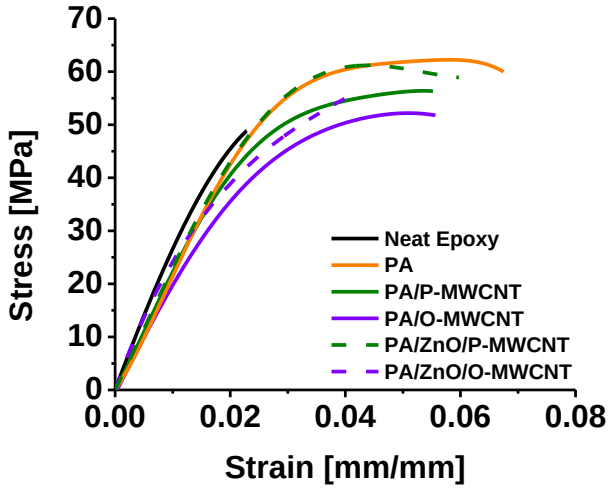

Figure 49. Tensile engineering stress vs. engineering strain curves for neat epoxy and ternary films.

Table 10. Tensile properties (Young's modulus, tensile strength, and percent elongation) of neat epoxy and ternary thin films tested on a UTM at a loading rate of 5 mm/min.

Samples	E [GPa]	σ_{UT} [MPa]	ε_B [%]
Neat Epoxy	2.71 ± 0.04	51 ± 5	2.7 ± 0.4
Epoxy/PA	2.44 ± 0.07	60 ± 2	6.1 ± 0.5
Epoxy/PA/P-MWCNT	2.41 ± 0.20	53 ± 5	4.3 ± 1.0
Epoxy/PA/O-MWCNT	2.33 ± 0.13	51 ± 4	5.4 ± 1.2
Epoxy/PA/ZnO/P-MWCNT	2.74 ± 0.35	59 ± 5	4.5 ± 2.1
Epoxy/PA/ZnO/O-MWCNT	2.75 ± 0.18	54 ± 4	4.1 ± 0.8

The concentrations of MWCNTs and PA are kept at 1.7 wt.% and 20 wt.% respectively. The addition of PA caused a reduction in the modulus (-10%), but improved

the tensile strength (15%) and ductility (126%) of the matrix. When PA is dispersed with P-MWCNTs into epoxy, the modulus decreases (-11%), the tensile strength remains, and the strain at break increases (59%). The addition of PA and O-MWCNTs to epoxy reduces the modulus (-14%), the tensile strengths remains, and the ductility increases (100%). In the ternary systems mentioned, the drop in modulus is likely due to the presence of a large number of soft thermoplastic particles, whereas the increased ductility is due to the ability of PA to undergo severe plastic deformation.

For the ternary samples containing functionalized MWCNTs, the Epoxy/PA/ZnO/P-MWCNT film exhibited no change in modulus, but enhanced tensile strength (13%) and strain at break (67%). The system containing PA/ZnO/O-MWCNTs exhibits similar behavior. The increased modulus is to be expected given the drastic improvement that was observed for the binary systems. This suggests that the reinforcement of the matrix due to the functionalized MWCNTs is able to counteract the large concentration of PA, which reduces the modulus of the matrix.

5.4 Conclusions

Ternary epoxy thin films containing ZnO-functionalized MWCNTs and PA microparticles were fabricated and their thermal, mechanical, and electrical behaviors were characterized as a function of filler type. The films were prepared with a simple two step approach whereby the degassed epoxy nanocomposite solutions were partially cured before being cast into thin films and subsequently cured. The hybrid films containing PA/P-MWCNTs and PA/ZnO/P-MWCNTs exhibited electrical conductivities high enough for anti-static films. The introduction of PA to the epoxy matrix resulted in a drop

in elastic modulus, which was not recovered when P-MWCNTs or O-MWCNTs were dispersed with them. However, when ZnO/MWCNTs were dispersed in the epoxy matrix alongside the PA microparticles, the modulus was recovered back to its original level. Unfortunately, the T_g of the PA/ZnO/P-MWCNT system decreased, but even so, the modulus was still acceptable. However, the T_g may be driven closer to the neat matrix value upon further curing at elevated temperature. This might lead to and embrittlement of the matrix, but if the reason for the drop in T_g is actually due to a change in the stoichiometric ratio because of other crosslinking reactions occurring between the ZnO and the epoxy, then the T_g is not fully recoverable.

CHAPTER VI

EFFECT OF ZNO-FUNCTIONALIZATION ON FRACTURE TOUGHNESS OF EPOXY NANOCOMPOSITE THIN FILMS CONTAINING MWCNTS AND PA

6.1 Introduction

Several studies have reported small improvements in fracture toughness of epoxy when using CNTs, but the specific mechanism(s) have yet to be identified [23, 29, 73, 210, 211]. A wide variety of research has been conducted over the years to develop brittle polymer matrices with improved fracture toughness [29, 39, 49, 55, 66-69, 71, 83, 85, 105, 173, 190, 193-196, 200, 201, 208, 243-250, 260-268, 270-273, 275, 276, 278-284, 293, 338-351]. Several approaches are generally used to improve the fracture toughness of brittle polymers: molecular flexibilization, soft particle (rubber, low T_g thermoplastics) toughening, rigid particle toughening (glass, silica, high T_g thermoplastics) toughening, and nanofiller toughening [29, 73, 84, 85, 173, 194, 196, 199, 238, 239, 244, 251, 260, 262, 264, 266, 268, 270, 272, 273, 279, 281, 283, 340-343, 352-355]. Unfortunately, the effectiveness of the particle to toughen is restricted by the ductility of the matrix [173, 238, 239].

Epoxy resins with low monomer molecular weight typically exhibit exceptional mechanical properties and high T_g, but are unable to form shear bands due to poor ductility [86, 87]. In systems where the matrix is unable to relive stress by forming shear bands, fillers must alter the stress state at the crack tip and undergo large-scale plastic strain or directly interfere with a propagating crack by crack bridging, deflection, bifurcation, pinning, etc. [65]. Most polymers exhibit a small natural crack tip radius and, as a result,

submicron particles are usually ineffective at bridging or deflecting an opening crack. If a submicron particle is dispersed in epoxy and is unable to relieve hydrostatic tension at the crack tip by debonding or have the ability to internally cavitate, then their toughening ability is significantly reduced [193, 195, 196, 266, 267]. The most likely candidates for CNT toughening are: aggregate formation leading to crack propagation interference and/or defect shielding, compliance of a functional group at the filler/matrix interface, or low crosslink density areas near MWCNTs due to heterogeneous curing (because of their high thermal conductivity) [13, 43, 56, 344, 356].

6.2 Experimental

6.2.1 Materials

A DGEBF liquid epoxy prepolymer, D.E.R.™ 354, donated by DOW Chemical, with an epoxide equivalent weight of 158 g/eq, was used as the matrix in this work. EPIKURE™ W, a DETDA hardener, was donated by Momentive Specialty Chemicals Inc. (Columbus, OH), with an amine equivalent weight of 43.29 g/eq. MWCNTs were donated by Arkema with reported inner and outer diameters of 2-6 nm and 10-15 nm, respectively, length of 0.1-10 μm, >90 % carbon content, and a reported density of ≈2.1 g/cm^3. Zinc acetate dihydrate and KOH were purchased from Sigma-Aldrich and used as received. Acetone and MeOH were purchased from Macron Fine Chemicals and Sigma-Aldrich and used as received. Release paper composed of a cellulose-based paper coated with PDMS was donated by Experia Specialty Solutions. Hybrid thin films with and without cracks were embedded in a mixture of DGEBF and D.E.H.™ 615. All

materials were dried at ≈70 °C overnight in a vacuum oven and used as received with the exception of MWCNTs, which were subjected to mild oxidation according to previous reports [73, 81, 104, 124, 332].

6.2.2 Pretreatment of MWCNTs

P-MWCNTs (250 mg) were added to a concentrated mixture of sulfuric (45 mL) and nitric acid (15 mL) at a 3:1 volume ratio and ultrasonicated in a sonication bath (Branson 2510) for 2 h at 25 °C. Next, 190 mL of deionized water (DI-H_2O) was added to hinder further oxidation and the solution was sonicated for another 1 h at 25 °C. After oxidation, the MWCNTs were isolated with a polyvinylidine fluoride (PVDF) filter membrane (Millipore, Durapore, 0.45 μm pore size) under vacuum. The O-MWCNTs were washed four times with DI-H_2O during the filtration process to remove any trace of acid residue. Then, the solution was washed with MeOH four times, and the O-MWCNTs were collected and resuspended in MeOH at a concentration of 1 mg/mL using ultrasonication for 1 h.

6.2.3 Synthesis of ZnO/MWCNTs

The synthesis of ZnO nanoparticles in MeOH is reported elsewhere [77, 313]. The procedure to prepare ZnO-functionalized MWCNTs is similar to the above method. P-MWCNTs (160 mg) and O-MWCNTs (160 mg) in MeOH were added to a flask and sonicated for 30 min to obtain a homogenous solution. Next, KOH (1 g) was added to the flask and dissolved via sonication for 10 min. Concurrently, zinc acetate dihydrate (1.96 g) was added to a separate flask with MeOH and dissolved via sonication for 5 min. After

both reactants were completely dissolved, the solutions were mixed at 60 °C while stirring at 300 RPM to initiate the reaction. Then, the solution was refluxed at 60 °C for 2 h to promote the growth of ZnO QDs. After initiation and growth, the ZnO/P-MWCNTs and ZnO/O-MWCNTs were filtered through a PVDF membrane (0.45 μm pore size) under vacuum with MeOH four times and then redispersed in MeOH via ultrasonication for 1 h. Their concentrations were determined by pipetting a predetermined amount of solution into an aluminum weighing dish and the weight recorded. Next, the solution was left in an oven overnight at 60 °C to slowly evaporate the solvent. Finally, the pan with dry ZnO/P-MWCNTs was weighed and the difference was divided by the initial solution volume to determine the concentration of ZnO/P-MWCNTs in MeOH.

6.2.4 Thin film composite preparation

DGEBF and DETDA were used as the matrix and curing agent in this study, respectively, to fabricate epoxy composite thin films. DGEBF (3.92 g) and DETDA (1.18 g) were added to a flask and degassed at 60 °C on a rotary evaporator under vacuum at 60-120 RPM for 30 min. The epoxy mixture was then B-staged in a preheated oven at 121 °C for 45 min to increase its viscosity for thin film processing. Once B-staged, the solution was poured onto an Elcometer 4340 Thin Film Coater preheated to 80 °C and cast at 5 mm/s to a thickness of 100-200 μm. Then, the film was placed in a preheated oven at 121 °C and cured for 2 h followed by a post-cure at 177 °C for 3 h. Composite films were fabricated according to the same procedure with a slight alteration. A PA/ZnO/P-MWCNT composite film was prepared by sonicating a predetermined amount of ZnO/P-MWCNTs in MeOH in a flask for 30 min. A specific amount of PA microparticles were dispersed in

an acetone solution in a separate flask via ultrasonication for 15 min. Next, the two solutions were mixed together and ultrasonicated for a further 15 min. DGEBF and DETDA were dissolved in acetone via sonication for 5 min and were subsequently added to the PA/ZnO/P-MWCNT MeOH/acetone solution with a final MeOH/acetone vol.%/vol.% of 2/1. The mixed composite solution was then sonicated for 15 min followed by removal of the solvent using a rotary evaporator at 60 °C for 15 min at 60-120 RPM. Next, the viscous resin was degassed in a vacuum oven at 80 °C for 2 h to ensure the complete removal of solvent. Then, the resin was carefully removed with a spatula and placed on a thin film coater preheated to 80 °C and cast at 5 mm/s to a thickness of 100-200 μm. For the O-MWCNT systems, the thin film coater was preheated to 100 °C due to their increased viscosity compared to the P-MWCNT systems. Once cast, the films were placed in an oven and cured at 121 °C for 2.75 h followed by a post cure at 177 °C for 3 h. The curing time and temperature were held constant at 2.75 h at 121 °C followed by 3 h at 177 °C to ensure the same degree of cure for all systems.

6.2.5 Characterization

Microtensile dogbones were fabricated with a steel cutting die with dimensions given in ASTM D1708-13 [335]. Single-edge notch tension (SENT) and double-edge notch tension (DENT) specimens were prepared, tested, and the data analyzed according to Klemann, Butkus, and Bose [184, 303, 304]. To summarize, newly punched dogbones were laid down on a glass plate that had a custom measuring grid on it. The specimen was properly aligned on the grid and the center line was marked with a permanent marker.

Next, the tip of a fresh razor blade was gently pushed into the specimen parallel to the specimen surface Figure 50.

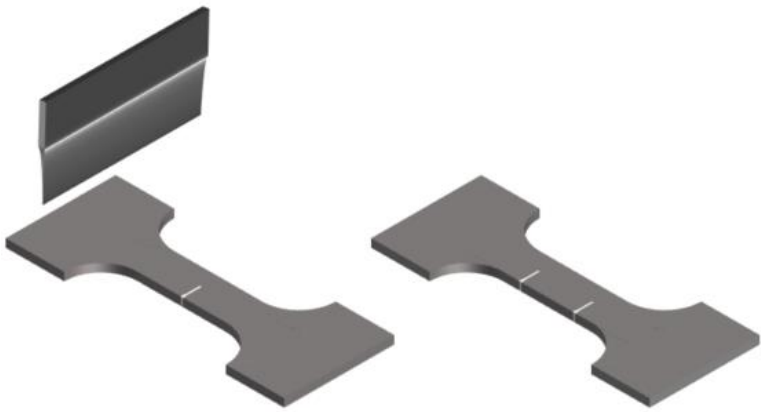

Figure 50. Schematic of SENT and DENT sample preparation. (A fresh razor blade was used for each sample)

For DENT samples, the center line was marked along with two lines 3 mm from the center line to ensure that the stress states in front of the cracks would not interact with each other. The notch (the length of the blade that is pushed into the sample) was kept to ≈1 mm. For a valid test, the full crack length was kept to a third of the overall width. Before testing, the cracks were imaged with an OM in reflectance mode (Olympus BX60 microscope with a Canon Mark 2 Digital Camera). Special care was taken to make sure that only sharp, natural cracks were produced, and the only those specimens were tested Figure 51.

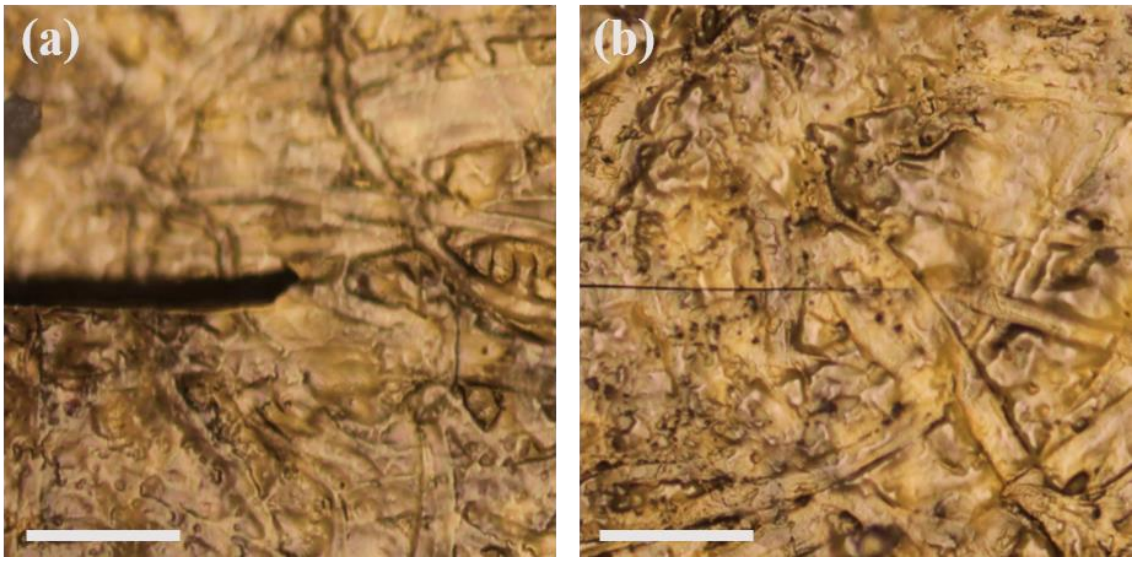

Figure 51. Reflective OM of surface of cracked thin films with (a) blunt crack and (b) sharp crack with scale bar = 100 μm.

If a specimen with a blunt crack was tested, it would exhibit an artificially large K_{IC} due to the small stress intensity factor requiring a much larger load to critically load the crack and cause it to propagate. The crack length was measured with ImageJ and recorded. The films were dried at ≈70 °C overnight in a vacuum oven and strained in uniaxial tension on an RSA-G2 DMA (TA Instruments) at a loading rate of 0.5 mm/min, at STP, with a data acquisition rate of 120 pts/s. A modified equation for Mode I fracture toughness was developed for thin polymeric films that follow linear-elastic fracture mechanics.

SEM (FEI Quanta 600 FE-SEM) was operated at 10 kV to investigate and identify the fracture mechanisms present on the post-fractured surface of the neat epoxy and composites. The fracture surfaces were isolated from the DENT samples and affixed to carbon tape that had been placed on the vertical face of a 90° specimen holder for SEM.

Two samples were pushed against the carbon tape to ensure that they would not debond from it during sputter coating or imaging. The samples were coated with 4 nm of Pt/Pd to make them conductive, thereby reducing the probability of charge buildup during the imaging process. The notch-to-natural crack transition was imaged along with the initial propagation zone. Special care was taken to clearly identify the initiation and propagation regions along the fracture surface.

TOM and TEM (FEI Tecnai G2 F20 ST FE-TEM) were used to identify the fracture mechanisms in the various systems by embedding sub-critically cracked samples into an embedding resin and using a Leica microtome to thick- and thin-section the materials. Sectioning was performed at STP after the crack tips were isolated by trimming away any excess material with a fresh razor blade to leave a trapezoid of material ≈1 mm x 0.5 mm exposed on the surface. Special care was taken to not cut off the crack tip of the embedded sample. However, in practice, this can be hard to do especially if the sample is of a dark color, which MWCNT/epoxy composites typically are. A MicroStar diamond knife, with a cutting angle of 4°, was used to section the materials at a cutting speed and feed of 0.30 mm/s and 5 μm for thick sections and 3.00 mm/s and 120 nm for thin sections. The diamond knife was overfilled with DI-H_2O and a small amount was pipetted out so that the surface of the water began to reflect the overhead light of the microtome so as to be able to see the interference pattern of the sections that come off. A number of sections (≤ 50) were obtained from each sample. The sections lay on top of the water due to surface tension and are corralled into groups of ≈5-10 with either a human eyelash that is affixed to a wooden stick, or a gold eyelash that is affixed to a special holder. Once the specimens

have been properly arranged on the surface of the water, a Deluxe Perfect Loop (Electron Microscopy Sciences) is used to collect and transfer them to a copper meshed grid. The Perfect Loop is dipped into DI-H_2O, then acetone, and DI-H_2O again to clean it and to impart a slightly hydrophilic nature on the surface of the loop. It should have a meniscus of water on the inside of the loop, if done correctly. Next, the loop is pushed down into the water far away from the intended sections, and then moved towards the sections until it lies directly beneath them. It is then pulled up and out of the water somewhat rapidly. If done correctly, the sections should lay within the meniscus of water within the loop. A Cu grid is placed on lens paper and the loaded loop is brought down so that they are concentric. As the two surfaces are brought together, the water is wicked away by the lens paper and the grid is allowed to dry before being taken to the TEM for observation. TEM was used to locate the crack tip and identify the fracture mechanisms, if any.

6.3 Results and discussion

6.3.1 Fracture toughness of hybrid epoxy thin films

As was previously mentioned, the dispersion of modified and unmodified MWCNTs in the presence of PA was observed to improve as a function of oxidation and surface functionalization. The systems containing P-MWCNTs (25%/40%), O-MWCNTs (38%/125%), PA (83%/265%), and PA/P-MWCNTs (106%/370%) exhibited K_{IC} and G_{IC} values that are similar to those that have been reported by previous members the Polymer Technology Center (Table 11, Figure 52, and Figure 53) [29, 73].

Table 11. Mode I critical stress intensity factor, K_{IC}, and critical strain energy release rate, G_{IC}, of neat epoxy and binary/ternary films. Average values and standard deviations are reported for at least 3 specimens/sample.

Samples	K_{IC} [MPa·√m]	G_{IC} [J/m^2]
Neat Epoxy	0.57 ± 0.08	121 ± 34
Epoxy/PA	0.71 ± 0.08	169 ± 39
Epoxy/P-MWCNT	0.78 ± 0.28	273 ± 152
Epoxy/O-MWCNT	1.25 ± 0.11	435 ± 78
Epoxy/ZnO/P-MWCNT	1.29 ± 0.15	412 ± 93
Epoxy/ZnO/O-MWCNT	1.04 ± 0.08	443 ± 63
Epoxy/PA/P-MWCNT	1.17 ± 0.05	570 ± 50
Epoxy/PA/O-MWCNT	1.55 ± 0.19	1050 ± 252
Epoxy/PA/ZnO/P-MWCNT	1.81 ± 0.05	1175 ± 66
Epoxy/PA/ZnO/O-MWCNT	1.15 ± 0.17	493 ± 141

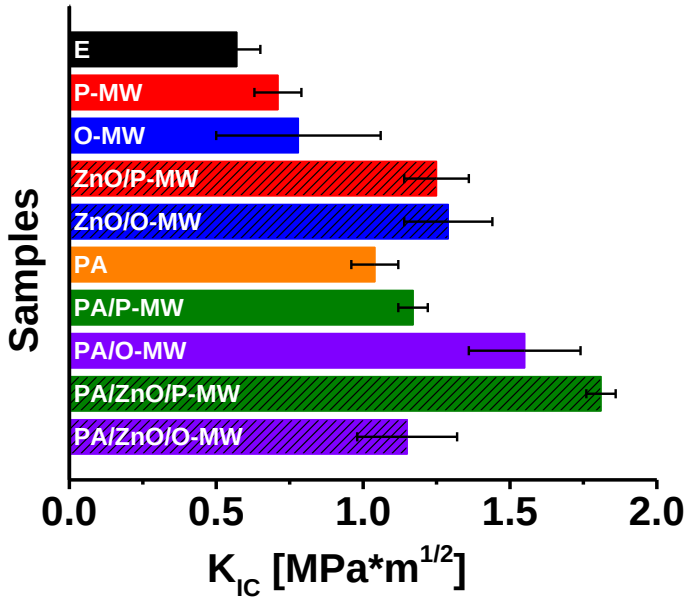

Figure 52. Mode I critical stress intensity factor, K_{IC}, of neat epoxy and composite films. Average values and standard deviations reported on at least 3 specimens/samples.

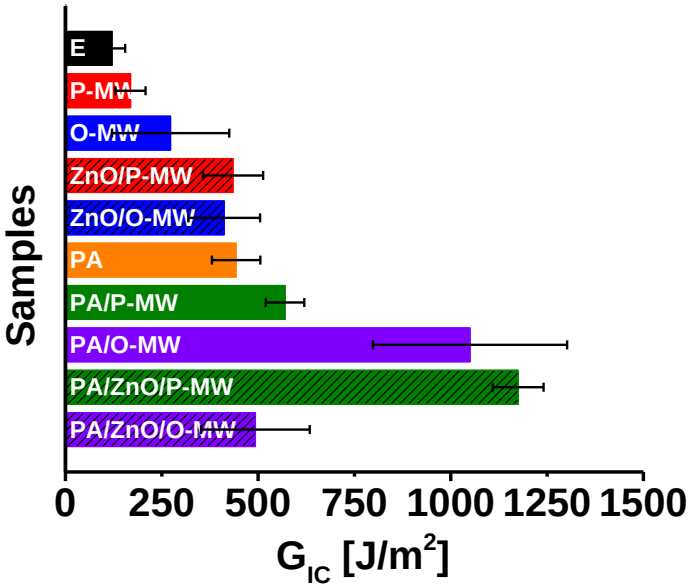

Figure 53. Mode I critical strain energy release rate, G_{IC}, of neat epoxy and composite films. Average values and standard deviations reported on at least 3 specimens/sample.

Somewhat surprising, is the fact that the systems containing ZnO/P-MWCNTs (119%/259%) and ZnO/O-MWCNTs (128%/240%) exhibited higher fracture toughness values than that of PA and PA/P-MWCNT toughened epoxy. Even more surprising is the observation that PA/O-MWCNTs and PA/ZnO/P-MWCNTs are able to enhance the fracture toughness by 172% and 218%, respectively. Unfortunately, the system containing PA/ZnO/O-MWCNTs (103%/307%) was unable to exceed the fracture toughness and critical strain energy release rate of PA/ZnO/P-MWCNTs (219%/869%). Furthermore, while the G_{IC} of every composite system was larger than that of the neat matrix, the system containing PA/ZnO/P-MWCNTs exhibited a remarkable increase in G_{IC} (871%), almost an order of magnitude compared to the neat matrix. The composite containing PA/O-MWCNTs exhibited a similar, albeit less, trend.

Sub-critical cracks in ZnO/P-MWCNT/epoxy and ZnO/O-MWCNT/epoxy films were investigated with TEM as seen in Figure 54.

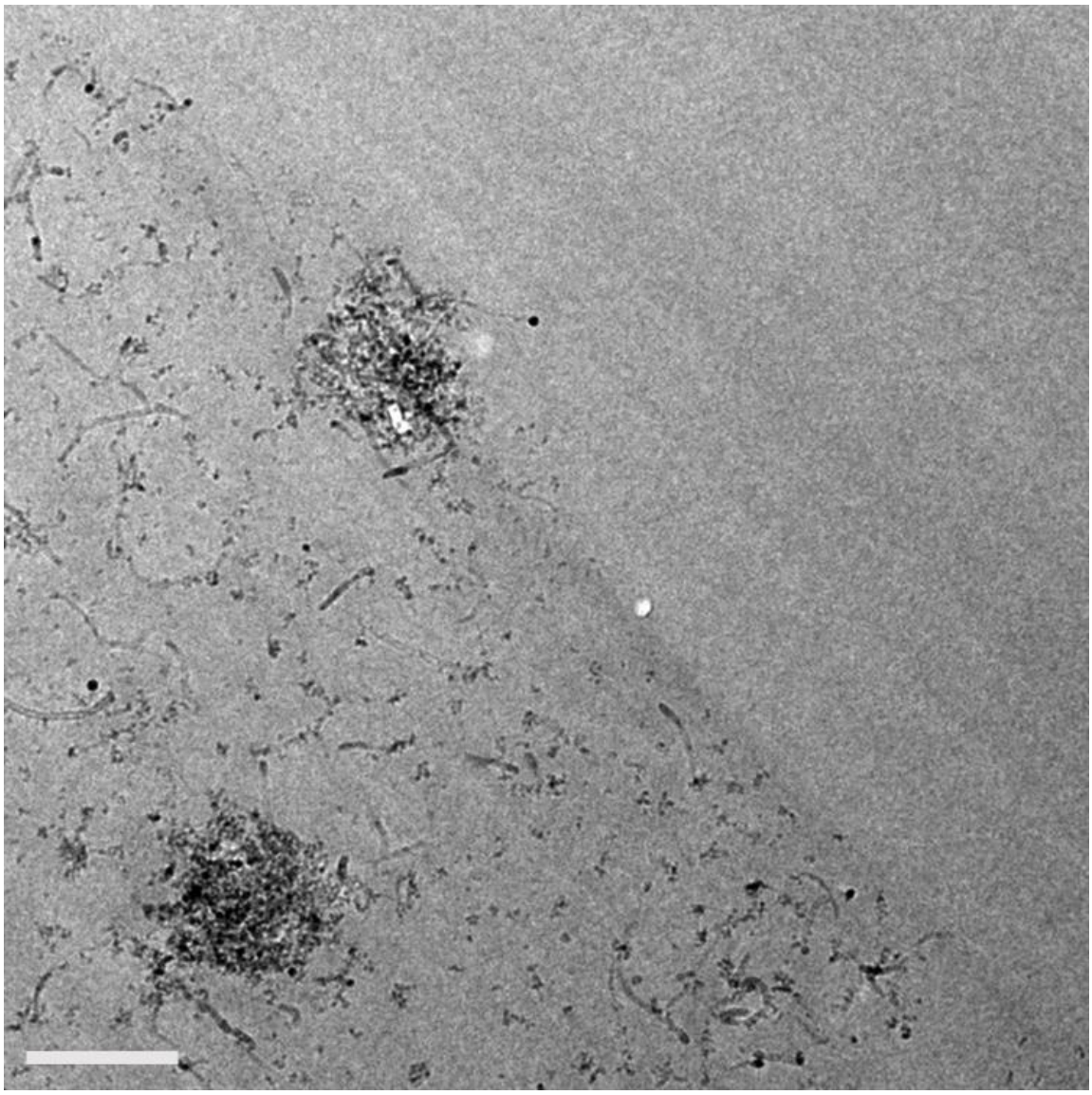

Figure 54. TEM of sub-critical crack in ZnO/P-MWCNT/epoxy thin film with scale bar = 400 nm.

Small aggregates of ZnO QDs can be seen alongside the crack in the ZnO/P-MWCNT/epoxy film. The crack tip in the ZnO/O-MWCNT/epoxy composite was observed and no tubes were seen bridging the crack. However, a fractured

ZnO/O-MWCNT can clearly be seen in front of the crack tip, which makes sense given the tensile stress state directly in front of the crack tip (Figure 55).

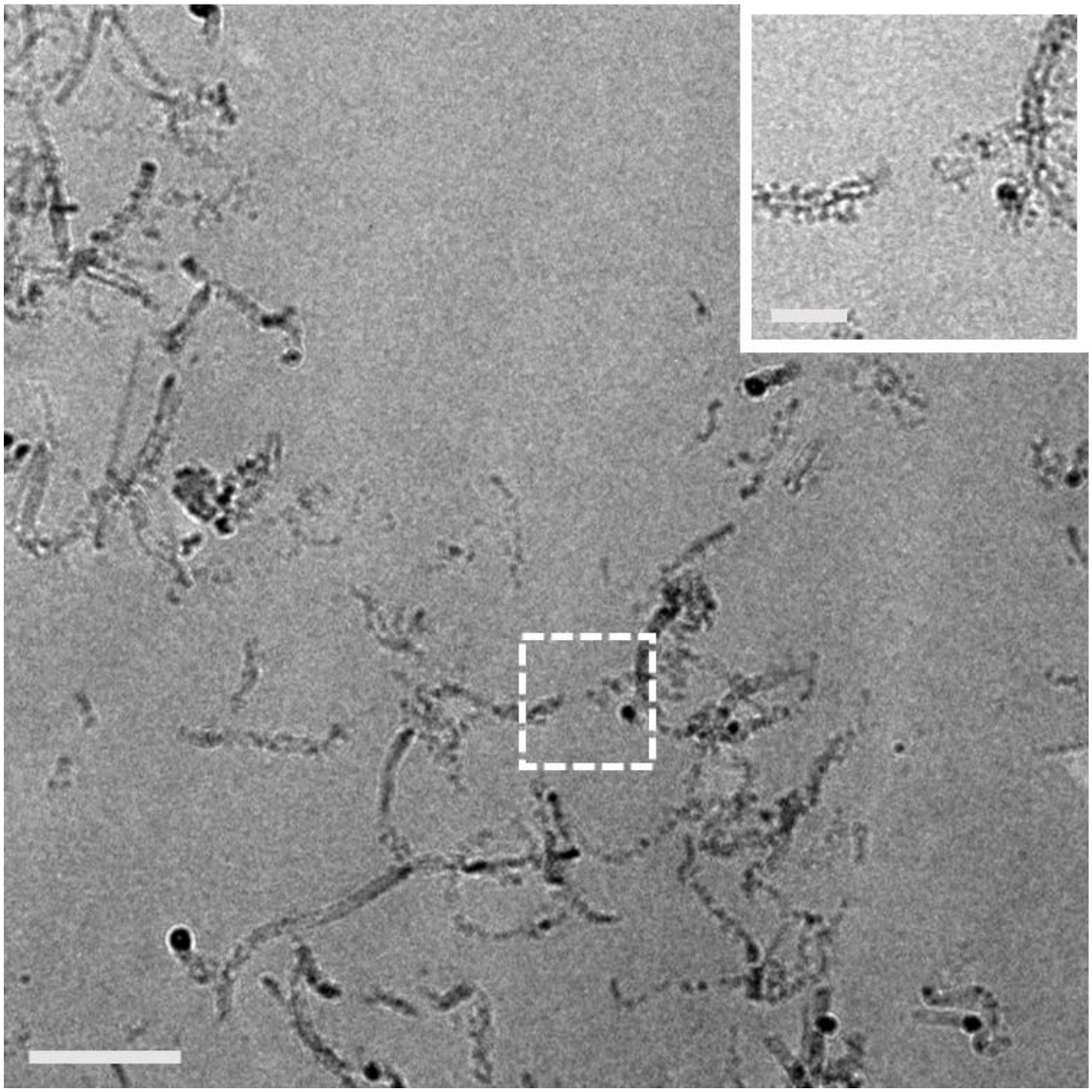

Figure 55. TEM of sub-critical crack in ZnO/O-MWCNT/epoxy film with scale bar = 200 nm. A fractured ZnO/O-MWCNT is clearly observed in the inset with scale bar = 50 nm.

Unfortunately, the other samples were not able to be imaged without the use of a cryotome.

TOM was used to observe the cracks in hybrid films containing ZnO/P-MWCNTs, ZnO/O-MWCNTs, PA/P-MWCNTs, PA/O-MWCNTs, PA/ZnO/P-MWCNTs, and PA/ZnO/O-MWCNTs. No apparent fracture mechanisms are observed in the ZnO/O-MWCNT/epoxy film, whereas for the ZnO/P-MWCNT film, an aggregate of CNTs is clearly observed to have fractured (Figure 56).

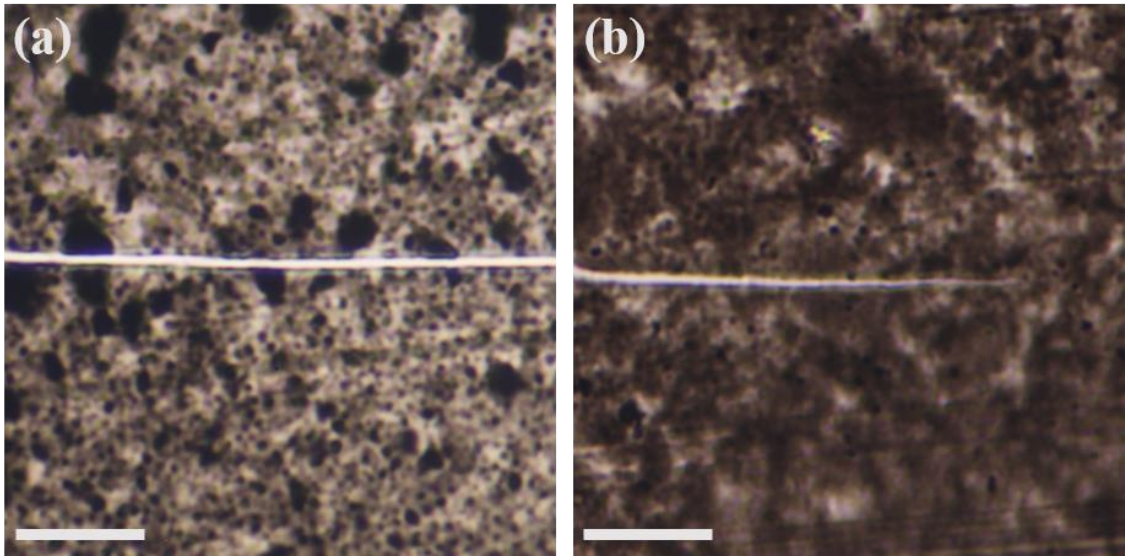

Figure 56. OM of sub-critical crack in (a) ZnO/P-MWCNT/epoxy and (b) ZnO/O-MWCNT/epoxy thin films with scale bar = 50 μm.

It is very likely that the observed increase in fracture toughness for the films containing ZnO/MWCNTs is due to nanoscale fracture mechanism that are only observable via SEM

or TEM. The epoxy films composed of PA/P-MWCNTs and PA/O-MWCNTs contain PA particles that clearly bridge the crack in Figure 57.

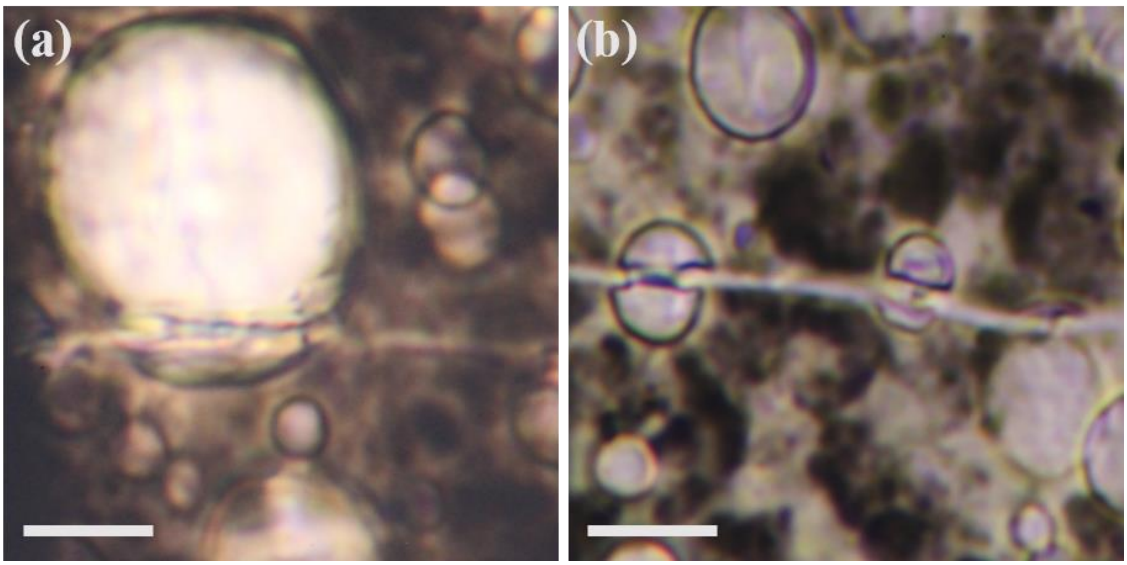

Figure 57. OM of sub-critical crack in (a) PA/P-MWCNT/epoxy and (b) PA/O-MWCNT/epoxy thin films with scale bar = 10 μm.

Trans-particle fracture is also observed in the film containing PA/O-MWCNTs. In the PA/ZnO/P-MWCNT/epoxy and PA/ZnO/O-MWCNT/epoxy systems, trans-particle fracture, crack bridging, and crack deflection are all observed (Figure 58).

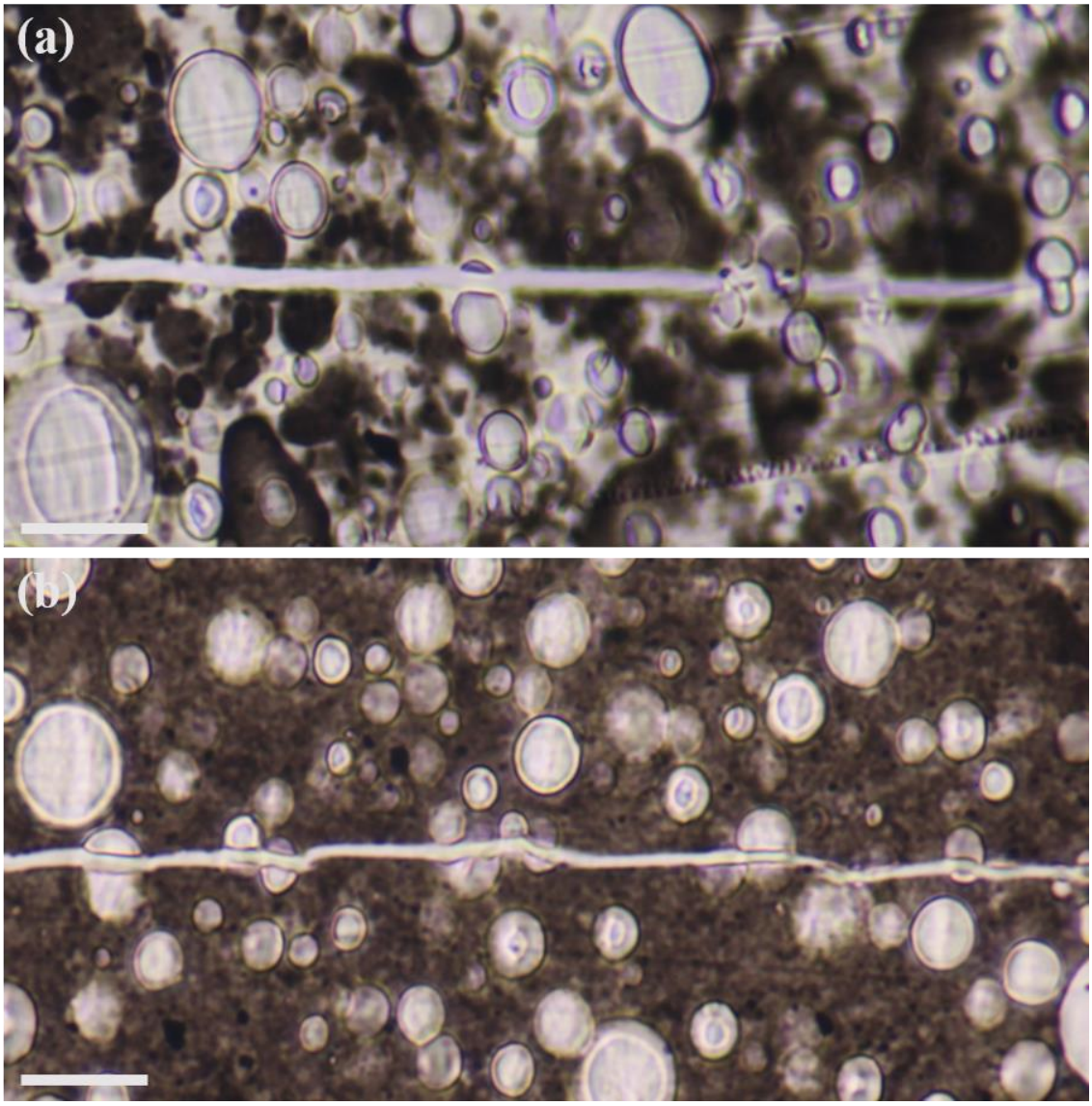

Figure 58. OM of sub-critical crack in (a) PA/ZnO/P-MWCNT/epoxy and (b) PA/ZnO/O-MWCNT/epoxy films with scale bar = 50 μm.

This is clearly one of the reasons for the incredible reinforcement of the fracture toughness in the PA/ZnO/P-MWCNT/epoxy film.

SEM was used to observe the fracture surfaces in hybrid epoxy films containing ZnO/P-MWCNTs, ZnO/O-MWCNTs, PA/P-MWCNTs, PA/O-MWCNTs, PA/ZnO/P-MWCNTs, and PA/ZnO/O-MWCNTs. The fracture surfaces of neat epoxy, PA/epoxy, P-MWCNT/epoxy, and O-MWCNT/epoxy were not imaged due to their K_{IC} values closely matching those reported in the literature and because they are not necessary for comparison with the other systems [29, 73]. In the epoxy film containing ZnO/P-MWCNTs, a large number of CNT ends, but not holes, were observed in the initial region after the crack propagated (Figure 59).

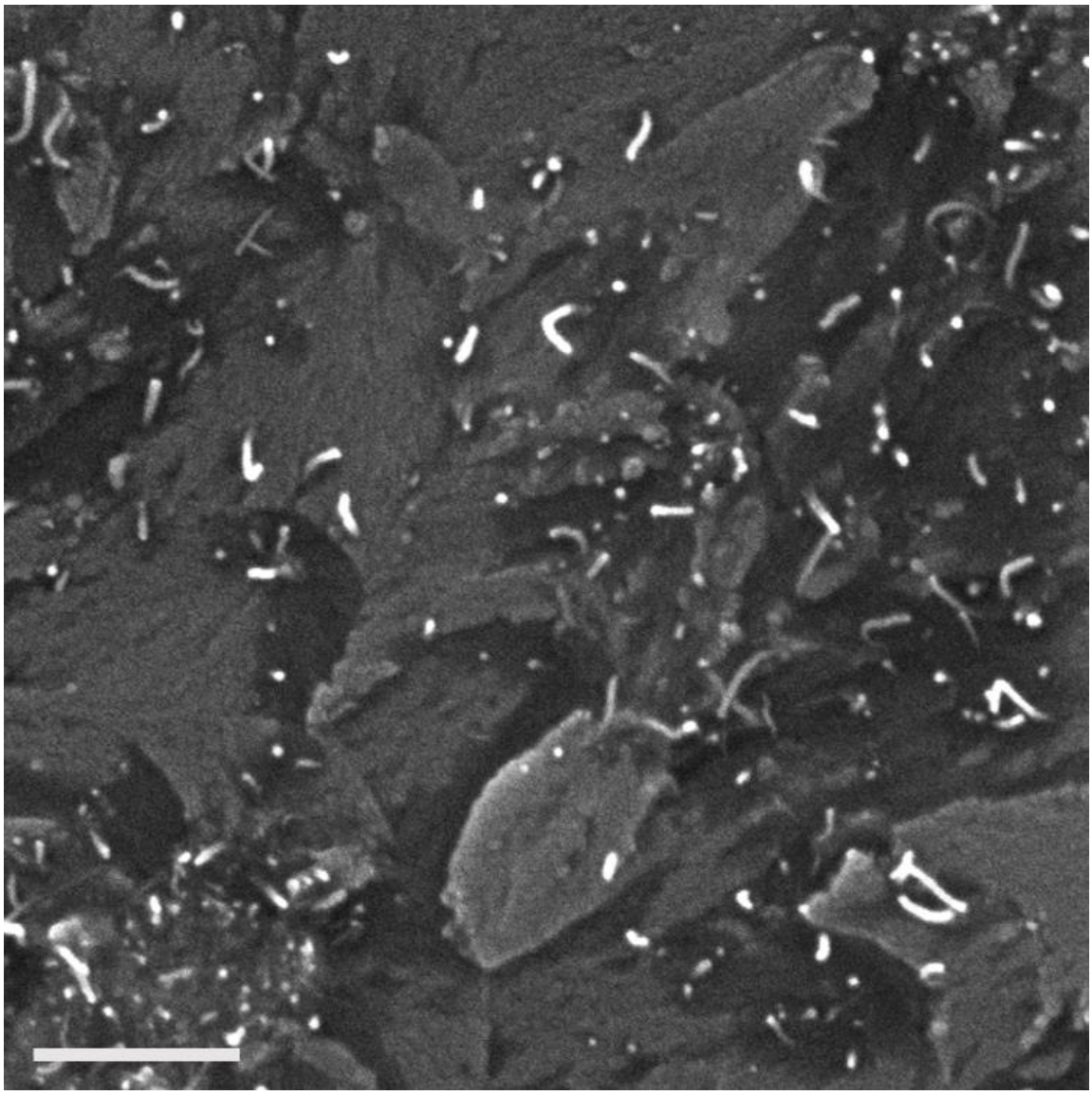

Figure 59. SEM micrograph of ZnO/P-MWCNT/epoxy film showing exposed tubes with scale bar = 1 μm.

Given the large number of exposed tubes in the ZnO/P-MWCNT system, tube pull-out on a global scale can be suggested as the toughening mechanism responsible for the significant increase in fracture toughness of the hybrid films containing ZnO-functionalized MWCNTs. High-resolution SEM or TEM need to be done to

determine if the ZnO QDs have been severed at the surface of the MWCNTs during pull-out or if they remain on the surface, and to what extent the matrix has been removed along with the MWCNTs during pull-out. If the ZnO QDs are severed, this would require a substantial amount of energy, resulting in a large amount of fracture energy being dissipated. Furthermore, if the ZnO QDs remain on the surface and scrape matrix material as the tube pulls out, this will also result in a significant amount of fracture energy dissipation. What appear to be aggregates of P-MWCNTs and ZnO QDs can also be seen in Figure 60.

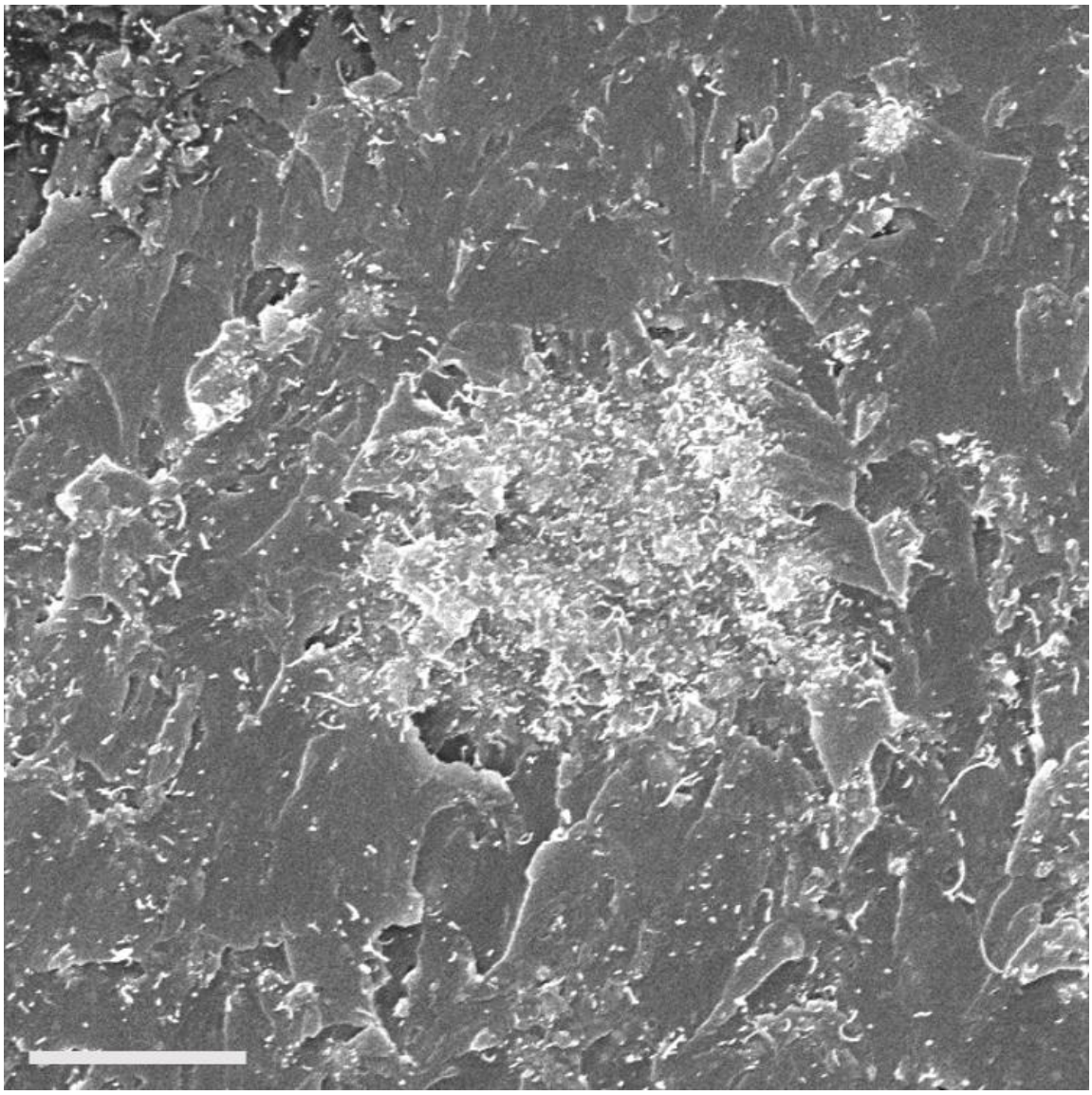

Figure 60. Cluster of tubes observed via SEM with scale bar = 3 μm.

After this region, a very rough and flaky appearance is observed. Ripple-like features are present on the fracture surface of ZnO/O-MWCNT/epoxy indicating that crack deflection took place (Figure 61).

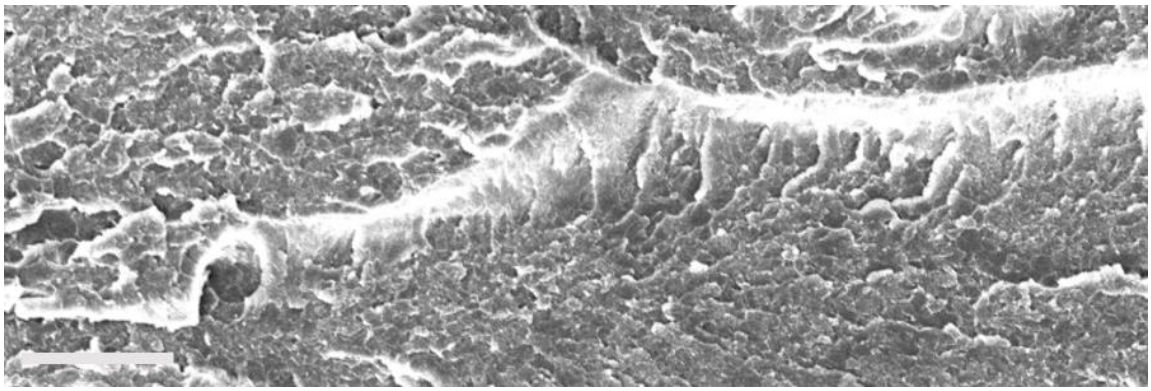

Figure 61. SEM of ZnO/O-MWCNT/epoxy fracture exhibiting a ripple-like step feature indicative of crack deflection with scale bar = 25 μm.

Very rough patches were also observed after this region; however, no exposed tubes were observed. In the PA/P-MWCNT/epoxy system, P-MWCNT agglomerates and the remains of drawn PA microparticles can be clearly seen on the fracture surface (Figure 62).

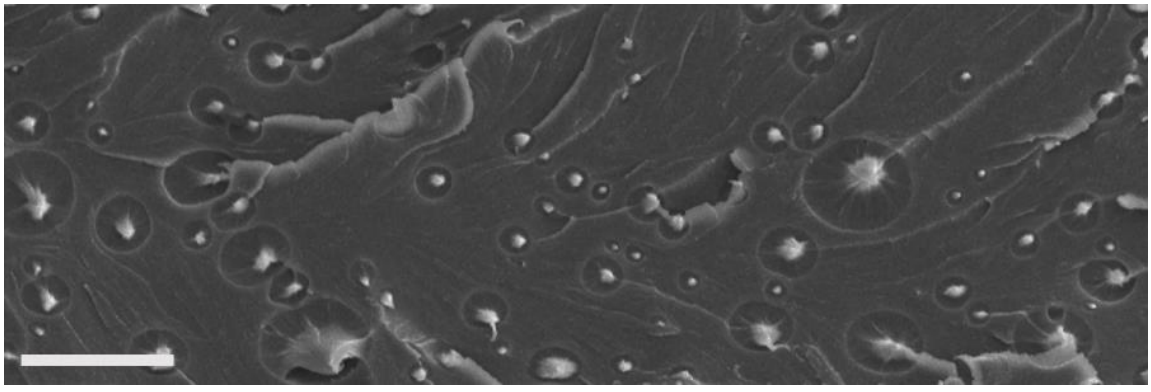

Figure 62. SEM micrograph of drawn PA particles on PA/P-MWCNT/epoxy fracture surface with scale bar = 25 μm.

A number of O-MWCNT aggregates can be clearly seen in the ternary system of PA/O-MWCNTs/epoxy. Upon further inspection, drawn PA can also be seen, and in larger numbers than observed in the PA/P-MWCNT/epoxy film (Figure 63).

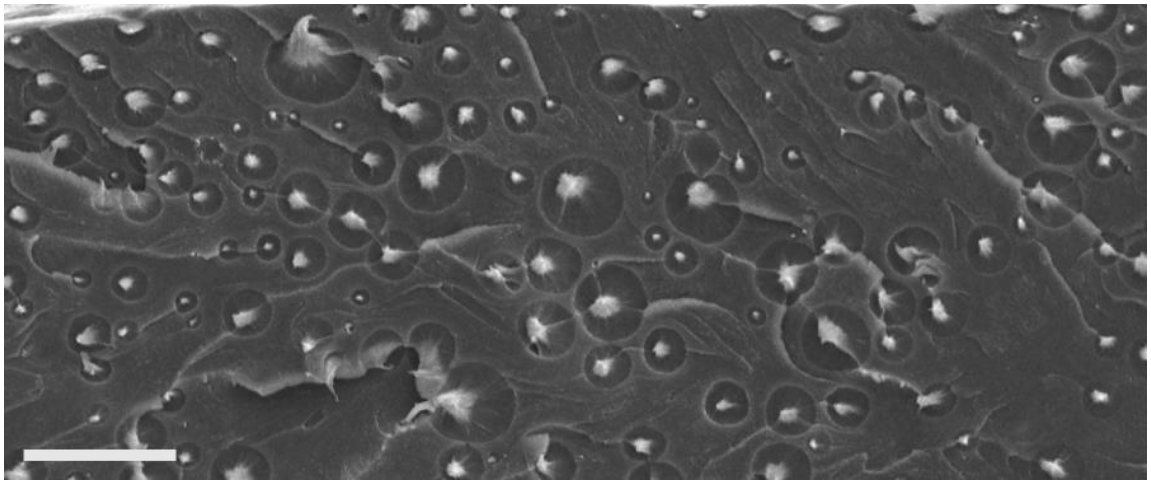

Figure 63. SEM micrograph of drawn PA particles clearly observable on the PA/O-MWCNT fracture surface with scale bar = 25 μm.

Moreover, at high magnification, what appear to be matrix cracks are observed in the divots left by the PA (Figure 64).

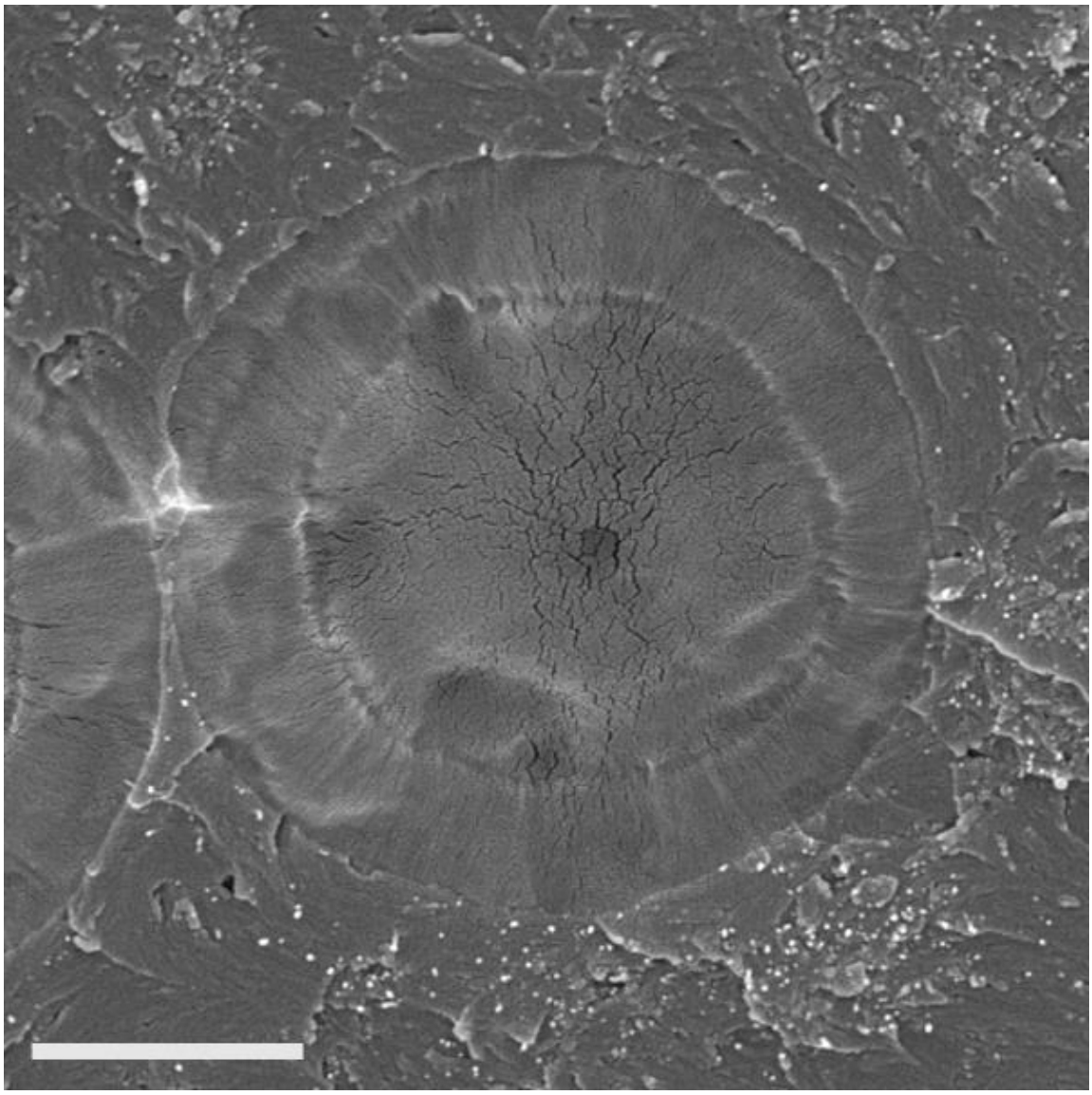

Figure 64. Microcracks in divots left by PA microparticles in PA/O-MWCNT/epoxy thin films with scale bar = 3 μm.

A much more uniform dispersion of CNTs is observed for the PA/ZnO/P-MWCNT/epoxy film. After the initial propagation region, the fracture surface is decorated with numerous divots where PA microparticles used to be, but also, sub-critically strained PA particles are observed (Figure 65).

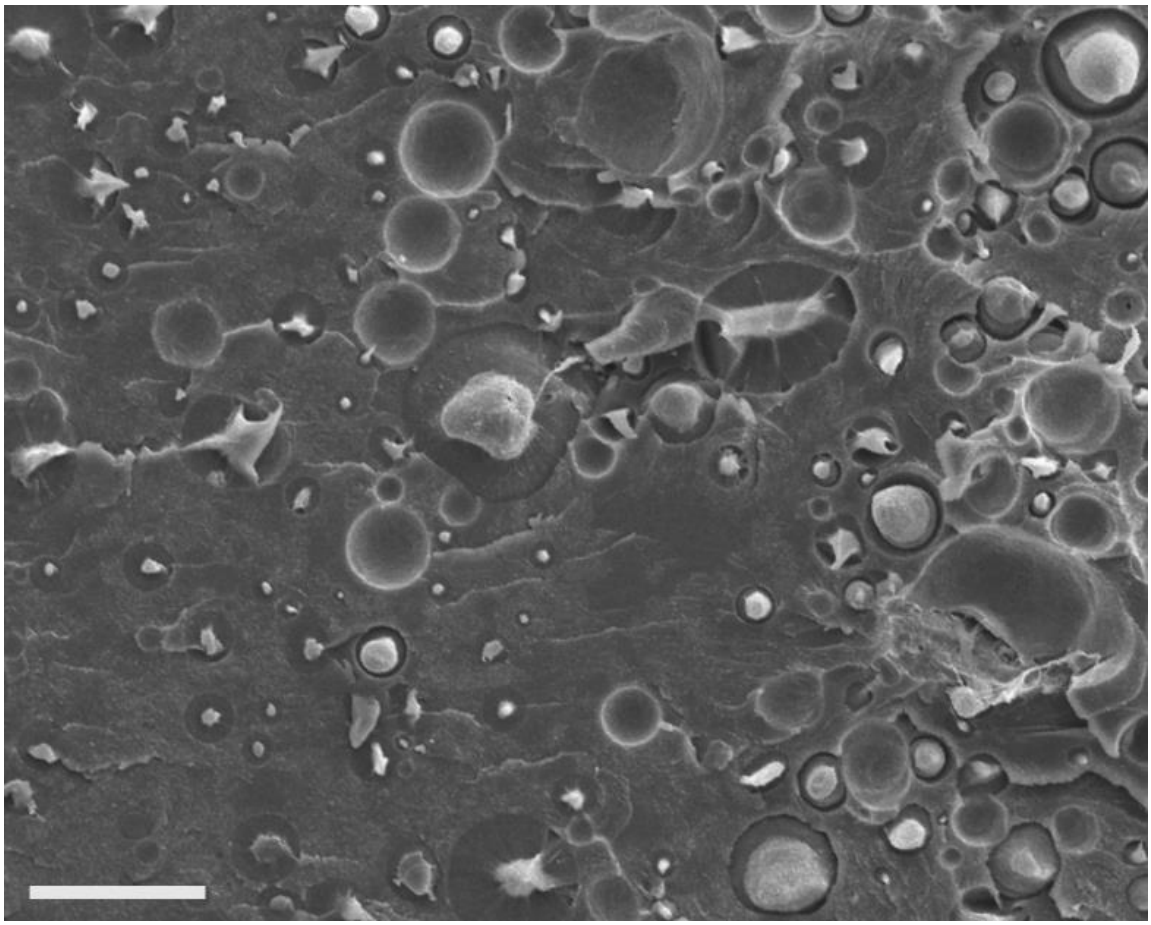

Figure 65. SEM micrograph of fracture surface of PA/ZnO/P-MWCNT/epoxy film with scale bar = 25 μm.

The appearance of a large number of PA particles that have not been completely drawn out of the fracture surface suggests that there is a force that keeps them from doing so. Perhaps, it is similar to the explanation given in Section 5.3.1, in which it was suggested that the presence of PA caused the ZnO QD aggregates to break apart and the surfaces of the PA and ZnO may engage in hydrogen bonding to a degree. The hybrid film of PA/ZnO/O-MWCNTs/epoxy also exhibits a well-dispersed system of MWCNTs. The fracture surface is littered with sparse populations of drawn PA microparticles (Figure 66).

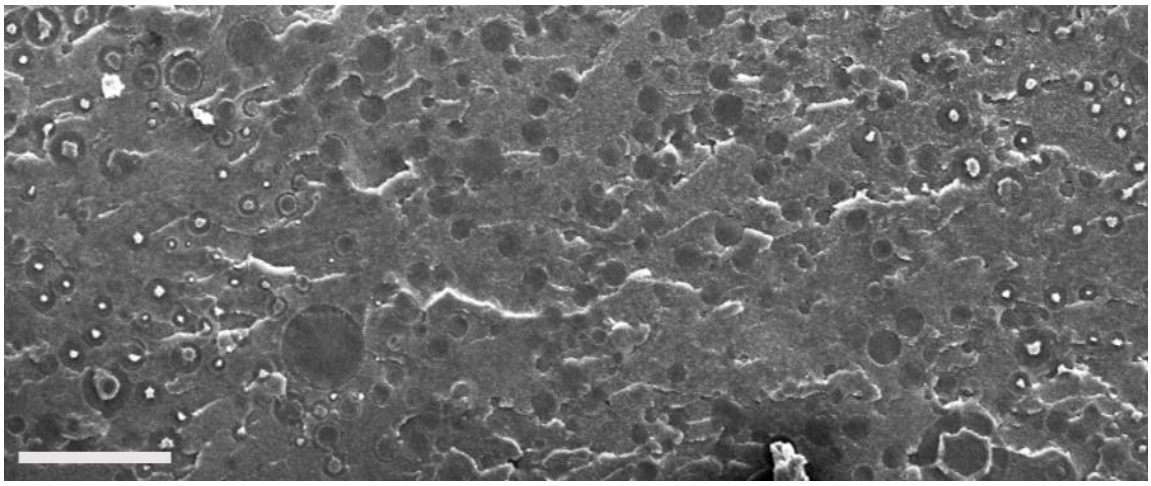

Figure 66. SEM micrograph of sparse populations of drawn PA microparticles in PA/ZnO/O-MWCNT/epoxy film with scale bar = 50 μm.

The final section of the fracture surface is covered with numerous drawn PA and divots from the particles on the other side of the fracture surface (Figure 67).

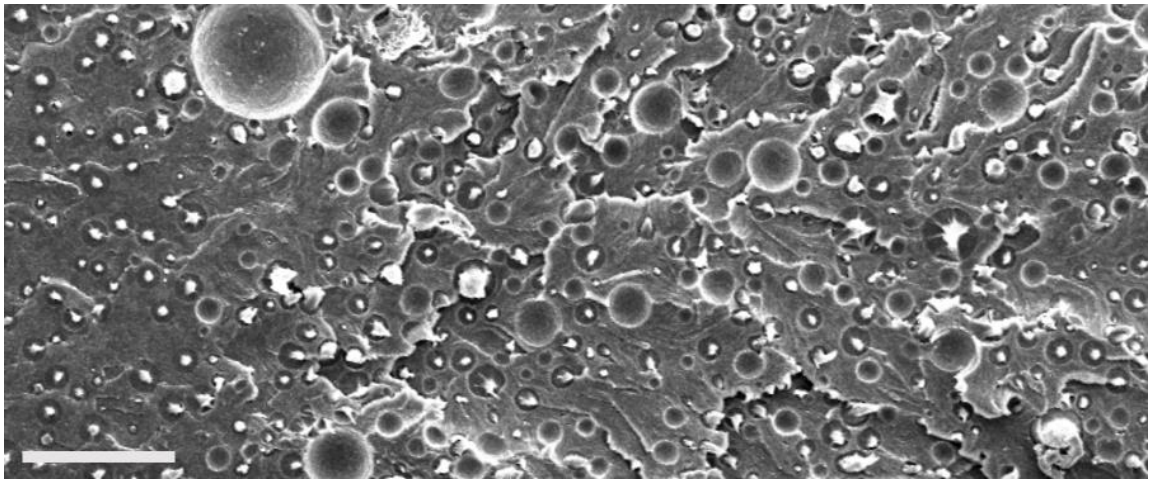

Figure 67. Evidence of divoting and drawing of PA particles via SEM of PA/ZnO/O-MWCNT/epoxy fracture surface with scale bar = 50 μm.

The Mode I critical stress intensity factor, K_{IC}, and critical strain energy release rate, G_{IC}, were evaluated using a SENT configuration. The fracture toughening mechanisms were identified via TOM, SEM, and TEM observation of thick- and thin-sections and metal-coated fracture surfaces. Various fracture mechanisms were identified in the binary and ternary systems. However, without cryotome, the fracture mechanisms associated with the MWCNTs in the ternary systems cannot be elucidated. The sectioning of those samples and their subsequent evaluations with TEM is left for future work.

6.4 Conclusions

Ternary systems containing P-MWCNTs, O-MWCNTs, ZnO, and PA, were fabricated and tested in SENT and DENT configurations to quantify the fracture toughness improvement and allow for the identification of the fracture mechanisms responsible for said improvement. The systems containing P-MWCNTs, O-MWCNTs, PA, and PA/P-MWCNTs exhibited K_{IC} and G_{IC} values that are similar to those that have been reported by previous members the Polymer Technology Center [29, 73]. Somewhat surprising, is the fact that the functionalized MWCNTs exhibited higher fracture toughness values than that of PA and PA/P-MWCNT toughened epoxy. Even more surprising is the observation that PA/O-MWCNTs and PA/ZnO/P-MWCNTs are able to enhance the fracture toughness by 172% and 218%, respectively. Unfortunately, the system containing PA/ZnO/O-MWCNTs was unable to exceed the fracture toughness of PA/ZnO/P-MWCNTs. Furthermore, while the G_{IC} of every composite system was larger

than that of the neat matrix, the system containing PA/ZnO/P-MWCNTs exhibited a drastic increase in G_{IC} (871%), almost an order of magnitude compared to the neat matrix.

Unfortunately, cryotomed sections were not obtained and/or presented here. Initial attempts at microtoming the ternary systems at RT yielded thin sections in which the PA particles are clearly pulled out of the matrix, having been plastically deformed. If the expectation that the ZnO QDs or the ZnO/O-MWCNTs themselves will be located near the PA microparticles, then RT sectioning will not yield adequate specimens. Therefore, cryotome is necessary in order to properly investigate and identify the morphology and fracture mechanisms of PA/MWCNTs in epoxy.

CHAPTER VII

CONCLUSIONS AND FUTURE WORK

7.1 Concluding remarks

The development of a new physical functionalization method was presented and summarized. The method is a simple two-step wet chemistry approach whereby ZnO QDs are grown in the presence of MWCNTs in a MeOH solution via refluxing at elevated temperature for 2 h. MWCNTs were observed to be well-covered with wurtzite ZnO QDs (with a small amount of clustering in systems containing O-MWCNTs) and were stable for up to a couple of months at concentrations of ≤ 3 mg/mL. Furthermore, the hybrid MWCNT solutions were observed to be well-dispersed when imaged with TOM. When an epoxy monomer and curing agent were dissolved in the solution with a small amount of acetone, the dispersion was observed to not change. Therefore, not only was a system of ZnO/MWCNTs stable and well-dispersed in organic solvent, but the presence of the epoxy monomer and curing agent did not negatively affect said dispersion. This suggested that the ZnO/MWCNTs would likely maintain their good dispersion state when the solvent was removed and the epoxy matrix cured.

The effect of ZnO/MWCNTs and PA on the fracture toughness, and tensile and electrical properties of hybrid epoxy thin film nanocomposites has been studied in this dissertation. Various fabrication and experimental techniques were used to account for the evolution of the morphology and dispersion of the fillers. These techniques include XRD, XPS, UV-Vis-NIR, TOM, TEM, DSC, and DMA. Several mechanical and fracture tests were also performed to investigate the effect of the filler type on the tensile, fracture, and

electrical behaviors of the thin film nanocomposites. The decoration of MWCNTs, with and without surface oxidation, enhanced the tensile modulus, tensile strength, and fracture toughness of the epoxy nanocomposite films. Furthermore, the addition of ZnO/P-MWCNTs led to the formation of a conductive network that exhibited an electrical conductivity an order of magnitude higher than that containing P-MWCNTs only. Moreover, all of the systems that contained O-MWCNTs, were not conductive. When PA was added to the MWCNT/epoxy composites, the modulus decreased, while the tensile strength, ductility, and toughness all improved. The ternary composites containing P-MWCNTs were conductive, but exhibited lower conductivities than their binary counterparts. This has been observed to be due to the breaking up of MWCNT aggregates due to the presence of PA microparticles.

The fracture mechanisms of the composites were investigated with TOM, SEM, and TEM. However, the presence of low T_g PA requires cryotome, microtoming at cryogenic temperature by using liquid nitrogen. However, this was unable to be performed and reported on in this dissertation and is left for future work. On the basis of TOM and SEM, the MWCNT aggregates present in the binary systems without functionalization broke apart, reducing their overall size. PA microparticles were observed bridging the crack, far behind the crack tip. Trans-particle fracture of PA was also observed behind the crack tip. However, without TEM, especially in the ternary systems, the fracture mechanisms attributed to MWCNT toughening were unable to be investigated and identified.

Multifunctional epoxy nanocomposite thin films were successfully fabricated and exhibited enhanced stiffness, strength, ductility, toughness, and electrical conductivity without a significant drop in processability of thermal stability. These films are ideal candidates for B-stage interleave toughening of CFRCs to improve the delamination toughness while not sacrificing through thickness conductivity or stiffness.

7.2 Future directions

The decoration of MWCNTs with ZnO QDs opens up the possibilities for further research and integration into various applications. Epoxy nanocomposite thin films can be fabricated with tailored properties for a given set of operating conditions without sacrificing their working temperature. Composites can be made that are conductive or insulative, have a high or low modulus, tensile strength, and ductility, or are toughened. Future work should focus on altering the concentration, filler chemistry, curing agent, decoration density to gain further insight into the processing-structure-property relationships in epoxy nanocomposites containing surface decorated MWCNTs.

7.2.1 Filler concentration and grafting density

The concentration of MWCNTs and the grafting density of ZnO QDs on their surfaces should be altered to determine the limiting concentrating with respect to property enhancement. MWCNTs, with and without functionalization, should be dispersed at concentrations ranging from 0.0 wt.% to 5.0 wt.% to determine the concentration at which a percolative network forms and the investigate the maximum possible conductivity attainable. The highest obtainable tensile and fracture properties should also be determined

as a function of concentration. Furthermore, the grafting density of ZnO QDs on the surface of MWCNTs has already been demonstrated to be tailorable from a wt.%/wt.% ratio of ZnO/MWCNT of 0/1 to 20/1. It has been observed that above a ratio of 8/1, ZnO/MWCNTs are not thermodynamically stable in organic solvent, so this challenge would need to be addressed.

7.2.2 Curing agent chemistry

The curing agent used in this study, DETDA, yields an epoxy matrix with a $T_g \approx 150$ °C, which is good for most structural applications. However, for more demanding applications where higher working temperatures or increased modulus are needed, different curing agents can be used. Furthermore, from a processing standpoint, asymmetric curing agents are crucial to limiting the extent of the crosslinking reaction so as to inhibit the buildup of viscosity during fabrication (hand layup, thin film processing, VaRTM, etc.). The limitation of viscosity during the early stages of cure provides sufficient time and increased mobility to form a conductive network or to more evenly disperse rather than be locked into place upon vitrification of the network. A separate curing agent may not be needed if the thermoplastic toughening particles or MWCNTs have surface chemistries that are able to crosslink with epoxide moieties. This would allow for solvent free processing, which comes with a processing penalty, but is less energy intensive.

7.2.3 Metal oxide reduction to metal and QD chemistry

Metal oxides are able to be reduced in various inert atmospheres are elevated temperatures, resulting in the change from exhibiting semi-conductive to conductive behavior and very likely a change in their colloidal stability. This would be very beneficial for tailoring the electrical properties of an epoxy composite for a given application. However, this change in surface chemistry would certainly alter the particle-particle and particle-matrix interactions, which may allow the vdW forces between MWCNTs to dominate causing them to bundle and form aggregates in solution and in the matrix. This would likely reduce any enhanced mechanical property that was previously observed for the system containing MWCNTs decorated with metallic oxide nanoparticles.

Various metal oxides and metals could be grown *in situ* on the MWCNT surface depending on the required application; the choice lies with the researcher. For applications that require a high dielectric constant, metallic oxides can be used, whereas for high electrical and/or thermal conductivity, metals can be use. However, the reaction conditions need to be well-documented because the growth and geometry of metal and metal oxide nanoparticles is highly dependent on pH, precursor concentration, solubility in a given solvent, etc. Furthermore, cost is another parameter that needs to be evaluated before deciding on a particular metal or metal oxide chemistry.

7.2.4 Thermoplastic toughening particle chemistry

In this study, preformed PA microparticles were dispersed into an epoxy matrix because previous studies have observed improved ductility, tensile strength, and fracture toughness. However, the introduction of a high concentration of low T_g (relatively soft)

thermoplastic particles has been shown to reduce the T_g of the composite. If high working temperature and high fracture toughness are needed for a given application, then high T_g (relatively rigid) thermoplastic particles such as PEI, PES, or PPE should be used. However, special care should be taken when using these rigid thermoplastic particles because their surface chemistries are different and could negatively influence the interaction between them and the MWCNTs used.

7.2.5 Hybrid b-staged interleaves for improved delamination toughness in carbon fiber-reinforced epoxy composites

B-stage interleave toughening is not a new concept, however, recent studies on epoxy interleaves containing PA have reported remarkable improvements in the delamination toughness of FRCs containing said interleaves. The preformed PA microparticles are able to absorb a significant amount of fracture energy by bridging the crack formed by the delamination between two plies at the mid-plane (the most common damage initiation zone) and undergoing extensive plastic deformation. However, the introduction of PA toughened epoxy interleaves has its drawbacks, specifically when it comes to stiffness, T_g, and electrical conductivity. When PA is dispersed into epoxy at a high concentration, the T_g and tensile modulus of the interleave drop as a result. Furthermore, the interleave, insulative in nature, acts to inhibit the conduction of electrons through the fiber-reinforced network of the composite. The systems studied in this dissertation are well-suited to address these concerns and should be optimized to take full advantage of reinforcing ability.

7.2.6 Anti-corrosive Zn-rich epoxy coatings containing ZnO/MWCNTs and/or PA

Corrosion is a thermodynamic inevitability in metals, even though extensive research has been conducted to understand and prevent it. As of yet, no ideal method or approach has been developed that can prevent corrosion indefinitely. However, the use of protective coatings has long since been used to address the need for anti-corrosive materials.

Epoxy is one of the most commonly used materials to prevent corrosion in severe environments (oil and gas). However, hydrophilic moieities intrinsic to epoxy, such as -OH, -COOH, and -NH_2, contain lone pairs of electrons that cause epoxy to leach water from its surroundings. This increased water uptake decreases the effectiveness of epoxy to prevent the corrosion of the metallic substrate upon which it coats. Therefore, numerous research studies have been conducted with the aim of improving the corrosion resistance of epoxies by introducing various fillers.

The incorporation of metal particles, such as Zn and Mg, is a common approach to improving the corrosion resistance of epoxy primers. If a homogenous dispersion of particles forms, the substrate will be protected by anodic protection, whereby the fillers, which are more active compared to the substrate, corrode when exposed to corrosive elements and act as a shield for the substrate. It is important for the fillers to form a conductive network so that any localized corrosion is delocalized across the entire surface of the coating. Unfortunately, a very high concentration of metal particles ($\geq$ 70%) is necessary and this has led to environmental concern over their incorporation. The need for such a high concentration of metal can be mitigated by introducing CNTs at a very low concentration, but enough to form a percolated network. This should allow for a much smaller amount of Zn particles to be used as sacrificial agents, reducing the weight and cost of anti-corrosive coatings and the growing environmental concern surrounding their use.

Nanoparticle-decorated MWCNTs and thermoplastic particles can be introduced into the Zn/epoxy coatings to address the need for a conductive network and improved fracture toughness [63, 233, 357-359]. Furthermore, CNT/epoxy composites have

exhibited improved wear and scratch resistance, which would help alleviate the localized corrosion of the substrate caused by surface damage. The systems presented in this dissertation would be excellent candidates for anti-corrosive coatings, especially if the ZnO QDs could be reduced to Zn particles and still provide enough stability for the MWCNTs to remain well-dispersed [359, 360].

7.2.7 Dielectric epoxy thin films containing ZnO/MWCNTs

Recent work into the dielectric response of epoxy composite films containing ZnO/MWCNTs has provided insight into their applicability for dielectric applications. The films containing ZnO/O-MWCNTs exhibited a dielectric constant of ≈32, which is more than two times greater than neat epoxy (≈14), over a range of frequencies from 0.11 Hz to 10 MHz (Figure 68).

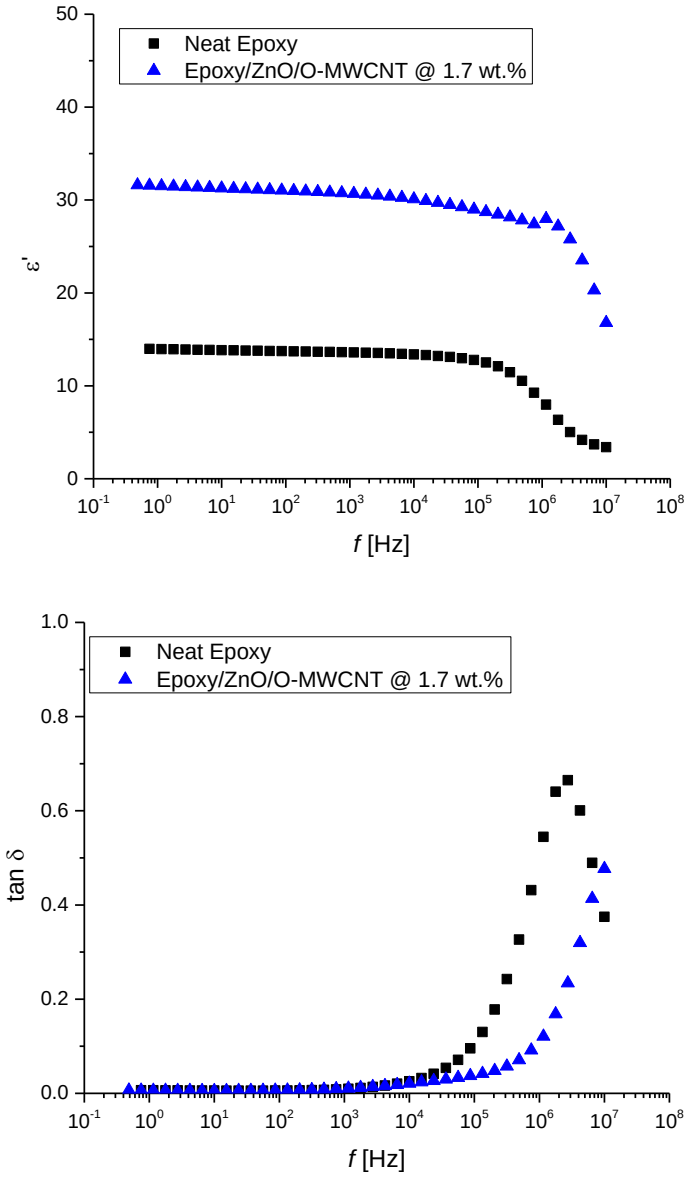

Figure 68. Dielectric constant and dielectric loss spectra of neat epoxy and ZnO/O-MWCNT/epoxy thin films.

Furthermore, both the neat epoxy and ZnO/O-MWCNT/epoxy exhibited essentially no dielectric loss. This is promising for dielectric applications, especially if dielectric

constant can be further improved without increasing the dielectric loss. If this is the case for epoxies with increased ZnO/O-MWCNT content, then these films could be used as thin film capacitors.

REFERENCES

[1] Baker AA, Dutton S, Kelly D. Composite Materials for Aircraft Structures. 2nd ed. Reston, Virginia: American Institute of Aeronautics and Astronautics; 2004.

[2] Ayatollahi MR, Shadlou S, Shokrieh MM. Correlation between aspect ratio of MWCNTs and mixed mode fracture of epoxy based nanocomposites. Materials Science and Engineering: A. 2011;528(19-20):6173-8.

[3] Hamer S, Leibovich H, Green A, Avrahami R, Zussman E, Siegmann A, et al. Mode I and Mode II fracture energy of MWCNT reinforced nanofibrilmats interleaved carbon/epoxy laminates. Composites Science and Technology. 2014;90:48-56.

[4] Zhang Q, Wu J, Gao L, Liu T, Zhong W, Sui G, et al. Dispersion stability of functionalized MWCNT in the epoxy–amine system and its effects on mechanical and interfacial properties of carbon fiber composites. Materials & Design. 2016;94:392-402.

[5] Bouhamed A, Müller C, Choura S, Kanoun O. Processing and characterization of MWCNTs/epoxy nanocomposites thin films for strain sensing applications. Sensors and Actuators A: Physical. 2017;257:65-72.

[6] Safadi B, Andrews R, Grulke EA. Multiwalled carbon nanotube polymer composites: Synthesis and characterization of thin films. Journal of Applied Polymer Science. 2002;84(14):2660-9.

[7] Thostenson ET, Chou T-W. Aligned multi-walled carbon nanotube-reinforced composites: Processing and mechanical characterization. Journal of Physics D: Applied Physics. 2002;35:L77-L80.

[8] Gojny FH, Nastalczyk J, Roslaniec Z, Schulte K. Surface modified multi-walled carbon nanotubes in CNT/epoxy-composites. Chemical Physics Letters. 2003;370(5-6):820-4.

[9] Gojny FH, Schulte K. Functionalisation effect on the thermo-mechanical behaviour of multi-wall carbon nanotube/epoxy-composites. Composites Science and Technology. 2004;64(15):2303-8.

[10] Martin C, Sandler J, Shaffer M, Schwarz M-K, Bauhofer W, Schulte K, et al. Formation of percolating networks in multi-wall carbon-nanotube–epoxy composites. Composites Science and Technology. 2004;64(15):2309-16.

[11] Kim YJ, Shin TS, Choi HD, Kwon JH, Chung Y-C, Yoon HG. Electrical conductivity of chemically modified multiwalled carbon nanotube/epoxy composites. Carbon. 2005;43(1):23-30.

[12] Moisala A, Li Q, Kinloch IA, Windle AH. Thermal and electrical conductivity of single- and multi-walled carbon nanotube-epoxy composites. Composites Science and Technology. 2006;66(10):1285-8.

[13] Thostenson ET, Chou T-W. Processing-structure-multi-functional property relationship in carbon nanotube/epoxy composites. Carbon. 2006;44(14):3022-9.

[14] Hernández-Pérez A, Avilés F, May-Pat A, Valadez-González A, Herrera-Franco PJ, Bartolo-Pérez P. Effective properties of multiwalled carbon nanotube/epoxy composites using two different tubes. Composites Science and Technology. 2008;68(6):1422-31.

[15] Kepple KL, Sanborn GP, Lacasse PA, Gruenberg KM, Ready WJ. Improved fracture toughness of carbon fiber composite functionalized with multi walled carbon nanotubes. Carbon. 2008;46(15):2026-33.

[16] Zhou Y, Pervin F, Lewis L, Jeelani S. Fabrication and characterization of carbon/epoxy composites mixed with multi-walled carbon nanotubes. Materials Science and Engineering: A. 2008;475(1-2):157-65.

[17] Guadagno L, Vertuccio L, Sorrentino A, Raimondo M, Naddeo C, Vittoria V, et al. Mechanical and barrier properties of epoxy resin filled with multi-walled carbon nanotubes. Carbon. 2009;47(10):2419-30.

[18] Nadler M, Werner J, Mahrholz T, Riedel U, Hufenbach W. Effect of CNT surface functionalisation on the mechanical properties of multi-walled carbon nanotube/epoxy-composites. Composites Part A: Applied Science and Manufacturing. 2009;40(6-7):932-7.

[19] Rosca ID, Hoa SV. Highly conductive multiwall carbon nanotube and epoxy composites produced by three-roll milling. Carbon. 2009;47(8):1958-68.

[20] Kostopoulos V, Baltopoulos A, Karapappas P, Vavouliotis A, Paipetis A. Impact and after-impact properties of carbon fibre reinforced composites enhanced with multi-wall carbon nanotubes. Composites Science and Technology. 2010;70(4):553-63.

[21] Martone A, Formicola C, Giordano M, Zarrelli M. Reinforcement efficiency of multi-walled carbon nanotube/epoxy nano composites. Composites Science and Technology. 2010;70(7):1154-60.

[22] Montazeri A, Javadpour J, Khavandi A, Tcharkhtchi A, Mohajeri A. Mechanical properties of multi-walled carbon nanotube/epoxy composites. Materials & Design. 2010;31(9):4202-8.

[23] Sumfleth J, Prehn K, Wichmann MH, Wedekind S, Schulte K. A comparative study of the electrical and mechanical properties of epoxy nanocomposites reinforced by CVD-and arc-grown multi-wall carbon nanotubes. Composites Science and Technology. 2010;70(1):173-80.

[24] Ayatollahi MR, Shadlou S, Shokrieh MM. Mixed mode brittle fracture in epoxy/multi-walled carbon nanotube nanocomposites. Engineering Fracture Mechanics. 2011;78(14):2620-32.

[25] Ayatollahi MR, Shadlou S, Shokrieh MM, Chitsazzadeh M. Effect of multi-walled carbon nanotube aspect ratio on mechanical and electrical properties of epoxy-based nanocomposites. Polymer Testing. 2011;30(5):548-56.

[26] Guadagno L, De Vivo B, Di Bartolomeo A, Lamberti P, Sorrentino A, Tucci V, et al. Effect of functionalization on the thermo-mechanical and electrical behavior of multi-wall carbon nanotube/epoxy composites. Carbon. 2011;49(6):1919-30.

[27] Khan SU, Li CY, Siddiqui NA, Kim J-K. Vibration damping characteristics of carbon fiber-reinforced composites containing multi-walled carbon nanotubes. Composites Science and Technology. 2011;71(12):1486-94.

[28] Montazeri A, Montazeri N. Viscoelastic and mechanical properties of multi walled carbon nanotube/epoxy composites with different nanotube content. Materials & Design. 2011;32(4):2301-7.

[29] White KL, Sue HJ. Electrical conductivity and fracture behavior of epoxy/polyamide-12/multiwalled carbon nanotube composites. Polymer Engineering & Science. 2011;51(11):2245-53.

[30] Chu C-C, White KL, Liu P, Zhang X, Sue H-J. Electrical conductivity and thermal stability of polypropylene containing well-dispersed multi-walled carbon nanotubes disentangled with exfoliated nanoplatelets. Carbon. 2012;50(12):4711-21.

[31] Saw LN, Mariatti M, Azura AR, Azizan A, Kim JK. Transparent, electrically conductive, and flexible films made from multiwalled carbon nanotube/epoxy composites. Composites Part B: Engineering. 2012;43(8):2973-9.

[32] Yang YK, Yu LJ, Peng RG, Huang YL, He CE, Liu HY, et al. Incorporation of liquid-like multiwalled carbon nanotubes into an epoxy matrix by solvent-free processing. Nanotechnology. 2012;23(22):225701.

[33] Chen Z, Dai XJ, Magniez K, Lamb PR, Rubin de Celis Leal D, Fox BL, et al. Improving the mechanical properties of epoxy using multiwalled carbon nanotubes functionalized by a novel plasma treatment. Composites Part A: Applied Science and Manufacturing. 2013;45:145-52.

[34] Yao H, Chu C-C, Sue H-J, Nishimura R. Electrically conductive superhydrophobic octadecylamine-functionalized multiwall carbon nanotube films. Carbon. 2013;53:366-73.

[35] Kausar A, Iqbal A, Hussain ST. Preparation and properties of polyamide/epoxy/multi-walled carbon nanotube nanocomposite. Journal of Plastic Film & Sheeting. 2014;30(2):205-24.

[36] White KL, Li P, Sumi Y, Sue HJ. Rheology of disentangled multiwalled carbon nanotubes dispersed in uncured epoxy fluid. J Phys Chem B. 2014;118(1):362-71.

[37] White KL, Yao H, Zhang X, Sue H-J. Rheology of electrostatically tethered nanoplatelets and multi-walled carbon nanotubes in epoxy. Polymer. 2016;84:223-33.

[38] Xu Y, Li Y, Bao J, Zhou T, Zhang A. Rigid thermosetting epoxy/multi-walled carbon nanotube foams with enhanced conductivity originated from a flow-induced concentration effect. RSC Advances. 2016;6(44):37710-20.

[39] Domun N, Hadavinia H, Zhang T, Sainsbury T, Liaghat GH, Vahid S. Improving the fracture toughness and the strength of epoxy using nanomaterials: A review of the current status. Nanoscale. 2015;7(23):10294-329.

[40] Ramasubramaniam R, Chen J, Liu H. Homogeneous carbon nanotube/polymer composites for electrical applications. Applied Physics Letters. 2003;83(14):2928-30.

[41] Gojny FH, Wichmann MHG, Köpke U, Fiedler B, Schulte K. Carbon nanotube-reinforced epoxy-composites: enhanced stiffness and fracture toughness at low nanotube content. Composites Science and Technology. 2004;64(15):2363-71.

[42] Xie X, Mai Y, Zhou X. Dispersion and alignment of carbon nanotubes in polymer matrix: A review. Materials Science and Engineering: R: Reports. 2005;49(4):89-112.

[43] Thostenson ET, Chou T-W. Fracture mechanisms in carbon nanotube-reinforced composites. 2006.

[44] Bekyarova E, Thostenson ET, Yu A, Itkis ME, Fakhrutdinov D, Chou T-W, et al. Functionalized single-walled carbon nanotubes for carbon fiber-epoxy composites. Journal of Physical Chemistry C. 2007;111:17865-71.

[45] Bekyarova E, Thostenson ET, Yu A, Kim H, Gao J, Tang J, et al. Multiscale carbon nanotube-carbon fiber reinforcement for advanced epoxy composites. Langmuir. 2007;23:3970-4.

[46] Godara A, Mezzo L, Luizi F, Warrier A, Lomov SV, van Vuure AW, et al. Influence of carbon nanotube reinforcement on the processing and the mechanical behaviour of carbon fiber/epoxy composites. Carbon. 2009;47(12):2914-23.

[47] Byrne MT, Gun'ko YK. Recent advances in research on carbon nanotube-polymer composites. Advanced Materials. 2010;22(15):1672-88.

[48] Qian H, Greenhalgh ES, Shaffer MSP, Bismarck A. Carbon nanotube-based hierarchical composites: a review. Journal of Materials Chemistry. 2010;20(23):4751.

[49] Hollertz R, Chatterjee S, Gutmann H, Geiger T, Nuesch FA, Chu BT. Improvement of toughness and electrical properties of epoxy composites with carbon nanotubes prepared by industrially relevant processes. Nanotechnology. 2011;22(12):125702.

[50] Pandey G, Thostenson ET. Carbon Nanotube-Based Multifunctional Polymer Nanocomposites. Polymer Reviews. 2012;52(3):355-416.

[51] Zhang Q, Huang JQ, Qian WZ, Zhang YY, Wei F. The road for nanomaterials industry: a review of carbon nanotube production, post-treatment, and bulk applications for composites and energy storage. Small. 2013;9(8):1237-65.

[52] Arash B, Wang Q, Varadan VK. Mechanical properties of carbon nanotube/polymer composites. Scientific Reports. 2014;4:6479.

[53] Liu Y, Kumar S. Polymer/carbon nanotube nano composite fibers: A review. ACS Appl Mater Interfaces. 2014;6(9):6069-87.

[54] Kausar A, Rafique I, Muhammad B. Review of Applications of Polymer/Carbon Nanotubes and Epoxy/CNT Composites. Polymer-Plastics Technology and Engineering. 2016;55(11):1167-91.

[55] Li M, Wang Z, Liu Q, Wang S, Gu Y, Li Y, et al. Carbon nanotube film/epoxy composites with high strength and toughness. Polymer Composites. 2017;38(3):588-96.

[56] Thostenson ET, Ren Z, Chou T-W. Advances in the science and technology of carbon nanotubes and their composites: A review. Composites Science and Technology. 2001;61:1899-912.

[57] Thostenson E, Li C, Chou T. Nanocomposites in context. Composites Science and Technology. 2005;65(3-4):491-516.

[58] Chou T-W, Gao L, Thostenson ET, Zhang Z, Byun J-H. An assessment of the science and technology of carbon nanotube-based fibers and composites. Composites Science and Technology. 2010;70(1):1-19.

[59] Kim SW, Kim T, Kim YS, Choi HS, Lim HJ, Yang SJ, et al. Surface modifications for the effective dispersion of carbon nanotubes in solvents and polymers. Carbon. 2012;50(1):3-33.

[60] Ma P-C, Siddiqui NA, Marom G, Kim J-K. Dispersion and functionalization of carbon nanotubes for polymer-based nanocomposites: A review. Composites Part A: Applied Science and Manufacturing. 2010;41(10):1345-67.

[61] Bandaru PR. Electrical Properties and Applications of Carbon Nanotube Structures. Journal of Nanoscience and Nanotechnology. 2007;7(4):1239-67.

[62] Yao H. Surface functionalization of 1-D and 2-D carbon-based nanomaterials and their applications. Texas A&M University, Doctor of Philosophy, 2015.

[63] Ates M. A review on conducting polymer coatings for corrosion protection. Journal of Adhesion Science and Technology. 2016;30(14):1510-36.

[64] Pearson RA, Yee AF. Toughening mechanisms in thermoplastic-modified epoxies. Polymer. 1992;34(17):3658-70.

[65] Pearson RA. Toughening epoxies using rigid thermoplastic particles-a review: American Chemical Society, Washington, DC (United States); 1993.

[66] Romano AM, Carbassi F, Braclia R. Rubber- and thermoplastic-toughened epoxy adhesive films. Journal of Applied Polymer Science. 1994;52:1775-83.

[67] Pasquale GD, Motta O, Recca A, Carter JT, McGrail PT, Acierno D. New high-performance thermoplastic toughened epoxy thermosets. Polymer. 1997;38(17):4345-8.

[68] Cardwell B, Yee AF. Toughening of epoxies through thermoplastic crack bridging. Journal of Materials Science. 1998;33(22):5473-84.

[69] Hodgkin JH, Simon GP, Varley RJ. Thermoplastic toughening of epoxy resins: A critical review. Polymers for Advanced Technologies. 1998;9:3-10.

[70] Zhang J, Guo Q, Fox BL. Study on thermoplastic-modified multifunctional epoxies: Influence of heating rate on cure behaviour and phase separation. Composites Science and Technology. 2009;69(7-8):1172-9.

[71] Brooker RD, Kinloch AJ, Taylor AC. The Morphology and Fracture Properties of Thermoplastic-Toughened Epoxy Polymers. The Journal of Adhesion. 2010;86(7):726-41.

[72] Xu X, Zhou Z, Hei Y, Zhang B, Bao J, Chen X. Improving compression-after-impact performance of carbon–fiber composites by CNTs/thermoplastic hybrid film interlayer. Composites Science and Technology. 2014;95:75-81.

[73] Sun L, Warren GL, Davis D, Sue HJ. Nylon toughened epoxy/SWCNT composites. Journal of Materials Science. 2011;46(1):207-14.

[74] White KL, Sue H-J. Delamination toughness of fiber-reinforced composites containing a carbon nanotube/polyamide-12 epoxy thin film interlayer. Polymer. 2012;53(1):37-42.

[75] Yang RD, Tripathy S, Li Y, Sue H-J. Photoluminescence and micro-Raman scattering in ZnO nanoparticles: The influence of acetate adsorption. Chemical Physics Letters. 2005;411(1-3):150-4.

[76] Sun D, Miyatake N, Sue H-J. Transparent PMMA/ZnO nanocomposite films based on colloidal ZnO quantum dots. Nanotechnology. 2007;18(21):215606.

[77] Sun D, Wong M, Sun L, Li Y, Miyatake N, Sue H-J. Purification and stabilization of colloidal ZnO nanoparticles in methanol. Journal of Sol-Gel Science and Technology. 2007;43(2):237-43.

[78] Sun D, Sue H-J, Miyatake N. Optical properties of ZnO quantum dots in epoxy with controlled dispersion. Journal of Physical Chemistry C. 2008;112:16002-10.

[79] Sun D, Sue H-J. Tunable ultraviolet emission of ZnO quantum dots in transparent poly(methyl methacrylate). Applied Physics Letters. 2009;94(25):253106.

[80] Wong M, Tsuji R, Nutt S, Sue H-J. Glass transition temperature changes of melt-blended polymer nanocomposites containing finely dispersed ZnO quantum dots. Soft Matter. 2010;6(18):4482.

[81] Sun D, Chu C-C, Sue H-J. Simple Approach for Preparation of Epoxy Hybrid Nanocomposites Based on Carbon Nanotubes and a Model Clay. Chemistry of Materials. 2010;22(12):3773-8.

[82] Groleau MR, Shi Y-B, Yee AF, Bertram JL, Sue HJ, Yang PC. Mode II fracture of composites interlayered with nylon particles. Composites Science and Technology. 1996;56(11):1223-40.

[83] Pearson R, Yee A. Toughening mechanisms in elastomer-modified epoxies. Journal of Materials Science. 1989;24(7):2571-80.

[84] Sue H-J. Fracture toughness and the corresponding toughening mechanisms of rubber-modified brittle epoxies. 1990.

[85] Pearson RA, Yee AF. Influence of particle size and particle size distribution on toughening mechanisms in rubber-modified epoxies. Journal of Materials Science. 1991;26:3828-44.

[86] Sue H-J. Study of rubber-modified brittle epoxy systems. Part I: Fracture toughness measurements using the double-notch four-point-bend method. Polymer Engineering and Science. 1991;31(4):270-4.

[87] Sue HJ. Study of rubber-modified brittle epoxy systems. Part II: Toughening mechanisms under mode-I fracture. Polymer Engineering & Science. 1991;31(4):275-88.

[88] Iijima S. Helical microtubules of graphitic carbon. Nature. 1991;354(6348):56-8.

[89] Novoselov AKGKS. The rise of graphene. Nature Materials. 2007;6:183-91.

[90] Prasek J, Drbohlavova J, Chomoucka J, Hubalek J, Jasek O, Adam V, et al. Methods for carbon nanotubes synthesis—review. Journal of Materials Chemistry. 2011;21(40):15872.

[91] Thess A, Lee R, Nikolaev P, Dai H, Petit P, Robert J, et al. Crystalline ropes of metallic carbon nanotubes. Science. 1996;273:483-7.

[92] Li C, Thostenson ET, Chou T-W. Dominant role of tunneling resistance in the electrical conductivity of carbon nanotube–based composites. Applied Physics Letters. 2007;91(22):223114.

[93] Li C, Thostenson ET, Chou T-W. Sensors and actuators based on carbon nanotubes and their composites: A review. Composites Science and Technology. 2008;68(6):1227-49.

[94] Li C, Thostenson ET, Chou T-W. Effect of nanotube waviness on the electrical conductivity of carbon nanotube-based composites. Composites Science and Technology. 2008;68(6):1445-52.

[95] Gao L, Chou T-W, Thostenson ET, Godara A, Zhang Z, Mezzo L. Highly conductive polymer composites based on controlled agglomeration of carbon nanotubes. Carbon. 2010;48(9):2649-51.

[96] Lu W, Chou T-W, Thostenson ET. A three-dimensional model of electrical percolation thresholds in carbon nanotube-based composites. Applied Physics Letters. 2010;96(22):223106.

[97] Allaoui A, Bai S, Cheng HM, Bai JB. Mechanical and electrical properties of a MWNT/epoxy composite. Composites Science and Technology. 2002;62:1993-8.

[98] Sandler JKW, Kirk JE, Kinloch IA, Shaffer MSP, Windle AH. Ultra-low electrical percolation threshold in carbon-nanotube-epoxy composites. Polymer. 2003;44(19):5893-9.

[99] Gojny FH, Wichmann MHG, Fiedler B, Kinloch IA, Bauhofer W, Windle AH, et al. Evaluation and identification of electrical and thermal conduction mechanisms in carbon nanotube/epoxy composites. Polymer. 2006;47(6):2036-45.

[100] Bauhofer W, Kovacs JZ. A review and analysis of electrical percolation in carbon nanotube polymer composites. Composites Science and Technology. 2009;69(10):1486-98.

[101] Min C, Shen X, Shi Z, Chen L, Xu Z. The Electrical Properties and Conducting Mechanisms of Carbon Nanotube/Polymer Nanocomposites: A Review. Polymer-Plastics Technology and Engineering. 2010;49(12):1172-81.

[102] Spitalsky Z, Tasis D, Papagelis K, Galiotis C. Carbon nanotube–polymer composites: Chemistry, processing, mechanical and electrical properties. Progress in Polymer Science. 2010;35(3):357-401.

[103] Gardea F. Electrical and thermal experimental characterization and modeling of carbon nanotube/epoxy composites. Texas A&M University, Master of Science, 2011.

[104] White KL, Shuai M, Zhang X, Sue H-J, Nishimura R. Electrical conductivity of well-exfoliated single-walled carbon nanotubes. Carbon. 2011;49(15):5124-31.

[105] Tang L-C, Wan Y-J, Peng K, Pei Y-B, Wu L-B, Chen L-M, et al. Fracture toughness and electrical conductivity of epoxy composites filled with carbon nanotubes and spherical particles. Composites Part A: Applied Science and Manufacturing. 2013;45:95-101.

[106] Gardea F, Lagoudas DC. Characterization of electrical and thermal properties of carbon nanotube/epoxy composites. Composites Part B: Engineering. 2014;56:611-20.

[107] Gu J, Liang C, Zhao X, Gan B, Qiu H, Guo Y, et al. Highly thermally conductive flame-retardant epoxy nanocomposites with reduced ignitability and excellent electrical conductivities. Composites Science and Technology. 2017;139:83-9.

[108] Guadagno L, Naddeo C, Raimondo M, Barra G, Vertuccio L, Russo S, et al. Influence of carbon nanoparticles/epoxy matrix interaction on mechanical, electrical and transport properties of structural advanced materials. Nanotechnology. 2017;28(9):094001.

[109] Balasubramanian K, Burghard M. Chemically functionalized carbon nanotubes. Small. 2005;1(2):180-92.

[110] Schadler LS, Giannaris SC, Ajayan PM. Load transfer in carbon nanotube epoxy composites. Applied Physics Letters. 1998;73(26):3842-4.

[111] Avilés F, Cauich-Rodríguez JV, Moo-Tah L, May-Pat A, Vargas-Coronado R. Evaluation of mild acid oxidation treatments for MWCNT functionalization. Carbon. 2009;47(13):2970-5.

[112] Chiang Y-C, Lin W-H, Chang Y-C. The influence of treatment duration on multi-walled carbon nanotubes functionalized by H2SO4/HNO3 oxidation. Applied Surface Science. 2011;257(6):2401-10.

[113] Hirsch A. Functionalization of single-walled carbon nanotubes. Angewandte Chemie International Edition. 2002;41(11):1853-9.

[114] Martinez-Rubi Y, Gonzalez-Dominguez JM, Anson-Casaos A, Kingston CT, Daroszewska M, Barnes M, et al. Tailored SWCNT functionalization optimized for compatibility with epoxy matrices. Nanotechnology. 2012;23(28):285701.

[115] Murphy H, Papakonstantinou P, Okpalugo TIT. Raman study of multiwalled carbon nanotubes functionalized with oxygen groups. Journal of Vacuum Science & Technology B: Microelectronics and Nanometer Structures. 2006;24(2):715.

[116] Bom D, Andrews R, Jacques D, Anthony J, Chen B, Meier MS, et al. Thermogravimetric Analysis of the Oxidation of Multiwalled Carbon Nanotubes:

Evidence for the Role of Defect Sites in Carbon Nanotube Chemistry. Nano Letters. 2002;2(6):615-9.

[117] Datsyuk V, Kalyva M, Papagelis K, Parthenios J, Tasis D, Siokou A, et al. Chemical oxidation of multiwalled carbon nanotubes. Carbon. 2008;46(6):833-40.

[118] Rosca ID, Watari F, Uo M, Akasaka T. Oxidation of multiwalled carbon nanotubes by nitric acid. Carbon. 2005;43(15):3124-31.

[119] Saleh TA. The influence of treatment temperature on the acidity of MWCNT oxidized by HNO3 or a mixture of HNO3/H2SO4. Applied Surface Science. 2011;257(17):7746-51.

[120] Stobinski L, Lesiak B, Kövér L, Tóth J, Biniak S, Trykowski G, et al. Multiwall carbon nanotubes purification and oxidation by nitric acid studied by the FTIR and electron spectroscopy methods. Journal of Alloys and Compounds. 2010;501(1):77-84.

[121] Wepasnick KA, Smith BA, Schrote KE, Wilson HK, Diegelmann SR, Fairbrother DH. Surface and structural characterization of multi-walled carbon nanotubes following different oxidative treatments. Carbon. 2011;49(1):24-36.

[122] Ziegler KJ, Gu Z, Peng H, Flor EL, Hauge RH, Smalley RE. Controlled Oxidative Cutting of Single-Walled Carbon Nanotubes. Journal of the American Chemical Society. 2005;127:1541-7.

[123] Wang S, Liang Z, Liu T, Wang B, Zhang C. Effective amino-functionalization of carbon nanotubes for reinforcing epoxy polymer composites. Nanotechnology. 2006;17(6):1551-7.

[124] Sun L, Warren GL, O'Reilly JY, Everett WN, Lee SM, Davis D, et al. Mechanical properties of surface-functionalized SWCNT/epoxy composites. Carbon. 2008;46(2):320-8.

[125] Yang K, Gu M, Guo Y, Pan X, Mu G. Effects of carbon nanotube functionalization on the mechanical and thermal properties of epoxy composites. Carbon. 2009;47(7):1723-37.

[126] Sahoo NG, Rana S, Cho JW, Li L, Chan SH. Polymer nanocomposites based on functionalized carbon nanotubes. Progress in Polymer Science. 2010;35(7):837-67.

[127] Yang S-Y, Ma C-CM, Teng C-C, Huang Y-W, Liao S-H, Huang Y-L, et al. Effect of functionalized carbon nanotubes on the thermal conductivity of epoxy composites. Carbon. 2010;48(3):592-603.

[128] Davis DC, Wilkerson JW, Zhu J, Hadjiev VG. A strategy for improving mechanical properties of a fiber reinforced epoxy composite using functionalized carbon nanotubes. Composites Science and Technology. 2011;71(8):1089-97.

[129] Gonzalez-Dominguez JM, Martinez-Rubi Y, Diez-Pascual AM, Anson-Casaos A, Gomez-Fatou M, Simard B, et al. Reactive fillers based on SWCNTs functionalized with matrix-based moieties for the production of epoxy composites with superior and tunable properties. Nanotechnology. 2012;23(28):285702.

[130] Kamat PV. Graphene-Based Nanoarchitectures. Anchoring Semiconductor and Metal Nanoparticles on a Two-Dimensional Carbon Support. The Journal of Physical Chemistry Letters. 2009;1:520-7.

[131] Kuilla T, Bhadra S, Yao D, Kim NH, Bose S, Lee JH. Recent advances in graphene based polymer composites. Progress in Polymer Science. 2010;35(11):1350-75.

[132] Potts JR, Dreyer DR, Bielawski CW, Ruoff RS. Graphene-based polymer nanocomposites. Polymer. 2011;52(1):5-25.

[133] Ang L, Hor TA, Xu G, Tung C, Zhao S, Wang J. Decoration of activated carbon nanotubes with copper and nickel. Carbon. 2000;38(3):363-72.

[134] Zhang N, Sun J, Jiang D, Feng T, Li Q. Anchoring zinc oxide quantum dots on functionalized multi-walled carbon nanotubes by covalent coupling. Carbon. 2009;47(5):1214-9.

[135] Park SH, Bandaru PR. Improved mechanical properties of carbon nanotube/polymer composites through the use of carboxyl-epoxide functional group linkages. Polymer. 2010;51(22):5071-7.

[136] Yao H, Jin L, Sue H-J, Sumi Y, Nishimura R. Facile decoration of Au nanoparticles on reduced graphene oxide surfaces via a one-step chemical functionalization approach. Journal of Materials Chemistry A. 2013;1(36):10783-9.

[137] Teng C-C, Ma C-CM, Lu C-H, Yang S-Y, Lee S-H, Hsiao M-C, et al. Thermal conductivity and structure of non-covalent functionalized graphene/epoxy composites. Carbon. 2011;49(15):5107-16.

[138] Gu Z, Peng H, Hauge RH, Smalley RE, Margrave JL. Cutting single-wall carbon nanotubes through fluorination. Nano Letters. 2002;2(9):1009-13.

[139] Stevens JL, Huang AY, Peng H, Chiang IW, Khabashesku VN, Margrave JL. Sidewall amino-functionalization of single-walled carbon nanotubes through fluorination and subsequent reactions with terminal diamines. Nano Letters. 2003;3(3):331-6.

[140] Charlier J-C. Defects in carbon nanotubes. Accounts of Chemical Research. 2002;35:1063-9.

[141] Ebbesen TW, Hiura H, Bisher ME, Treacy MM, Shreeve-Keyer JL, Haushalter RC. Decoration of carbon nanotubes. Advanced Materials. 1996;8(2):155-7.

[142] Satishkumar B, Vogl EM, Govindaraj A, Rao C. The decoration of carbon nanotubes by metal nanoparticles. Journal of Physics D: Applied Physics. 1996;29(12):3173.

[143] Jiang L, Gao L. Modified carbon nanotubes: an effective way to selective attachment of gold nanoparticles. Carbon. 2003;41(15):2923-9.

[144] Jiang L, Gao L. Fabrication and characterization of ZnO-coated multi-walled carbon nanotubes with enhanced photocatalytic activity. Materials Chemistry and Physics. 2005;91(2-3):313-6.

[145] Landi BJ, Castro SL, Ruf HJ, Evans CM, Bailey SG, Raffaelle RP. CdSe quantum dot-single wall carbon nanotube complexes for polymeric solar cells. Solar Energy Materials and Solar Cells. 2005;87(1-4):733-46.

[146] Biju V, Itoh T, Makita Y, Ishikawa M. Close-conjugation of quantum dots and gold nanoparticles to sidewall functionalized single-walled carbon nanotube templates. Journal of Photochemistry and Photobiology A: Chemistry. 2006;183(3):315-21.

[147] Chen CS, Chen XH, Yi B, Liu TG, Li WH, Xu LS, et al. Zinc oxide nanoparticle decorated multi-walled carbon nanotubes and their optical properties. Acta Materialia. 2006;54(20):5401-7.

[148] Landi BJ, Evans CM, Worman JJ, Castro SL, Bailey SG, Raffaelle RP. Noncovalent attachment of CdSe quantum dots to single wall carbon nanotubes. Materials Letters. 2006;60(29-30):3502-6.

[149] Li X, Liu Y, Fu L, Cao L, Wei D, Wang Y. Efficient synthesis of carbon nanotube–nanoparticle hybrids. Advanced Functional Materials. 2006;16(18):2431-7.

[150] Pan B, Cui D, He R, Gao F, Zhang Y. Covalent attachment of quantum dot on carbon nanotubes. Chemical Physics Letters. 2006;417(4-6):419-24.

[151] Tzitzios V, Georgakilas V, Oikonomou E, Karakassides M, Petridis D. Synthesis and characterization of carbon nanotube/metal nanoparticle composites well dispersed in organic media. Carbon. 2006;44(5):848-53.

[152] Bittencourt C, Felten A, Ghijsen J, Pireaux J, Drube W, Erni R, et al. Decorating carbon nanotubes with nickel nanoparticles. Chemical Physics Letters. 2007;436(4):368-72.

[153] Dai K, Shi L, Fang J, Zhang Y. Synthesis of silver nanoparticles on functional multi-walled carbon nanotubes. Materials Science and Engineering: A. 2007;465(1):283-6.

[154] Georgakilas V, Gournis D, Tzitzios V, Pasquato L, Guldi DM, Prato M. Decorating carbon nanotubes with metal or semiconductor nanoparticles. Journal of Materials Chemistry. 2007;17(26):2679-94.

[155] Jiang H, Zhu L, Moon K-s, Wong C. The preparation of stable metal nanoparticles on carbon nanotubes whose surfaces were modified during production. Carbon. 2007;45(3):655-61.

[156] Lee KY, Kim M, Lee YW, Lee J-J, Han SW. Fabrication of metal nanoparticles–carbon nanotubes composite materials in solution. Chemical Physics Letters. 2007;440(4):249-52.

[157] Du Y, Hao C, Wang G. Preparation of floral-patterned ZnO/MWCNT heterogeneity structure using microwave irradiation heating method. Materials Letters. 2008;62(1):30-2.

[158] Ma PC, Tang BZ, Kim J-K. Effect of CNT decoration with silver nanoparticles on electrical conductivity of CNT-polymer composites. Carbon. 2008;46(11):1497-505.

[159] Stobinski L, Peszke J, Tomasik P, Lin H-M. Decoration of carboxylated multi-wall carbon nanotubes with quantum dots. Journal of Alloys and Compounds. 2008;455(1-2):137-41.

[160] Wang X, Xia B, Zhu X, Chen J, Qiu S, Li J. Controlled modification of multiwalled carbon nanotubes with ZnO nanostructures. Journal of Solid State Chemistry. 2008;181(4):822-7.

[161] Xu P, Cui D, Pan B, Gao F, He R, Li Q, et al. A facile strategy for covalent binding of nanoparticles onto carbon nanotubes. Applied Surface Science. 2008;254(16):5236-40.

[162] Gonzalez-Campo A, Orchard KL, Sato N, Shaffer MS, Williams CK. One-pot, in situ synthesis of ZnO-carbon nanotube-epoxy resin hybrid nanocomposites. Chem Commun (Camb). 2009(27):4034-6.

[163] Zhu L-P, Liao G-H, Huang W-Y, Ma L-L, Yang Y, Yu Y, et al. Preparation, characterization and photocatalytic properties of ZnO-coated multi-walled carbon nanotubes. Materials Science and Engineering: B. 2009;163(3):194-8.

[164] Klanwan J, Akrapattangkul N, Pavarajarn V, Seto T, Otani Y, Charinpanitkul T. Single-step synthesis of MWCNT/ZnO nanocomposite using co-chemical vapor deposition method. Materials Letters. 2010;64(1):80-2.

[165] Sameera I, Bhatia R, Prasad V. Preparation, characterization and electrical conductivity studies of MWCNT/ZnO nanoparticles hybrid. Physica B: Condensed Matter. 2010;405(7):1709-14.

[166] Tan Z, Chua DHC. ZnO tip-coated CNT core-shell structures for photoluminescence and electron emission properties. Journal of The Electrochemical Society. 2011;4:112-6.

[167] Wu B, Kuang Y, Zhang X, Chen J. Noble metal nanoparticles/carbon nanotubes nanohybrids: synthesis and applications. Nano Today. 2011;6(1):75-90.

[168] Xin F, Li L. Decoration of carbon nanotubes with silver nanoparticles for advanced CNT/polymer nanocomposites. Composites Part A: Applied Science and Manufacturing. 2011;42(8):961-7.

[169] Peng Y, Chen Q. Fabrication of one-dimensional Ag/multiwalled carbon nanotube nano-composite. Nanoscale Research Letters. 2012;7:195.

[170] Daneshvar-Fatah F, Nasirpouri F. A study on electrodeposition of Ni-noncovalently treated carbon nanotubes nanocomposite coatings with desirable mechanical and anti-corrosion properties. Surface and Coatings Technology. 2014;248:63-73.

[171] Shao D, Sun H, Gao J, Xin G, Aguilar MA, Yao T, et al. Flexible, thorn-like ZnO-multiwalled carbon nanotube hybrid paper for efficient ultraviolet sensing and photocatalyst applications. Nanoscale. 2014;6(22):13630-6.

[172] Nasirpouri F, Daneshvar-Fattah F, Samardak A, Sukovatitsina E, Ognev A, Chebotkevich L. Magnetic properties of electrodeposited nickel-multiwall carbon nanotube composite films. IEEE Transactions on Magnetics. 2015;51(11):1-4.

[173] Bagheri R, Marouf BT, Pearson RA. Rubber-Toughened Epoxies: A Critical Review. Polymer Reviews. 2009;49(3):201-25.

[174] Liew KM, Lei ZX, Zhang LW. Mechanical analysis of functionally graded carbon nanotube reinforced composites: A review. Composite Structures. 2015;120:90-7.

[175] Meer S, Kausar A, Iqbal T. Trends in Conducting Polymer and Hybrids of Conducting Polymer/Carbon Nanotube: A Review. Polymer-Plastics Technology and Engineering. 2016;55(13):1416-40.

[176] Gantayat S, Rout D, Swain SK. Carbon Nanomaterial–Reinforced Epoxy Composites: A Review. Polymer-Plastics Technology and Engineering. 2017:1-16.

[177] Thostenson ET, Chou T-W. Carbon nanotube-based health monitoring of mechanically fastened composite joints. Composites Science and Technology. 2008;68(12):2557-61.

[178] Warren GL, Sun L, Hadjiev VG, Davis D, Lagoudas D, Sue H-J. B-staged epoxy/single-walled carbon nanotube nanocomposite thin films for composite reinforcement. Journal of Applied Polymer Science. 2009;112(1):290-8.

[179] White KL. Improvement in the mechanical properties of B-staged carbon nanotube/epoxy based thin film systems. Texas A&M University, Bachelor of Science, 2009.

[180] Sun L, Warren GL, Sue H-J. Partially cured epoxy/SWCNT thin films for the reinforcement of vacuum-assisted resin-transfer-molded composites. Carbon. 2010;48(8):2364-7.

[181] Sager RJ, Klein PJ, Davis DC, Lagoudas DC, Warren GL, Sue H-J. Interlaminar fracture toughness of woven fabric composite laminates with carbon nanotube/epoxy interleaf films. Journal of Applied Polymer Science. 2011;121(4):2394-405.

[182] Ishai O, Rosenthal H, Sela N, Drukker E. Effect of selective adhesive interleaving on interlaminar fracture toughness of graphite/epoxy composite laminates. Composites. 1988;19(1):49-54.

[183] Sela N, Ishai O, Banks-Sills L. The effect of adhesive thickness on interlaminar fracture toughness of interleaved CFRP specimens. Composites. 1989;20(3):257-64.

[184] Butkus LM, Mathern PD, Johnson WS. Tensile Properties and Plane-Stress Fracture Toughness of Thin Film Aerospace Adhesives. The Journal of Adhesion. 1998;66(1-4):251-73.

[185] Novák I, Krupa I, Chodák I. Analysis of correlation between percolation concentration and elongation at break in filled electroconductive epoxy-based adhesives. European Polymer Journal. 2003;39(3):585-92.

[186] Feng C-W. Prediction of long-term creep behavior of epoxy adhesives for structural applications. Texas A&M University, Master of Science, 2004.

[187] Feng CW, Keong CW, Hsueh YP, Wang YY, Sue HJ. Modeling of long-term creep behavior of structural epoxy adhesives. International Journal of Adhesion and Adhesives. 2005;25(5):427-36.

[188] Jiang H, Browning R, Liu P, Chang TA, Sue H-J. Determination of epoxy coating wet-adhesive strength using a standardized ASTM/ISO scratch test. Journal of Coatings Technology and Research. 2010;8(2):255-63.

[189] Quan D, Carolan D, Rouge C, Murphy N, Ivankovic A. Carbon nanotubes and core–shell rubber nanoparticles modified structural epoxy adhesives. Journal of Materials Science. 2016;52(8):4493-508.

[190] Zotti A, Zuppolini S, Zarrelli M, Borriello A. Fracture Toughening Mechanisms in Epoxy Adhesives. 2016.

[191] Kinloch AJ, Shaw SJ, Hunston DL. Deformation and fracture behaviour of a rubber-toughened epoxy: 2. Failure criteria. Polymer. 1983;24:1355-63.

[192] Kinloch AJ, Shaw SJ, Tod DA, Hunston DL. Deformation and fracture behaviour of a rubber-toughened epoxy: 1. Microstructure and fracture studies. Polymer. 1983;24:1341-54.

[193] Sue H-J, Meitin EIG, Pickelman DM, Bott CJ. Fracture mechanisms in rigid core-shell particle modified high performance epoxies. Colloid and Polymer Science. 1996;274:342-9.

[194] Gam KT, Miyamoto M, Nishimura R, Sue H-J. Fracture behavior of core-shell rubber-modified clay-epoxy nanocomposites. Polymer Engineering and Science. 2003;43(10):1635-45.

[195] Wetzel B, Rosso P, Haupert F, Friedrich K. Epoxy nanocomposites – fracture and toughening mechanisms. Engineering Fracture Mechanics. 2006;73(16):2375-98.

[196] Liu J, Sue H-J, Thompson ZJ, Bates FS, Dettloff M, Jacob G, et al. Effect of crosslink density on fracture behavior of model epoxies containing block copolymer nanoparticles. Polymer. 2009;50(19):4683-9.

[197] Zheng N, Huang Y, Liu H-Y, Gao J, Mai Y-W. Improvement of interlaminar fracture toughness in carbon fiber/epoxy composites with carbon nanotubes/polysulfone interleaves. Composites Science and Technology. 2017;140:8-15.

[198] Bose S, Khare RA, Moldenaers P. Assessing the strengths and weaknesses of various types of pre-treatments of carbon nanotubes on the properties of polymer/carbon nanotubes composites: A critical review. Polymer. 2010;51(5):975-93.

[199] Jia J, Sun X, Lin X, Shen X, Mai Y-W, Kim J-K. Exceptional electrical conductivity and fracture resistance of 3D interconnected graphene foam/epoxy composites. ACS Nano. 2014;8(6):5774–83.

[200] Ladani RB, Wu S, Kinloch AJ, Ghorbani K, Zhang J, Mouritz AP, et al. Improving the toughness and electrical conductivity of epoxy nanocomposites by using

aligned carbon nanofibres. Composites Science and Technology. 2015;117:146-58.

[201] Lim YJ, Carolan D, Taylor AC. Simultaneously tough and conductive rubber–graphene–epoxy nanocomposites. Journal of Materials Science. 2016;51(18):8631-44.

[202] Xu Y, Li Y, Hua W, Zhang A, Bao J. Light-Weight Silver Plating Foam and Carbon Nanotube Hybridized Epoxy Composite Foams with Exceptional Conductivity and Electromagnetic Shielding Property. ACS Appl Mater Interfaces. 2016;8(36):24131-42.

[203] Teng K, Ni Y, Wang W, Wang H, Xu Z, Chen L, et al. Adjustable micro-structure, higher-level mechanical behavior and conductivities of preformed graphene architecture/epoxy composites via RTM route. Composites Part A: Applied Science and Manufacturing. 2017;94:178-88.

[204] Špitalský Z, Krontiras CA, Georga SN, Galiotis C. Effect of oxidation treatment of multiwalled carbon nanotubes on the mechanical and electrical properties of their epoxy composites. Composites Part A: Applied Science and Manufacturing. 2009;40(6-7):778-83.

[205] Ghaleb ZA, Mariatti M, Ariff ZM. Properties of graphene nanopowder and multi-walled carbon nanotube-filled epoxy thin-film nanocomposites for electronic applications: The effect of sonication time and filler loading. Composites Part A: Applied Science and Manufacturing. 2014;58:77-83.

[206] Fogel M, Parlevliet P, Geistbeck M, Olivier P, Dantras É. Thermal, rheological and electrical analysis of MWCNTs/epoxy matrices. Composites Science and Technology. 2015;110:118-25.

[207] Wang X, Yong ZZ, Li QW, Bradford PD, Liu W, Tucker DS, et al. Ultrastrong, Stiff and Multifunctional Carbon Nanotube Composites. Materials Research Letters. 2012;1(1):19-25.

[208] Mikhalchan A, Gspann T, Windle A. Aligned carbon nanotube–epoxy composites: the effect of nanotube organization on strength, stiffness, and toughness. Journal of Materials Science. 2016;51(22):10005-25.

[209] Coleman JN, Khan U, Blau WJ, Gun'ko YK. Small but strong: A review of the mechanical properties of carbon nanotube–polymer composites. Carbon. 2006;44(9):1624-52.

[210] Gojny F, Wichmann M, Fiedler B, Schulte K. Influence of different carbon nanotubes on the mechanical properties of epoxy matrix composites – A comparative study. Composites Science and Technology. 2005;65(15-16):2300-13.

[211] Fiedler B, Gojny FH, Wichmann MH, Nolte MC, Schulte K. Fundamental aspects of nano-reinforced composites. Composites Science and Technology. 2006;66(16):3115-25.

[212] Guo P, Chen X, Gao X, Song H, Shen H. Fabrication and mechanical properties of well-dispersed multiwalled carbon nanotubes/epoxy composites. Composites Science and Technology. 2007;67(15-16):3331-7.

[213] Ma PC, Kim J-K, Tang BZ. Effects of silane functionalization on the properties of carbon nanotube/epoxy nanocomposites. Composites Science and Technology. 2007;67(14):2965-72.

[214] Guo P, Song H, Chen X. Interfacial properties and microstructure of multiwalled carbon nanotubes/epoxy composites. Materials Science and Engineering: A. 2009;517(1-2):17-23.

[215] Kathi J, Rhee K-Y, Lee JH. Effect of chemical functionalization of multi-walled carbon nanotubes with 3-aminopropyltriethoxysilane on mechanical and morphological properties of epoxy nanocomposites. Composites Part A: Applied Science and Manufacturing. 2009;40(6-7):800-9.

[216] Kim H-C, Kim S-K, Kim JT, Rhee K-Y, Kathi J. Thermal and Tensile Properties of Epoxy Nanocomposites Reinforced by Silane-functionalized Multiwalled Carbon Nanotubes. Journal of Macromolecular Science, Part B. 2010;49(1):132-42.

[217] Montazeri A, Montazeri N, Farzaneh S. Thermo-Mechanical Properties of Multi-Walled Carbon Nanotube (MWCNT)/Epoxy Composites. International Journal of Polymer Analysis and Characterization. 2011;16(3):199-210.

[218] Shanmugharaj AM, Choi WS, Ryu SH. Physical properties of phenol-anchored multiwall carbon nanotube/epoxy nanocomposite. Polymer Bulletin. 2011;67(8):1721-30.

[219] Zhang J, Jiang D. Interconnected multi-walled carbon nanotubes reinforced polymer-matrix composites. Composites Science and Technology. 2011;71(4):466-70.

[220] Srikanth I, Kumar S, Kumar A, Ghosal P, Subrahmanyam C. Effect of amino functionalized MWCNT on the crosslink density, fracture toughness of epoxy and mechanical properties of carbon–epoxy composites. Composites Part A: Applied Science and Manufacturing. 2012;43(11):2083-6.

[221] Cui L-J, Wang Y-B, Xiu W-J, Wang W-Y, Xu L-H, Xu X-B, et al. Effect of functionalization of multi-walled carbon nanotube on the curing behavior and mechanical property of multi-walled carbon nanotube/epoxy composites. Materials & Design. 2013;49:279-84.

[222] Shirkavand Hadavand B, Mahdavi Javid K, Gharagozlou M. Mechanical properties of multi-walled carbon nanotube/epoxy polysulfide nanocomposite. Materials & Design. 2013;50:62-7.

[223] Singh BP, Prasanta, Choudhary V, Saini P, Pande S, Singh VN, et al. Enhanced microwave shielding and mechanical properties of high loading MWCNT–epoxy composites. Journal of Nanoparticle Research. 2013;15(4).

[224] Revathi A, Rao S, Rao KV, Rajendra Prakash M, Sendil Murugan M, Srihari S, et al. Influence of temperature on tensile behavior of multiwalled carbon nanotube modified epoxy nanocomposites. Journal of Materials Research. 2014;29(15):1635-41.

[225] Zhang J, Wang Y, Wang X, Ding G, Pan Y, Xie H, et al. Effects of amino-functionalized carbon nanotubes on the properties of amine-terminated butadiene-acrylonitrile rubber-toughened epoxy resins. Journal of Applied Polymer Science. 2014;131(13):n/a-n/a.

[226] Ghosh PK, Kumar K, Chaudhary N. Influence of ultrasonic dual mixing on thermal and tensile properties of MWCNTs-epoxy composite. Composites Part B: Engineering. 2015;77:139-44.

[227] Wu J, Yu K, Qian K, Jia Y. One step fabrication of multi-walled carbon nanotubes/graphene nanoplatelets hybrid materials with excellent mechanical property. Fibers and Polymers. 2015;16(7):1540-6.

[228] Gazderazi M, Jamshidi M. Hybridizing MWCNT with nano metal oxides and TiO2in epoxy composites: Influence on mechanical and thermal performances. Journal of Applied Polymer Science. 2016;133(34).

[229] Lee S-E, Lee MY, Lee M-K, Jeong E, Lee Y-S. Effect of fluorination on the mechanical behavior and electromagnetic interference shielding of MWCNT/epoxy composites. Applied Surface Science. 2016;369:189-95.

[230] Ozaytekin I, Turedi HE, Ahmetli G. Preparation of epoxy composites with CTAB-modified BN and MWCNTs. Polymer Composites. 2016;37(12):3423-32.

[231] Zhang X, Zhao D, Luan D, Bi C. Fabrication and mechanical properties of multiwalled carbon nanotube/nanonickel reinforced epoxy resin composites. Applied Physics A. 2016;122(12).

[232] Ghaleb ZA, Mariatti M, Ariff ZM. Synergy effects of graphene and multiwalled carbon nanotubes hybrid system on properties of epoxy nanocomposites. Journal of Reinforced Plastics and Composites. 2017;36(9):685-95.

[233] Kumar A, Ghosh PK, Yadav KL, Kumar K. Thermo-mechanical and anti-corrosive properties of MWCNT/epoxy nanocomposite fabricated by innovative dispersion technique. Composites Part B: Engineering. 2017;113:291-9.

[234] Wu Y, Gu Z, Chen M, Zhu C, Liao H. Effect of functionalization of multi-walled carbon nanotube on mechanical and viscoelastic properties of polysulfide-modified epoxy nanocomposites. High Performance Polymers. 2017;29(2):151-60.

[235] Garg AC, Mai Y-W. Failure mechanisms in toughened epoxy resins - A review. Composites Science and Technology. 1988;31:179-223.

[236] Rider AN, Yeo E, Gopalakrishna J, Thostenson ET, Brack N. Hierarchical composites with high-volume fractions of carbon nanotubes: Influence of plasma surface treatment and thermoplastic nanophase-modified epoxy. Carbon. 2015;94:971-81.

[237] Carrillo-Escalante HJ, Alvarez-Castillo A, Valadez-Gonzalez A, Herrera-Franco PJ. Effect of fiber-matrix adhesion on the fracture behavior of a carbon fiber reinforced thermoplastic-modified epoxy matrix. Carbon Letters. 2016;19:47-56.

[238] Meeks AC. Fracture and mechanical properties of epoxy resins and rubber-modified epoxy resins. Polymer. 1974;15(10):675-81.

[239] Bucknall CB, Yoshii T. Relationship between structure and mechanical properties in rubber-toughened epoxy resins. British Polymer Journal. 1978;10(1):53-9.

[240] Sue H-J. Craze-like damage in a core-shell rubber-modified epoxy. 1991.

[241] Sue H, Garcia-Meitin E, Pickelman D. Toughening Concept in Rubber-Modified High Performance Epoxies. Elastomer Technology Handbook, N Cheremisinoff, Ed, CRC, Boca Raton. 1993;661.

[242] Sue H-J, Bertram JL, Garcia-Meitin EI, Wilchester JW, Walker LL. Fracture behavior of core-shell rubber-modified crosslinkable epoxy thermoplastics. Colloid and Polymer Science. 1994;272:456-66.

[243] Du J, Thouless MD, Yee AF. Development of a process zone in rubber-modified epoxy polymers. International Journal of Fracture. 1998;92(3):271-86.

[244] Gam KT. Structure-property relationship in core-shell rubber toughened epoxy nanocomposites. Texas A&M University, Doctor of Philosophy, 2003.

[245] Ma J, Mo M-S, Du X-S, Dai S-R, Luck I. Study of epoxy toughened by in situ formed rubber nanoparticles. Journal of Applied Polymer Science. 2008;110(1):304-12.

[246] Mafi ER, Ebrahimi M. Role of core-shell rubber particle cavitation resistance on toughenability of epoxy resins. Polymer Engineering & Science. 2008;48(7):1376-80.

[247] Abadyan M, Bagheri R, Kouchakzadeh MA. Fracture toughness of a hybrid-rubber-modified epoxy. I. Synergistic toughening. Journal of Applied Polymer Science. 2012;125(3):2467-75.

[248] Abadyan M, Kouchakzadeh MA, Bagheri R. Fracture toughness of a hybrid rubber modified epoxy. II. Effect of loading rate. Journal of Applied Polymer Science. 2012;125(3):2476-83.

[249] Zhou H, Xu S. A new method to prepare rubber toughened epoxy with high modulus and high impact strength. Materials Letters. 2014;121:238-40.

[250] Quan D, Ivankovic A. Effect of core–shell rubber (CSR) nano-particles on mechanical properties and fracture toughness of an epoxy polymer. Polymer. 2015;66:16-28.

[251] Caldona EB, De Leon ACC, Pajarito BB, Advincula RC. A Review on Rubber-Enhanced Polymeric Materials. Polymer Reviews. 2017;57(2):311-38.

[252] McGarry FJ, Willner AM. Toughening of an epoxy resin by an elastomer second phase. 1968.

[253] Sultan JN, Laible RC, McGarry FJ. Microstructure of two-phase polymers. Applied Polymer Symposium. 1971;16:127-36.

[254] Gorton BS. Interaction of nylon polymers with epoxy resins in adhesive blends. Journal of Applied Polymer Science. 1964;8:1287-95.

[255] Kim S, Kim J, Lim SH, Jo WH, Choe CR. Effects of mixing temperatures on the morphology and toughness of epoxy/polyamide blends. Journal of Applied Polymer Science. 1999;72:1055-63.

[256] Bakar M, Wojtania I, Legocka I, Gospodarczyk J. Property enhancement of epoxy resins by using a combination of polyamide and montmorillonite. Advances in Polymer Technology. 2007;26(4):223-31.

[257] Bucknall CB, Partridge IK. Addition of polyethersulphone to epoxy resins. British Polymer Journal. 1983;15:71.

[258] Bucknall CB, Partridge IK. Phase separation in epoxy resins containing polyethersulphone. Polymer. 1983;24:639-44.

[259] Singh S, Partridge IK. Mixed-mode fracture in an interleaved carbon-fibre/epoxy composite. Composites Science and Technology. 1995;55:319-27.

[260] Sue HJ, Gam KT, Bestaoui N, Clearfield A, Miyamoto M, Miyatake N. Fracture behavior of α-zirconium phosphate-based epoxy nanocomposites. Acta Materialia. 2004;52(8):2239-50.

[261] Wang K, Chen L, Wu J, Toh ML, He C, Yee AF. Epoxy nanocomposites with highly exfoliated clay: Mechanical properties and fracture mechanisms. Macromolecules. 2005;38:788-800.

[262] Boo WJ, Liu J, Sue HJ. Fracture behaviour of nanoplatelet reinforced polymer nanocomposites. Materials Science and Technology. 2006;22(7):829-34.

[263] Johnsen BB, Kinloch AJ, Mohammed RD, Taylor AC, Sprenger S. Toughening mechanisms of nanoparticle-modified epoxy polymers. Polymer. 2007;48(2):530-41.

[264] Adachi T, Osaki M, Araki W, Kwon S-C. Fracture toughness of nano- and micro-spherical silica-particle-filled epoxy composites. Acta Materialia. 2008;56(9):2101-9.

[265] Kim BC, Park SW, Lee DG. Fracture toughness of the nano-particle reinforced epoxy composite. Composite Structures. 2008;86(1-3):69-77.

[266] Liang Y, Pearson R. Toughening mechanisms in epoxy–silica nanocomposites (ESNs). Polymer. 2009;50(20):4895-905.

[267] Liu J. Toughening of epoxies based on self-assembly of nano-sized amphiphilic block copolymer micelles. Texas A&M University, Doctor of Philosophy, 2009.

[268] Thompson ZJ, Hillmyer MA, Liu JD, Sue H-J, Dettloff M, Bates FS. Block copolymer toughened epoxy: Role of cross-link density. Macromolecules. 2009;42:2333-5.

[269] Fang M, Zhang Z, Li J, Zhang H, Lu H, Yang Y. Constructing hierarchically structured interphases for strong and tough epoxy nanocomposites by amine-rich graphene surfaces. Journal of Materials Chemistry. 2010;20(43):9635.

[270] Hsieh TH, Kinloch AJ, Masania K, Taylor AC, Sprenger S. The mechanisms and mechanics of the toughening of epoxy polymers modified with silica nanoparticles. Polymer. 2010;51(26):6284-94.

[271] Hsieh TH, Kinloch AJ, Taylor AC, Kinloch IA. The effect of carbon nanotubes on the fracture toughness and fatigue performance of a thermosetting epoxy polymer. Journal of Materials Science. 2011;46(23):7525-35.

[272] Hsieh TH, Kinloch AJ, Taylor AC, Sprenger S. The effect of silica nanoparticles and carbon nanotubes on the toughness of a thermosetting epoxy polymer. Journal of Applied Polymer Science. 2011;119(4):2135-42.

[273] Bray DJ, Dittanet P, Guild FJ, Kinloch AJ, Masania K, Pearson RA, et al. The modelling of the toughening of epoxy polymers via silica nanoparticles: The effects of volume fraction and particle size. Polymer. 2013;54(26):7022-32.

[274] Lee C-F, Sue H-J, Fiscus DM. Refined fixture design for effective essential work of fracture toughness characterization of m-LLDPE thin films. Polymer Testing. 2013;32(2):256-64.

[275] Li Y, Umer R, Isakovic A, Samad YA, Zheng L, Liao K. Synergistic toughening of epoxy with carbon nanotubes and graphene oxide for improved long-term performance. RSC Advances. 2013;3(23):8849.

[276] Ghadami F, Dadfar MR, Kazazi M. Hot-cured epoxy-nanoparticulate-filled nanocomposites: Fracture toughness behavior. Engineering Fracture Mechanics. 2016;162:193-200.

[277] Konnola R, Nair CPR, Joseph K. High strength toughened epoxy nanocomposite based on poly(ether sulfone)-grafted multi-walled carbon nanotube. Polymers for Advanced Technologies. 2016;27(1):82-9.

[278] Li T, He S, Stein A, Francis LF, Bates FS. Synergistic Toughening of Epoxy Modified by Graphene and Block Copolymer Micelles. Macromolecules. 2016;49(24):9507-20.

[279] Liu S, Fan X, He C. Improving the fracture toughness of epoxy with nanosilica-rubber core-shell nanoparticles. Composites Science and Technology. 2016;125:132-40.

[280] Marouf BT, Mai Y-W, Bagheri R, Pearson RA. Toughening of Epoxy Nanocomposites: Nano and Hybrid Effects. Polymer Reviews. 2016;56(1):70-112.

[281] Wang F, Drzal LT, Qin Y, Huang Z. Enhancement of fracture toughness, mechanical and thermal properties of rubber/epoxy composites by incorporation

of graphene nanoplatelets. Composites Part A: Applied Science and Manufacturing. 2016;87:10-22.

[282] Zhang J, Deng S, Wang Y, Ye L. Role of rigid nanoparticles and CTBN rubber in the toughening of epoxies with different cross-linking densities. Composites Part A: Applied Science and Manufacturing. 2016;80:82-94.

[283] Kang W-S, Rhee KY, Park S-J. Influence of surface energetics of graphene oxide on fracture toughness of epoxy nanocomposites. Composites Part B: Engineering. 2017;114:175-83.

[284] Thitsartarn W, Fan X, Sun Y, Yeo JCC, Yuan D, He C. Simultaneous enhancement of strength and toughness of epoxy using POSS-Rubber core–shell nanoparticles. Composites Science and Technology. 2015;118:63-71.

[285] Colyer M, Ball T, Campbell MP. The work of fracture of epoxy resins. Cryogenics. 1974:281-3.

[286] Grayson MA, Fanter DL. A method for casting thin epoxy films. Journal of Applied Polymer Science. 1984;29:2677-8.

[287] Xu X, Thwe MM, Shearwood C, Liao K. Mechanical properties and interfacial characteristics of carbon-nanotube-reinforced epoxy thin films. Applied Physics Letters. 2002;81(15):2833-5.

[288] Guan C, Lü C-L, Liu Y-F, Yang B. Preparation and characterization of high refractive index thin films of TiO2/epoxy resin nanocomposites. Journal of Applied Polymer Science. 2006;102(2):1631-6.

[289] Yamada Y, Chung DDL. Epoxy-based carbon films with high electrical conductivity attached to an alumina substrate. Carbon. 2008;46(13):1798-801.

[290] Warren GL. Epoxy/single walled carbon nanotube nanocomposite thin films for composites reinforcement. Texas A&M University, Master of Science, 2009.

[291] Foo E, Jaafar M, Aziz A, Sim LC. Properties of spin coated epoxy/silica thin film composites: Effect of nano- and micron-size fillers. Composites Part A: Applied Science and Manufacturing. 2011;42(10):1432-7.

[292] Li J, Gao Y, Ma W, Liu L, Zhang Z, Niu Z, et al. High performance, freestanding and superthin carbon nanotube/epoxy nanocomposite films. Nanoscale. 2011;3(9):3731-6.

[293] Yahyaie H, Ebrahimi M, Tahami HV, Mafi ER. Toughening mechanisms of rubber modified thin film epoxy resins. Progress in Organic Coatings. 2013;76(1):286-92.

[294] Li P, Huang T-C, White KL, Hawkins S, Kotaki M, Nishimura R, et al. Spray-coated epoxy barrier films containing high aspect ratio functionalized graphene nanosheets. RSC Adv. 2015;5(124):102633-42.

[295] Liu P, Lam A, Fan Z, Tran TQ, Duong HM. Advanced multifunctional properties of aligned carbon nanotube-epoxy thin film composites. Materials & Design. 2015;87:600-5.

[296] Li K, Li Y, Lian Q, Cheng J, Zhang J. Influence of cross-linking density on the structure and properties of the interphase within supported ultrathin epoxy films. Journal of Materials Science. 2016;51(19):9019-30.

[297] McAninch IM, La Scala JJ, Palmese GR, Robinette EJ. Thin film initiation of cracks for fracture toughness measurements in epoxy resins. Journal of Applied Polymer Science. 2017;134(1).

[298] Hinkley JA, Mings SL. Fracture toughness of polyimide films. Polymer. 1990;31:75-7.

[299] Tobushi H, Hara H, Yamada E, Hayashi S. Thermomechanical properties in a thin film of shape memory polymer of polyurethane series. SPIE. 1996;2716:46-57.

[300] Kilwon Cho DL, Min Soo Lee and Chan Eon Park. Fracture behaviour of thin polyimide films. Polymer. 1997;38(7):1615-23.

[301] Giannakopoulos I, Taylor AC. An essential work of fracture study of the toughness of thermoset polyester coatings. Progress in Organic Coatings. 2015;78:265-74.

[302] Hawkins SA, Yao H, Wang H, Sue H-J. Tensile properties and electrical conductivity of epoxy composite thin films containing zinc oxide quantum dots and multi-walled carbon nanotubes. Carbon. 2017;115:18-27.

[303] Klemann BM, DeVilbiss T. The fracture toughness of thin polymeric films. Polymer Engineering & Science. 1996;36(1):126-34.

[304] Bose WW, Landes JD. Fracture toughness of thin polymer films using miniature specimens. Journal of Testing and Evaluation. 2003;31(4):1-7.

[305] Zhang S, Sun D, Fu Y, Du H. Toughness measurement of thin films: a critical review. Surface and Coatings Technology. 2005;198(1-3):74-84.

[306] Hosokawa H, Desai AV, Haque MA. Plane stress fracture toughness of freestanding nanoscale thin films. Thin Solid Films. 2008;516(18):6444-7.

[307] Zhu X-K, Joyce JA. Review of fracture toughness (G, K, J, CTOD, CTOA) testing and standardization. Engineering Fracture Mechanics. 2012;85:1-46.

[308] Han C, Yang M-Q, Weng B, Xu Y-J. Improving the photocatalytic activity and anti-photocorrosion of semiconductor ZnO by coupling with versatile carbon. Physical Chemistry Chemical Physics. 2014;16(32):16891-903.

[309] Liu J, Li X, Dai L. Water-Assisted Growth of Aligned Carbon Nanotube–ZnO Heterojunction Arrays. Advanced Materials. 2006;18(13):1740-4.

[310] Chrissanthopoulos A, Baskoutas S, Bouropoulos N, Dracopoulos V, Tasis D, Yannopoulos SN. Novel ZnO nanostructures grown on carbon nanotubes by thermal evaporation. Thin Solid Films. 2007;515(24):8524-8.

[311] Ok JG, Lee JY, Baac HW, Tawfick SH, Guo LJ, Hart AJ. Rapid anisotropic photoconductive response of ZnO-coated aligned carbon nanotube sheets. ACS Applied Materials and Interfaces. 2014;6(2):874-81.

[312] Sun J, Gao L, Iwasa M. Nonvocalent attachment of oxide nanoparticles onto carbon nanotubes using water-in-oil microemulsions. Chemical Communications. 2004;7:832-3.

[313] Meulenkamp EA. Synthesis and growth of ZnO nanoparticles. Journal of Physical Chemistry B. 1998;102:5566-72.

[314] Saleh TA, Gondal MA, Drmosh QA, Yamani ZH, Al-yamani A. Enhancement in photocatalytic activity for acetaldehyde removal by embedding ZnO nano particles

on multiwall carbon nanotubes. Chemical Engineering Journal. 2011;166(1):407-12.

[315] Tan Z, Chua DH. ZnO Tip-Coated Carbon Nanotubes Core–Shell Structures for Photoluminescence and Electron Emission Properties. Journal of The Electrochemical Society. 2011;158(4):K112-K6.

[316] Hosono E, Fujihara S, Kimura T, Imai H. Non-basic solution routes to prepare ZnO nanoparticles. Journal of Sol-Gel Science and Technology. 2004;29(2):71-9.

[317] Ishibashi K, Moriyama S, Fuse T, Yamaguchi T. Carbon nanotubes as building blocks of quantum dots. Physica E: Low-dimensional Systems and Nanostructures. 2006;35(2):338-43.

[318] Li X, Qi W, Mei D, Sushko ML, Aksay I, Liu J. Functionalized Graphene Sheets as Molecular Templates for Controlled Nucleation and Self-Assembly of Metal Oxide-Graphene Nanocomposites. Advanced Materials. 2012;24(37):5136-41.

[319] Sun D, Everett WN, Chu CC, Sue HJ. Single-walled carbon-nanotube dispersion with electrostatically tethered nanoplatelets. Small. 2009;5(23):2692-7.

[320] Zhang X, Sue H-J, Nishimura R. Electrostatically controlled isolation of debundled single-walled carbon nanotubes from nanoplatelet dispersant. Journal of Materials Chemistry. 2012;22(13):6156.

[321] Xie Y, Heo SH, Yoo SH, Ali G, Cho SO. Synthesis and photocatalytic activity of anatase TiO2 nanoparticles-coated carbon nanotubes. Nanoscale Research Letters. 2010;5(3):603-7.

[322] Kuo F-L, Li Y, Solomon M, Du J, Shepherd ND. Workfunction tuning of zinc oxide films by argon sputtering and oxygen plasma: an experimental and computational study. Journal of Physics D: Applied Physics. 2012;45(6):065301.

[323] Yao H, Sue H-J. New Approach to Disperse Carbon Nanotube in Solvent Through Inorganic Nanoparticles and Their Application in Visible-Light Photocatalyst. In Preparation.

[324] Bethune DS, Klang CH, de Vries MS, Gorman G, Savoy R, Vazquez J, et al. Cobalt-catalysed growth of carbon nanotubes with single-atomic-layer walls. Nature. 1993;363(6430):605-7.

[325] Zhu J, Wei S, Yadav A, Guo Z. Rheological behaviors and electrical conductivity of epoxy resin nanocomposites suspended with in-situ stabilized carbon nanofibers. Polymer. 2010;51(12):2643-51.

[326] Salvetat J-P, Bonard J-M, Thomson N, Kulik A, Forro L, Benoit W, et al. Mechanical properties of carbon nanotubes. Applied Physics A. 1999;69(3):255-60.

[327] Berber S, Kwon Y-K, Tománek D. Unusually high thermal conductivity of carbon nanotubes. Physical Review Letters. 2000;84(20):4613.

[328] Yu M-F, Lourie O, Dyer MJ, Moloni K, Kelly TF, Ruoff RS. Strength and breaking mechanism of multiwalled carbon nanotubes under tensile load. Science. 2000;287(5453):637-40.

[329] Dai H. Carbon nanotubes: synthesis, integration, and properties. Accounts of Chemical Research. 2002;35(12):1035-44.

[330] Seidel RV, Graham AP, Rajasekharan B, Unger E, Liebau M, Duesberg GS, et al. Bias dependence and electrical breakdown of small diameter single-walled carbon nanotubes. Journal of Applied Physics. 2004;96(11):6694-9.

[331] Kovacs JZ, Velagala BS, Schulte K, Bauhofer W. Two percolation thresholds in carbon nanotube epoxy composites. Composites Science and Technology. 2007;67(5):922-8.

[332] Liu P, White KL, Sugiyama H, Xi J, Higuchi T, Hoshino T, et al. Influence of trace amount of well-dispersed carbon nanotubes on structural development and tensile properties of polypropylene. Macromolecules. 2013;46:463-73.

[333] Zhang Y, Tang Z-R, Fu X, Xu Y-J. Engineering the unique 2D mat of graphene to achieve graphene-TiO2 nanocomposite for photocatalytic selective transformation: what advantage does graphene have over its forebear carbon nanotube? ACS nano. 2011;5(9):7426-35.

[334] ASTM. D638-14 Standard Test Method for Tensile Properties of Plastics. West Conshohocken, Pennsylvania: ASTM International 2014.

[335] ASTM. D1708-13 Standard Test Method for Tensile Properties of Plastics by Use of Microtensile Specimens. West Conshohocken, Pennsylvania: ASTM International 2013.

[336] Geng H-Z, Kim KK, So KP, Lee YS, Chang Y, Lee YH. Effect of Acid Treatment on Carbon Nanotube-Based Flexible Transparent Conducting Films. Journal of the American Chemical Society. 2007;129:7758-9.

[337] Andriotis AN, Menon M, Froudakis GE. Various bonding configurations of transition-metal atoms on carbon nanotubes: Their effect on contact resistance. Applied Physics Letters. 2000;76:3890.

[338] Sue H-J, Jones RE, Garcia-Meitin EI. Fracture behaviour of model toughened composites under Mode I and Mode II delaminations. Journal of Materials Science. 1993;28:6381-91.

[339] Wei G, Sue H-J. Fracture mechanisms in preformed polyphenylene oxide particle-modified bismaleimide resins. Journal of Applied Polymer Science. 1999;74:2539-45.

[340] Lee J, Yee AF. Role of inherent matrix toughness on fracture of glass bead filled epoxies. Polymer. 2000;41:8375-85.

[341] Lee J, Yee AF. Inorganic particle toughening I: Micro-mechanical deformations in the fracture of glass bead filled epoxies. Polymer. 2001;42:577-88.

[342] Lee J, Yee AF. Inorganic particle toughening II: Toughening mechanisms of glass bead filled epoxies. Polymer. 2001;42:589-97.

[343] Liu JD, Sue H-J, Thompson ZJ, Bates FS, Dettloff M, Jacob G, et al. Nanocavitation in self-assembled amphiphilic block copolymer-modified epoxy. Macromolecules. 2008;41:7616-24.

[344] Zhang W, Srivastava I, Zhu YF, Picu CR, Koratkar NA. Heterogeneity in epoxy nanocomposites initiates crazing: significant improvements in fatigue resistance and toughening. Small. 2009;5(12):1403-7.

[345] Tang L-C, Zhang H, Sprenger S, Ye L, Zhang Z. Fracture mechanisms of epoxy-based ternary composites filled with rigid-soft particles. Composites Science and Technology. 2012;72(5):558-65.

[346] Chen J, Kinloch AJ, Sprenger S, Taylor AC. The mechanical properties and toughening mechanisms of an epoxy polymer modified with polysiloxane-based core-shell particles. Polymer. 2013;54(16):4276-89.

[347] Koo B, Subramanian N, Chattopadhyay A. Molecular dynamics study of brittle fracture in epoxy-based thermoset polymer. Composites Part B: Engineering. 2016;95:433-9.

[348] Nash NH, Young TM, Stanley WF. The influence of a thermoplastic toughening interlayer and hydrothermal conditioning on the Mode-II interlaminar fracture toughness of Carbon/Benzoxazine composites. Composites Part A: Applied Science and Manufacturing. 2016;81:111-20.

[349] Rahul R, Kitey R. Effect of cross-linking on dynamic mechanical and fracture behavior of epoxy variants. Composites Part B: Engineering. 2016;85:336-42.

[350] Van Velthem P, Ballout W, Horion J, Janssens YA, Destoop V, Pardoen T, et al. Morphology and fracture properties of toughened highly crosslinked epoxy composites: A comparative study between high and low Tg tougheners. Composites Part B: Engineering. 2016;101:14-20.

[351] Liu W, Wang Y, Wang P, Li Y, Jiang Q, Hu X, et al. A biomimetic approach to improve the dispersibility, interfacial interactions and toughening effects of carbon nanofibers in epoxy composites. Composites Part B: Engineering. 2017;113:197-205.

[352] Kawaguchi T, Pearson RA. The effect of particle–matrix adhesion on the mechanical behavior of glass filled epoxies: Part 1. A study on yield behavior and cohesive strength. Polymer. 2003;44(15):4229-38.

[353] Kawaguchi T, Pearson RA. The effect of particle–matrix adhesion on the mechanical behavior of glass filled epoxies. Part 2. A study on fracture toughness. Polymer. 2003;44(15):4239-47.

[354] Bortz DR, Heras EG, Martin-Gullon I. Impressive Fatigue Life and Fracture Toughness Improvements in Graphene Oxide/Epoxy Composites. Macromolecules. 2012;45(1):238-45.

[355] Boo W, Sun L, Liu J, Clearfield A, Sue H, Mullins M, et al. Morphology and mechanical behavior of exfoliated epoxy/α-zirconium phosphate nanocomposites. Composites Science and Technology. 2007;67(2):262-9.

[356] Putz KW, Palmeri MJ, Cohn RB, Andrews R, Brinson LC. Effect of cross-link density on interphase creation in polymer nanocomposites. Macromolecules. 2008;41(18):6752-6.

[357] Macutkevic J, Kuzhir PP, Paddubskaya AG, Banys J, Maksimenko SA, Stefanutti E, et al. Broadband dielectric/electric properties of epoxy thin films filled with multiwalled carbon nanotubes. Journal of Nanophotonics. 2013;7.

[358] Cubides Y, Castaneda H. Corrosion protection mechanisms of carbon nanotube and zinc-rich epoxy primers on carbon steel in simulated concrete pore solutions in the presence of chloride ions. Corrosion Science. 2016;109:145-61.

[359] Ramezanzadeh B, Attar MM, Farzam M. A study on the anticorrosion performance of the epoxy–polyamide nanocomposites containing ZnO nanoparticles. Progress in Organic Coatings. 2011;72(3):410-22.

[360] Ramezanzadeh B, Attar MM. Studying the effects of micro and nano sized ZnO particles on the corrosion resistance and deterioration behavior of an epoxy-polyamide coating on hot-dip galvanized steel. Progress in Organic Coatings. 2011;71(3):314-28.